2008

FLEXURAL DESIGN OF SHAPE MEMORY ALLOY REINFORCED CONCRETE SECTIONS FOR STRENGTH AND SERVICEABILITY REQUIREMENTS

Yamen Ibrahim Elbahy

FLEXURAL DESIGN OF SHAPE MEMORY ALLOY REINFORCED CONCRETE SECTIONS FOR STRENGTH AND SERVICEABILITY REQUIREMENTS

(**Spine Title:** Flexural Design of SMA RC sections)

(Thesis Format: Integrated Article)

By

Yamen Ibrahim **Elbahy**

Graduate Program

In

Engineering Science

Department of Civil and Environmental Engineering

Submitted in partial fulfillment
of the requirements for the degree of
Master of Engineering Science

School of Graduate and Postdoctoral Studies
The University of Western Ontario
London, Ontario
August, 2008

ABSTRACT

Superelastic shape memory alloys (SMAs) have the ability to recover plastic deformations upon unloading. This unique property has motivated researchers to utilize them as primary reinforcement for RC structures located in seismic regions. The lack of understanding the behaviour of SMA RC sections is constraining their use. This thesis investigates the flexural behaviour of SMA RC sections. The validity of the flexural design equations provided by the Canadian Standards for SMA RC sections is evaluated. The load-deflection behaviour of SMA RC members is also investigated. The results are used to assess the applicability of available deflection models for SMA RC members. Artificial neural networks (ANNs) are used to develop a new deflection model. The thesis provides flexural design equations that allow engineers to accurately design SMA RC members for strength and serviceability requirements.

Keywords: reinforced concrete, shape memory alloys, moment-curvature, load-deflection, artificial neural networks, ultimate concrete strain, sectional analysis, moment-area method.

CO-AUTHORSHIP

This thesis has been prepared in accordance with the regulation of manuscript format stipulated by the School of Graduate and Postdoctoral Studies at The University of Western Ontario. Substantial parts of this thesis were either published in or submitted for publication to peer-reviewed technical journals and international conferences. All data analysis, modelling process, and writing the initial version of all publications listed below were carried out by the candidate himself. The contribution of his research advisor and co-advisor consisted of either providing advice, and/or helping in the development of final versions of publications:

[1] Elbahy Y.I., Youssef M.A., Nehdi M. (2008). "Flexural Behaviour of Concrete Members Reinforced with Shape Memory Alloys." 2nd Canadian Conference on Effective Design of Structures CCEDS-II, Sustainability of Civil Engineering Structures, Hamilton, ON, Canada, pp. 477-486.

[2] Elbahy Y.I., Youssef M.A., Nehdi M. "Stress Block Parameters for Concrete Flexural Members Reinforced with Superelastic Shape Memory Alloys." Submitted to the Materials and Structures Journal.

To: *My father AHMED,*

My mother AMIRA,

My brother HESHAM, and

My sister Yusra

ACKNOWLDGEMENT

The author would like to convey his sincere appreciation and gratitude to his advisors, Dr. Maged Youssef and Dr. Moncef Nehdi for their guidance, advice and encouragement throughout the course of this research. Their mentorship, support and patience were a great essence and are greatly acknowledged.

Special thanks are due to my friends and colleagues Mr. Ahmed Soliman, Mr. Mahmoud El-Feky, and Dr. Mohamed Bassuoni for the many constructive discussions we had during the course of this work. The author would also like to thank all technicians and staff at The Department of Civil and Environmental Engineering who contributed directly or indirectly to the accomplishment of this thesis.

Finally, the author would like to express his genuine gratitude and appreciation for his father, mother, brother, and sister for their continuous support and encouragement.

TABLE OF CONTENT

LIST OF TABLES

LIST OF FIGURES

LIST OF APPENDICES

LIST OF ABBREVIATION, SYMBOLS, AND NOMENCLATURE

$\overline{Y}$	Distance between point of action of the concrete compressive force and the centroidal axis.
A'_s	Compressive reinforcement area.
AAE	Average absolute error.
A_e	Effective area of concrete in tension surrounding tensile reinforcement.
A_f	Austenite finish temperature.
A_g	Area of concrete section.
AGE	Average algebraic error.
AI	Artificial intelligence.
ALI	Axial load index which represents the ratio between the applied axial load to the axial capacity of the cross-section.
ANN	Artificial Neural Network.
A-phase	Austenite phase.
A_s	Tensile reinforcement area.
b	Cross-section width.
b'	Width of beam at centroid of tensile reinforcement.
BCJ	Beam-column joint.
C	Compression zone height.
cc	Point at which concrete reaches its crushing strain.

C_c	Compressive force in concrete.
d	Effective depth of beam to centroid of tensile reinforcement.
D	The bar diameter.
d_b	Bar diameter.
d_c	Thickness of concrete cover measured from the extreme tension fibre to centre of bar located closest thereto.
E	Modulus of elasticity of the reinforcement.
e	Vector of the network errors.
E_{FRP}	Modulus of elasticity of FRP.
E_{p1}	SMA post-first yielding modulus of elasticity.
E_{p2}	SMA modulus of elasticity in the martensite phase.
E_s	Modulus of elasticity of steel.
$E_{u\text{-}s}$	Steel plastic modulus of elasticity.
$E_{u\text{-}SMA}$	SMA post-second yielding modulus of elasticity.
$E_{y\text{-}s}$	Steel elastic modulus of elasticity.
$E_{y\text{-}SMA}$	SMA modulus of elasticity in the austenite phase.
f	Neuron nonlinear activation function.
f_c	Concrete compressive stress.
f_c	Concrete compressive stress.
f_c'	Concrete compressive strength.
f_{cr}	Cracking stress.
f_f	Maximum stress in the FRP reinforcement at service load level.

FFBP	Feed-forward back-propagation.
f_o	Stress in the FRP bar at any specified load.
f_{p1}	SMA maximum recovery stress.
f_{p2}	Second SMA yielding stress.
FRP	Fibre reinforced polymers.
f_s	Steel stress.
f_{SMA}	SMA stress.
f_t'	The tensile strength of concrete and can be taken as $[7.5(f_c')^{0.5}]$.
f_{T1}	Martensite-to-austenite starting stress.
f_{T2}	Martensite-to-austenite finishing stress.
$f_{u\text{-}s}$	Steel ultimate stress.
$f_{u\text{-}SMA}$	SMA ultimate stress.
f_y	Austenite-to-martensite starting stress.
f_y	Yielding Stress.
$f_{y\text{-}s}$	Steel yielding stress.
$f_{y\text{-}SMA}$	First SMA yielding stress which represents the start of the masrtensite stress induced transformation
$f_{y\text{-}SMA}$	SMA yielding stress.
H	Point at which strain in the SMA bars exceeds ε_{p1}.
h	Cross-section height.
I_{cr}	Moment of inertia for the cracked section.
I_e	Effective moment of inertia.

I_g	Moment of inertia for the un-cracked section.
I_T	Un-cracked moment of inertia of the transformed section.
J	Jacobian matrix.
J_T	Transpose of the Jacobian matrix.
k_1	Factor that is equal to 1.6 for plain bars and 0.8 for deformed bars.
K_2	Factor that is equal to 0.5 for members subjected to bending and 1.0 for members subjected to tension.
k_b	A bond dependent factor.
K_f	Factor takes into account the behaviour of FRP bars.
K_g	Factor that is equal to 11 x 10^{-6} for steel conventionally steel reinforced concrete members.
L	Beam span.
M	Moment.
m	Order of the equation.
M_a	Applied moment.
M_{code}	Moment obtained using A23.3 (2004) recommended values (Equation [3-1].
M_{cr}	Cracking moment.
M_f	The failure moment.
MLP	Multi-layer perceptron.
M-phase	Martensite phase.
M_r	Moment obtained using the proposed equations for α_1, and β_1.

M_s	Martensite start temperature.
M_u	Ultimate moment.
M_y	Yielding moment.
n	Number of neurons in layer (l-1).
NSC	Normal strength concrete.
P	Axial load.
r	Point at which rupture of reinforcing bars occurs.
R	Coefficient of determination.
RC	Reinforced Concrete.
RMSE	Root mean square error.
SMAs	Shape memory alloys.
T_s	Tensile force in the SMA bars.
U_j^l	Neuron net input.
W	Tensile face surface crack width.
W_{ji}^l	Connection weight (strength) that connects the neuron j in layer l to neuron i in layer (l-1).
W_k	Vector of current weights and biases.
X_i^{l-1}	Input coming from neuron i in layer l-1 to neuron j in layer l.
y	Point at which bars reach f_y.
Y_j^l	Neuron output value.
Z	Slope of compressive strain softening branch.
α	Bond dependent coefficient. It can be taken as 0.5.

α_1, β_1	Stress block parameters.
β	Reduction factor for the calculation of the effective moment of inertia.
ε_l	Superelastic plateau strain length.
ε_c	Concrete compressive strain.
$\varepsilon_{c\text{-}max}$	Concrete maximum strain corresponding to the peak moment.
ε_{cu}	Ultimate concrete compressive strain.
ε_{end}	End part of the bar strain.
ε_{mid}	Middle part of the bar strain.
ε_{p1}	SMA maximum recovery stress.
ε_{p2}	Second SMA yielding strain.
ε_{p2}	Second SMA yielding strain.
ε_{SMA}	SMA strain.
$\varepsilon_{SMA\text{-}avg.}$	SMA average bar strain.
ε_{top}	Top compressive strain.
$\varepsilon_{u\text{-}s}$	Steel strain at failure.
$\varepsilon_{u\text{-}SMA}$	SMA strain at failure.
$\varepsilon_{y\text{-}s}$	Steel yielding strain.
$\varepsilon_{y\text{-}SMA}$	First SMA yielding strain.
θ_j^l	Threshold value assigned to neuron j in layer l.
μ	Learning rate
μ_m	The maximum bond stress.

ρ	Tensile reinforcement ratios.
ρ	Reinforcement ratio.
ρ'	Compressive reinforcement ratios.
ρ_b	The reinforcement ratio of the balanced section.
ρ_{FRP}	The reinforcement ratio of the FRP RC section.
Φ	Curvature.
Φ_{max}	Curvature corresponding to the peak moment.
Φ_u	Ultimate curvature.
Φ_y	Curvature corresponding to the yielding stress.

Chapter 1 Introduction and Thesis Organization

1.1 Introduction

Reinforced concrete (RC) structures are designed to function under predefined set of loads specified by design standards. However, experiencing unexpected severe loading may result in permanent damage. For instance, under a severe earthquake, the steel reinforcement would yield and permanent deformations are expected. Repairing these damaged structures might not be feasible and they might need to be demolished and replaced. Thus, there is a need for smart structures that can adjust their response to unexpected loading. These types of structures can be achieved by utilizing smart materials such as shape memory alloys (SMAs).

SMAs are special alloys that can undergo large deformations and return to their undeformed shape upon unloading or heating. Superelasticity, shape memory effect, and behaviour under cyclic loading are unique properties of SMAs which make them distinctive compared to other metals and alloys (Janke et al. 2005). These unique properties have motivated researchers to utilize them in civil and earthquake engineering applications. Some of these applications include using SMAs as bracing members (Mazzolan et al. 2004), ties (Auricchio et al. 2001), anchors for columns (Tamai et al. 2003), dampers (Clark et al. 1995, Krumme et al. 1995), and restrainers for steel beam-column joints (Ocel et al. 2004). The applicability of using SMAs as reinforcing bars was

experimentally investigated by Saiidi et al. (2007). The SMA RC beam-column joint tested by Youssef et al. (2008) showed superior performance compared to conventional steel reinforcement in recovering joint deformations under reversed cyclic loading.

The lack of understanding of the behaviour of SMA RC sections is considered a primary restrain to utilize them as primary reinforcement. Thus, more research is needed to investigate the behaviour of SMA RC sections, and to provide design equations to simplify the design process. This study investigates the flexural behaviour of SMA RC members and provide design equations to satisfy both strength and serviceability requirements.

1.2 Research objectives

The main objectives of the current research are:

1) Summarize the fundamental characteristics and unique properties of SMAs, and provide a literature review of their use as primary reinforcement for reinforced and prestressed concrete structures.
2) Study the flexural behaviour of SMA RC sections at different axial load levels, and provide design equations for SMA flexural members.
3) Study the load-deflection behaviour of SMA RC members and provide an assessment of existing deflection models for SMA RC members.
4) Utilize artificial neural network to develop a new model to predict the deflection of SMA RC members.

1.3 Outline of the thesis

This thesis is based on the "Integrated-Article Format" described in the University of Western Ontario School of Graduate and Postdoctoral Studies Thesis Regulation Manual. Chapters 3 to 5 have been written in a format suitable for submission to scholarly journal and have their own tables, figures, references, and appendices.

A literature review on shape memory alloys is introduced in Chapter 2. It includes the basic characteristics of SMAs from the civil engineering point of view. SMAs fabrication process, material modelling, unique properties, and applications as primary reinforcement are discussed.

In Chapter 3, the suitability of using sectional analysis to evaluate the moment-curvature relationship for SMA RC sections is confirmed. A parametric study is then conducted to identify the characteristics of this relationship for steel and SMA RC sections. Results are used to judge on the design equations given in the Canadian standards and to propose equations to estimate their recommended values.

The load-deflection behaviour of SMA RC members is investigated in Chapter 4 through a parametric study. Moment-curvature analysis is utilized to calculate deflections using the moment-area method. The results are used to judge on the validity of available models to calculate the deflection of SMA RC members.

In Chapter 5, artificial neural networks (ANN) are utilized to predict the deflection of SMA RC members. A new model is developed to predict the effective moment of inertia of SMA RC members. Design example is discussed to show the applicability of the model for design purposes.

Chapter 6 provides a general discussion of the entire thesis and restates important conclusions.

To overcome the limitations of the moment-area method in accounting for the deformations in the column and joint of the beam-column joint tested by Youssef et al. (2008), non-linear finite element analysis that accounts for non-linearity in material and geometry is carried out and summarized in Appendix I.

The calculation of the crack width for SMA RC members is investigated in Appendix II. Different available models are used to predict the crack width for the beam-column joint tested by Youssef et al. (2008). Suitable models are recommended.

The prediction of the developed ANN model are compared to predictions the existing models and summarized in Appendix III.

1.4 References

Auricchio, F., Faravelli, L., Magonette, G. and Torra, V. (2001). Shape Memory Alloys, Advances in Modelling and Applications, Artes Graficas Torres 17, 08029 Barcelona, Spain.

Clark, P. W., Aiken, I. D., Kelly, J. M., Higashino, M. and Krumme, R.C. (1995). "Experimental and Analytical Studies of Shape Memory Alloy Dampers for Structural Control." Smart Structures and Materials: Passive Damping, Proceedings of SPIE, 2445, 241-251.

Janke, L., Czaderski, C., Motavalli, M., Ruth, J. (2005). "Applications of Shape Memory Alloys in Civil Engineering Structures - Overview, Limits and New Ideas." Materials and Structures/Materiaux et Constructions, 38(279), 578-592.

Krumme, R., Hayes, J., and Sweeney, S. (1995). "Structural Damping with Shape Memory Alloys: One Class of Devices." Smart Structures and Materials: Passive Damping, Proceedings of SPIE, 2445, 225-240.

Mazzolani, F. M., Corte, G. D. And Faggiano, B. (2004). "Seismic Upgrading of RC Building y Means of Advanced Techniques: The ILVA-IDEM Project." The proceeding of the 13th World Conference on Earthquake Engineering, Paper no. 2703, Canada.

Ocel, J., DesRoches, R., Leon, R. T., Hess, W. G., Krumme, R., Hayes, J. R., Sweeney, S. (2004). "Steel Beam-Column Connections using Shape Memory Alloys." ASCE, Journal of Structural Engineering, 130(5), 732-740.

Saiidi, M.S., Sadrossadat-Zadeh, M., Ayoub, C., Itani, A. (2007). "Pilot Study of Behavior of Concrete Beams Reinforced with Shape Memory Alloys." ASCE, Journal of Materials in Civil Engineering, 19(6), 454-461.

Chapter 2 Utilizing Shape Memory Alloys as Reinforcement for Reinforced and Prestressed Concrete Structures

2.1 Introduction

The seismic design of steel reinforced concrete (RC) structures is mainly dependent on the energy dissipated by yielding of reinforcing bars. This philosophy results in structures behaving within the life safety performance level. However, repairing these structures following a seismic event is a critical issue. Damaged structures during seismic event might need to be demolished and replaced. Extensive research has been performed to improve the seismic design of concrete structures. Shape memory alloys (SMAs) were found to have unique properties, which motivated researchers to utilize them in civil structures (Janke et al. 2005). During an earthquake, SMA would yield. However, after the load removal, it has the ability to recover all of its deformations (Otsuka and Wayman 1998, Eucken 1991).

Some of the applications of SMA in civil structures include using them as anchors for columns (Tamai et al. 2003), restrainers for steel beam-column joints (Ocel et al. 2004), dampers (Clark et al. 1995, Krumme et al. 1995), ties (Auricchio et al. 2001), and bracing members (Mazzolan et al. 2004). Saiidi et al. (2007) experimentally investigated the applicability of SMA as reinforcing bars. Elbahy et al. (2008) studied the flexural behaviour of SMA reinforced concrete sections. Using the SMA in the critical regions of

reinforced concrete beam-column joints (BCJs) was investigated experimentally by Youssef et al. (2008).

This chapter introduces the basic characteristics of SMAs from the civil engineering point of view. SMAs fabrication process, material modeling, and unique properties are discussed in details in this chapter. Moreover, a review of the work done to utilize SMAs as primary reinforcement for concrete structures and as prestressing tendons for prestressed concrete is summarized.

2.2 Fabrication of SMAs

The fabrication process of SMAs starts by melting the alloys in a high vaco. The second stage of the manufacturing process includes shaping the hot or cold alloy to the desired shape such as: wire, ribbon, tube, sheet or bar. Finally, the shape memory treatment is performed to the alloy to obtain the unique properties such as shape memory effect and superelasticity. A summary for different SMA types and their chemical composition are summarized in Table 2-1.

Table 2-1: Chemical composition of different types of SMAs

Type	Composition [atomic %]
Cu-Al-Ni	28-29 Al, 3.0-4.5 Ni
Cu-Sn	15 Sn
Cu-Zn (brass)	38.5-41.5 Zn
Fe-Cr-Ni-Mn-Si	9 Cr, 5 Ni, 14 Mn, 6 Si
Fe-Mn-Si	28-33 Mn, 4-6 Si
Fe-Ni-C	31 Ni, 0.4 C
Fe-Ni-Co-Ti	33 Ni, 10 Co, 4 Ti
Fe-Ni-Nb	31 Ni, 7 Nb
Mn-Cu	5-35 Cu
Ni-Al	36-38 Al
Ni-Ti	49-51 Ni
Ni-Ti-Cu	8-20u

2.3 Phase transformation

Like other types of alloys, SMAs exhibit different phase transformations. There are two unique crystal structures or phases of the SMAs, which are martensite (M-phase) and austenite (A-phase), Figure 2-1. These two phases are mainly dependent on the thermo-mechanical parameters, which are the material temperature, load or stress level, and strain. As shown in Figure 2-1, there are some characteristic temperatures at which the alloys start to transform from one phase to another. For instance, the SMA starts to transform from austenite phase when its temperature drops below the martensite start temperature (M_s). The complete transformation to the martensite phase occurs when the alloy temperature reaches the martensite finish temperature (M_f). In the martensite phase, the alloy behaves ferro-elastically, and can be easily manipulated at large strains (Figure

2-2). Heating the alloy to the austenite start temperature (A_s) and then to the austenite finish temperature (A_f) will result in a complete transformation from martensite to austenite phase. In between A_f and M_f temperatures, both phases co-exist in the alloy with different percentages.

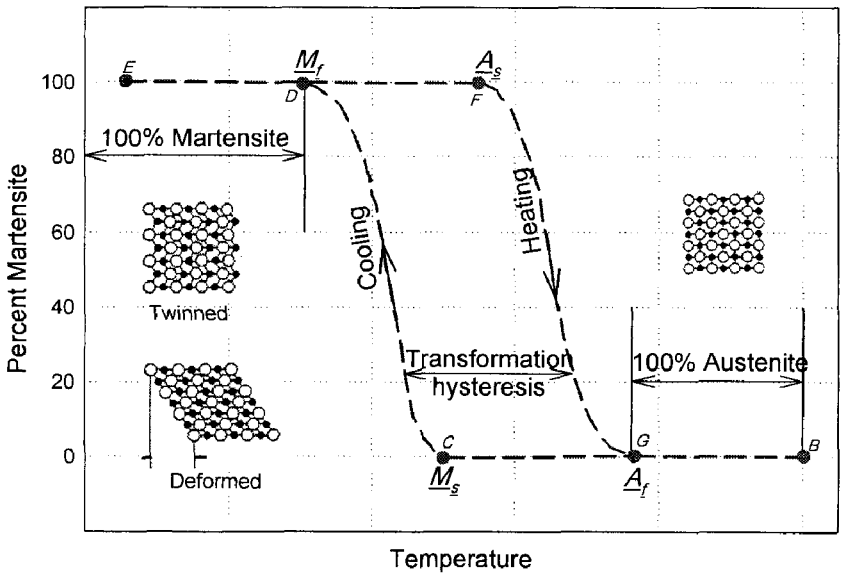

Figure 2-1: Phase Transformation and change in crystalline structure of SMA

Transformation temperature can vary considerably for different types of SMAs. It is highly dependent on the alloy composition, thermo-mechanical treatment during the manufacturing process, and type and level of loading. This should be considered if a certain phase is required under a certain mechanical load. Moreover, the number of the loading cycles or loading rate can also have an effect on the transformation temperatures.

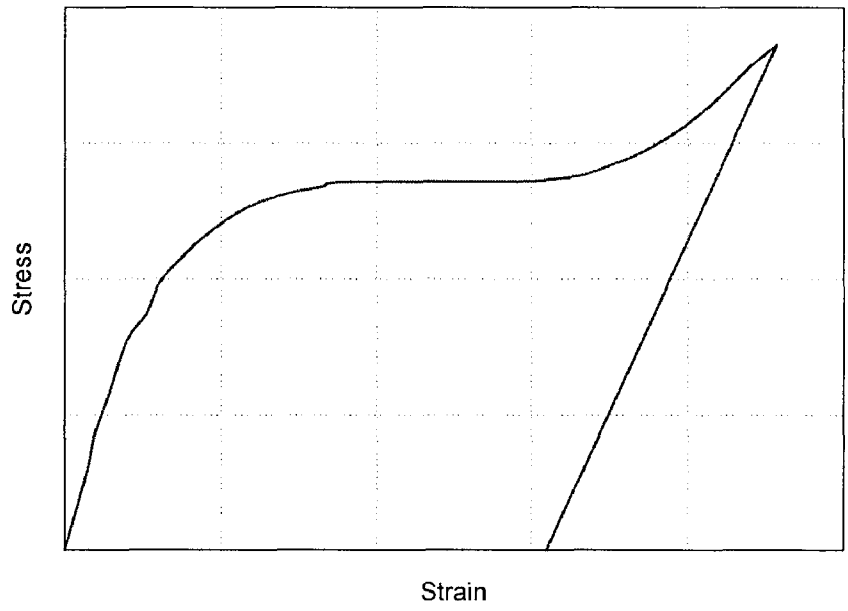

Figure 2-2: SMA stress-strain relationship at 100% martensite state

2.4 Unique properties of SMA

Many types of SMAs with different chemical compositions have been introduced in the market. Among these types, Ni-Ti (Nickel-Titanium based SMA) was found to be the most appropriate for civil engineering applications because of its high strain recoverable strain range. These applications utilize the Shape Memory Effect (SME), Superelasticity (SE), Damping hysteresis, high fatigue resistance, and high corrosion resistance of SMAs (Janke et al. 2005).

Shape memory effect (also known as 'one-way shape memory effect' or pseudo-platicity) defines the ability of certain types of alloys to recover their undeformed shape upon heating (Otsuka and Wayman 1998). Mechanical stresses occur in the alloy if the alloy is

restrained to recover the deformations. These stresses can be used in structural applications such as prestressing concrete members (El-Tawil and Ortega 2004).

Some types of SMAs have the ability to remember two different shapes based on the alloy temperature. This property is called 'two-way shape memory effect'. In order to achieve this property, special thermo-mechanical training is required (Janke et al. 2005).

The second unique property of SMA is the superelasticity. It is also known as pseudo-elasticity (Otsuka and Wayman 1998, Eucken 1991). SMA can reach high strain ranges (up to 10%) and return to its undeformed shape upon unloading (Figure 2-3). This property, pseudo-elasticity, exists in the alloy when it is above austenite finish A_f temperature. Increasing the external stresses during the loading phase without changing the temperature results in phase transformation from austenite to martensite. Once unloading starts, reverse transformation from martensite to austenite phase automatically occurs. This gives the SMA the ability to undergo hundreds of deformation cycles without keeping residual deformations.

Saadat et al. (1999) showed that SMA has high damping properties in both austenite and martensite phases. However, it is slightly higher in martensite phase because of the stress-induced martensite transformation, and the reorientation of the martensite variants under external loading. However, the damping hysteresis is affected by the internal and external factors such as the alloy temperature, loading frequency, strain range, alloy chemical composition, the ratio of the martensite to the austenite phase.

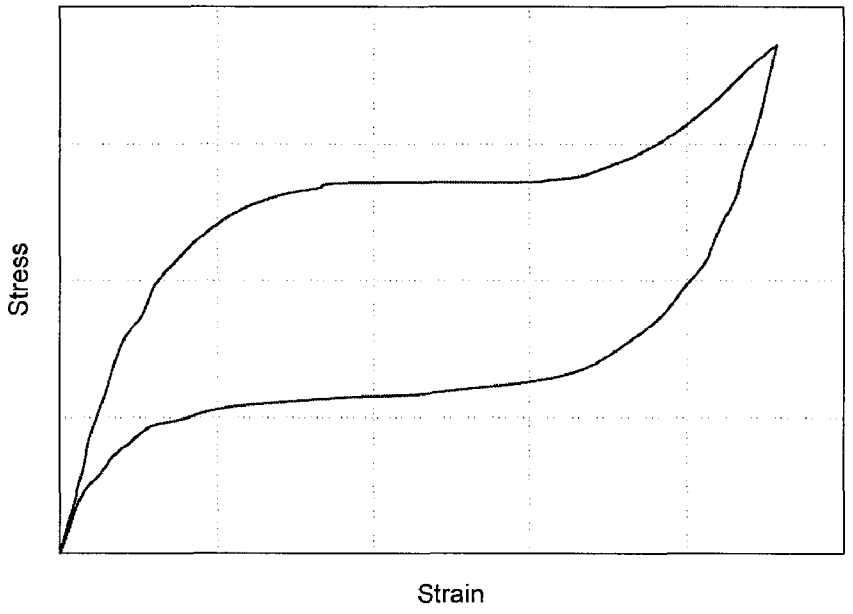

Figure 2-3: SMA stress-strain relationship at 100% austenite state

Fatigue is a critical property of the material when long time operation of the structure is considered. For SMAs, two types of fatigue should be considered. These types are structural fatigue (known as classical mechanical fatigue) and functional fatigue (known as shape memory fatigue) (Eggeler et al. 2004, Hornboge 2004). Structural fatigue represents the formation and growth of surface cracks in addition to the micro-structural defects leading to rupture of the material. Functional fatigue is the gradual degradation of either shape memory effect or damping capacity as a result of the micro-structural changes. The functional fatigue is associated with changes in the stress-strain relationship under cyclic loading.

2.5 Material modeling

SMAs have many applications in different fields such as medical sciences, aerospace, mechanical and civil engineering. Thus, the development of a proper constitutive model became an important issue. As most of the civil engineering applications utilize the SMAs as bars and wires, one-dimensional phenomenological models are enough. Some uniaxial phenomenological model have been proposed by Tanaka and Nagaki (1982), Liang and Rogers (1990), Brinson (1993), and Auricchio and Lubliner (1997).

Many finite element packages have recently included a model for the SMA material. Figure 2-4 shows the one-dimensional stress-strain model of SMA that is being used by SeismoStruct (2008). Six parameters are used to define the model which are: (1) Modulus of elasticity E, (2) Austenite-to-martensite starting stress f_y, (3) Austenite-to-martensite finishing stress f_{pl}, (4) Martensite-to-austenite starting stress f_{Tl}, (5) Martensite-to-austenite finishing stress f_{T2}, and (6) Superelastic plateau strain length ε_l.

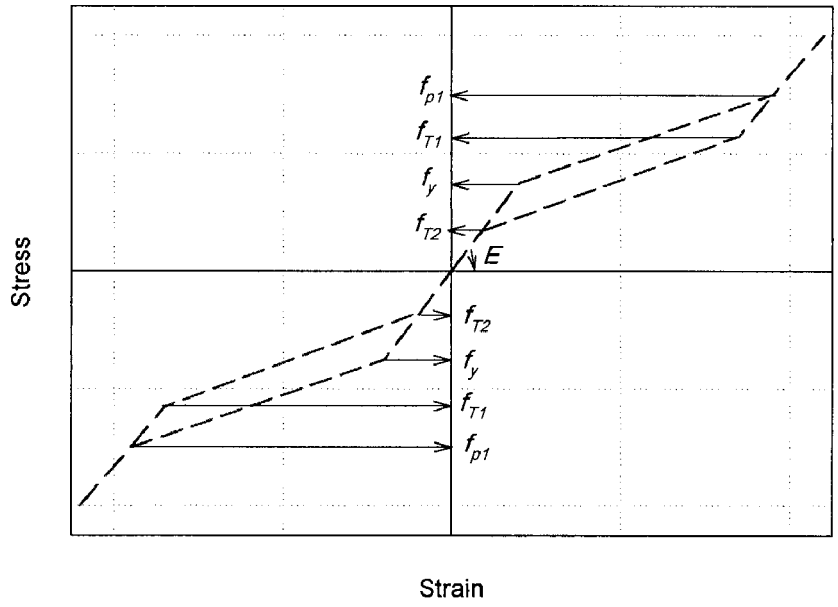

Figure 2-4: One-dimensional model of superelastic SMA (Auricchio and Sacco 1997)

2.6 Applications of SMA reinforcing bars

2.6.1 Reinforcement for concrete elements

Using the SMA as longitudinal reinforcing bars in the plastic hinge regions of RC columns was investigated experimentally by Saiidi and Wang (2006). Two quarter-scale spiral RC columns, one with SMA longitudinal reinforcement in the plastic hinge area while the second with conventional steel reinforcement, were designed, constructed, and tested using a shaking table. Details of the tested specimen are shown in Figure 2-5. Test results indicated superior performance of SMA RC columns compared to conventional steel RC columns in limiting relative column top displacement and column residual displacement. The damaged SMA RC column specimen was repaired with engineering cementations composites. The repaired specimen was retested using the same approach as

the initial test. Test results showed better performance for the repaired specimen compared to the original specimen in terms of force-displacement capacity and ductility.

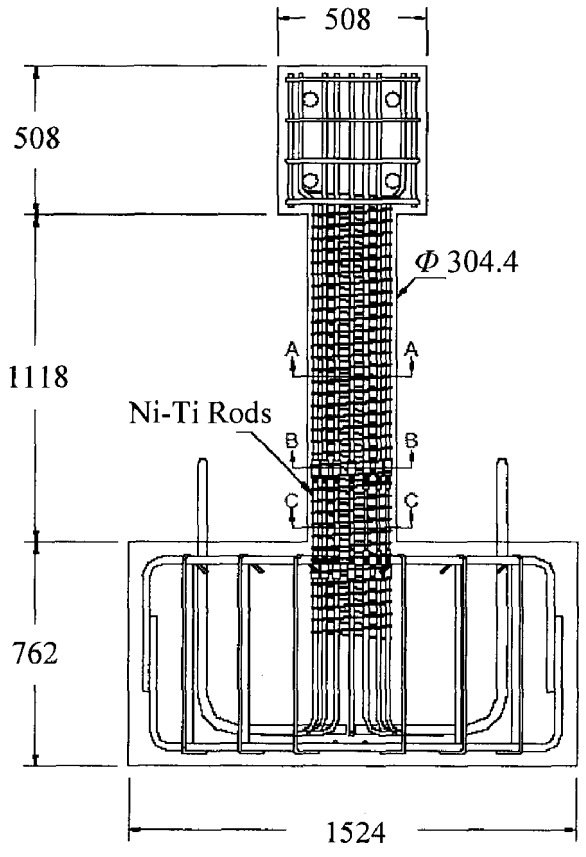

Figure 2-5: Details of tested specimen (Saiidi and Wang 2006)

The applicability of superelastic SMA bars for self-restoration of bridge decks and girders was investigated by Sakai et al. (2003). Three mortar beams, two of them were reinforced with SMA wires while the third was reinforced with steel wires, were tested under static one-point load up to the inelastic range. Test results showed that the SMA reinforced beams were able to return to one-tenth of their maximum deflection. The SMA RC beams reached deflections more than seven times the deflection of the steel RC

beams, which indicates much higher ductility. Cracks of the SMA RC beams were almost closed after unloading, Figure 2-6.

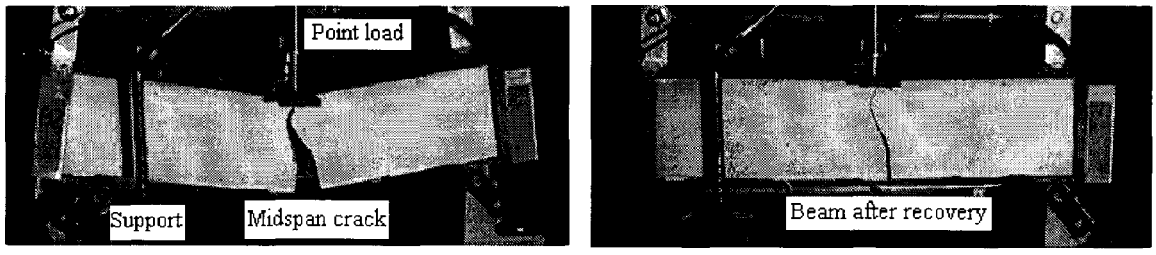

(a) Cracks at maximum deflection (b) Cracks after unloading

Figure 2-6: Cracking behaviour of SMA mortar beams (after Sakai et al. 2003)

The possibility of producing RC beams with variable stiffness and strength was investigated by Czoderski et al. (2005). The experimental program consisted of two RC beams. One beam was reinforced with SMA wires while the second was reinforced with steel wires. The two beams were tested under four-point loading. Heating the SMA wires resulted in phase transformation of the SMA, and as a result an increase of the beam strength and stiffness. This technique can help designing smart structures, which can intelligently respond to the applied loading.

Saiidi et al. (2007) experimentally investigated the ability of Ni-Ti reinforcement to recover deformations and dissipate energy under cyclic loading. Eight beams that have the same dimensions but differ in the reinforcement type and amount were used in the experimental program. To use the SMA bars with more than one beam, the beams were externally reinforced (Figure 2-7). Test results showed that the average residual deformations in SMA RC beams were much smaller than steel RC beams (one-fifth).

Moreover, the SMA bars showed superelastic behaviour when used as longitudinal reinforcement in the beam specimen, as the bars almost recovered the full deformations.

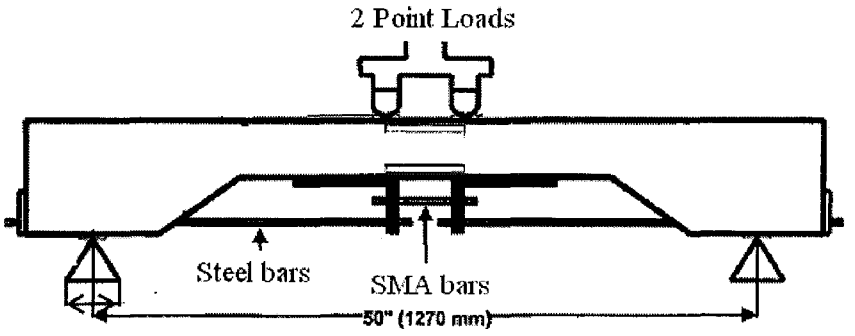

Figure 2-7: Test setup (after Saiidi et al. 2007)

The use of superelastic SMA bars in the critical regions of the beams-column joints was experimentally investigated by Youssef et al. (2008). Two three-quarter scale BCJs were tested under reversed cyclic loading. One of the two joints was reinforced with superelastic SMA in the plastic hinge region (Figure 2-8), while the other was reinforced with conventional steel. Test results showed very small residual displacement in case of SMA reinforcement compared to the steel reinforcement case. After the test, the residual strains in the SMA longitudinal bars were negligible, while the longitudinal steel bars experienced much larger strains compared to the SMA bars.

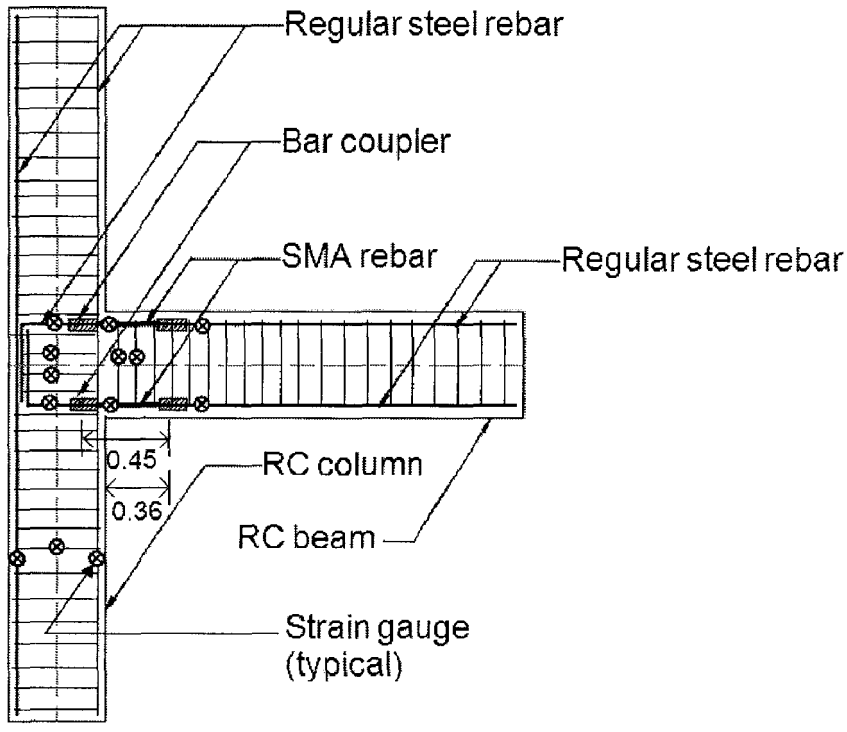

Figure 2-8: Details of the tested BCJ by Youssef et al. (2008)

2.6.2 Prestressing concrete elements

An extensive research has been conducted on utilizing the SMA tendons/wires in prestressing concrete elements. Both pre-tensioning and post-tensioning techniques can be performed using SMAs. Some benefits are associated with using the SMAs in the prestressing process such as: (1) active control on the amount of prestressing, (2) the absence of jacking or strands cutting process, and (3) elimination of losses associated with elastic shortening, friction, and anchorage losses.

Maji and Negret (1998) utilized the shape memory effect of Ni-Ti strands for prestressing concrete. The SMA strands were elongated beyond their plastic limit, and embedded in the beam forms. After casting of concrete, the strands were heated to recover the

deformations (Figure 2-9). This resulted in a significant prestressing force in concrete. The strands showed good bonding behaviour with concrete.

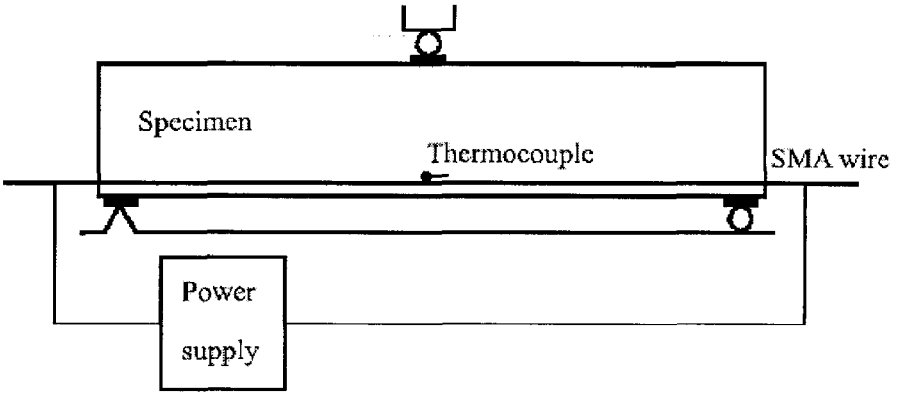

Figure 2-9: Using SMA in pre-tensioning concrete beams (after Li et al. 2007)

El-Tawil and Ortega (2004) studied the availability of using SMAs in permanent prestressing of concrete using post-tensioning technique. Mortar beams with 380 mm x 25mm x 38 mm were used (Figure 2-10). Two types of SMAs were used, Ni-Ti and Ni-Ti-Nb alloys. The second type showed better solution for permanent prestressing as the first type lost the recovery stresses after turning the electric current source off (i.e. temperature drop). The beams were tested under four-point testing, and the test results showed that a significant prestressing was achieved

Opara and Naaman (2000) studied the ability of SMAs to prestress concrete elements by utilizing their ability to recover plastic deformations (Figure 2-11). Plate shaped samples were used in the experimental work. Two of the samples were plain mortar, five were reinforced with steel, and two were reinforced with SMA. The results from the tests

showed that the SMA deformations were fully recovered, and that cracks were fully closed.

(a) SMA Martensite Phase

(b) Pre-stretch SMA at room temperature and transport to construction site

(c) Pour Concrete, and after hardening, install tendon in post-tensioning ducts. Alternatively, tendon could be installed in formwork prior to concrete placement.

(d) Anchor and trigger tendons using electrical source

Figure 2-10: Using SMA in post-tensioning concrete beams (after El-Tawil and Ortega 2004)

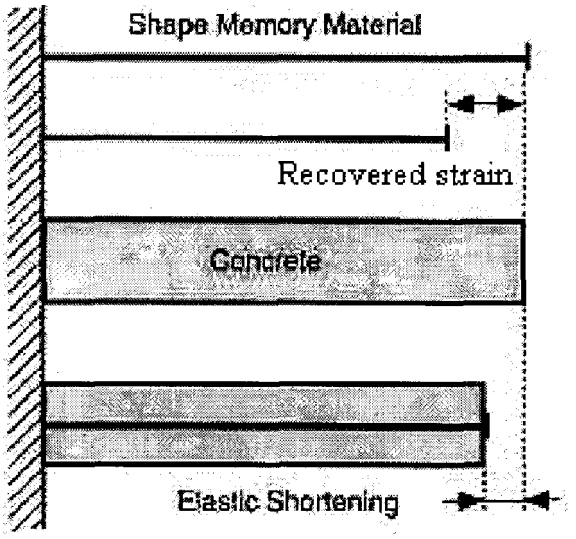

Figure 2-11: SMA self-healing (after Opara and Naaman 2000)

2.7 Limitations on SMAs

Although there is a high potential to utilize SMAs in civil engineering applications, its high cost is a hindrance for its use. A significant reduction in the cost of SMAs was observed in the last ten years. Although SMAs are still considered relatively expensive, the continuous on going research is expected to significantly reduce their cost. For example, Janke et al (2005) introduced a new type of SMAs that have different chemical composition (Fe-based SMA). This new composition resulted in cost reduction of 8.0% to 13.0% correspond to Nickel-Titanium based SMA.

Other research by Bruno and Valente (2002) on the feasibility of using SMA materials and devices in full scale construction projects, considered various costs such as direct costs (structural and non-structural) and indirect costs (injuries and deaths). The SMA devices have been found much preferable as they do not need additional costs for

maintenance or replacement. Moreover, Bruno and Valente (2002) found that using SMA devices reduced economic losses, and minimized human risk associated with natural disaster events.

2.8 Conclusions

The basic characteristics of SMAs from the civil engineering point of view have been introduced in this chapter. The SMA manufacturing process, material modeling, and unique properties were discussed in details. The availability of SMAs in different shapes in addition to their unique properties including shape memory effect, superleasticity, behaviour under cyclic loading, and the high fatigue and corrosion resistance have made them ideal for reinforced and prestressed concrete structures. A number of experimental and analytical work was carried out to study the advantages of using SMAs as reinforcing bars. Test results showed superior performance of superelastic SMAs in recovering deformations upon unloading and closing concrete cracks.

The research done on utilizing SMA as prestressing strands has showed many advantages such as: the ability to control the amount of prestressing, the absence of strands jacking and cutting process, and the elimination of elastic shortening, friction, and anchorage losses. However, more research is still needed in this field to reach the optimum design of SMA reinforced and prestressed concrete structures.

2.9 References

Auricchio, F. and Lubliner, J. (1997). "Uniaxial model for shape-memory alloys." International Journal of Solids and Structures, 34, 3601-3618.

Auricchio, F., Faravelli, L., Magonette, G. and Torra, V. (2001). Shape Memory Alloys, Advances in Modelling and Applications, Artes Graficas Torres 17, 08029 Barcelona, Spain.

Brinson, L.C. (1993). "One-Dimensional Constitutive Behavior of Shape Memory Alloys: Thermomechanical Derivation with Non-Constant Material Functions and Redefined Martensite Internal Variable." Journal of Intelligent Material Systems and Structures, 4, 229-242.

Bruno, S., and Valente, C. (2002). "Comparative Response Analysis of Conventional and Innovative Seismic Protection Strategies." Earthquake Engineering and Structural Dynamics, 31, 1067-1092.

Clark, P. W., Aiken, I. D., Kelly, J. M., Higashino, M. and Krumme, R.C. (1995). "Experimental and Analytical Studies of Shape Memory Alloy Dampers for Structural Control." Smart Structures and Materials: Passive Damping, Proceedings of SPIE, 2445, 241-251.

Czaderski. C., Hahnebach. B., and Motavalli, M. (2006). "RC Beam with Variable Stiffness and Strength." Construction and Building Materials, 20, 824-833.

Eggeler, G., Hornbogen, E., Yawny, A., Heckmann, A. and Wagner, M. (2004). "Structural and Functional Fatigue of NiTi Shape Memory Alloys." Journal of Material science and Engineering: A, 378 (1-2), 24-33.

Elbahy, Y.I., Youssef, M.A., Nehdi, M. (2008). "Flexural Behaviour of Concrete Memebers Reinforced with Shape Memory Alloys." 2nd Canadian Conference on Effective Design of Structures, McMaster University, Hamilton, Ontario, Canada.

El-Tawil, S., and Ortega-Rosales, J. (2004). "Prestressing Concrete using Shape Memory Alloy Tendons." ACI Structural Journal, 101(6), 846-851.

Eucken, S. (1991). Progress in Shape Memory Alloys, Alle Rechte Vorbehalten.

Hornbogen, E. (2004). "Review: Thermo-mechanical fatigue of shape memory alloys." Journal of Materials Science, 39 (2), 385-399.

Janke, L., Czaderski, C., Motavalli, M., Ruth, J. (2005). "Applications of Shape Memory Alloys in Civil Engineering Structures - Overview, Limits and New Ideas." Materials and Structures/Materiaux et Constructions, 38(279), 578-592.

Krstulovic-Opara, N. and Naaman, A.E. (2000). "Self-Stressing Fiber Composites." ACI structural Journal, 97-S38, 335-344.

Krumme, R., Hayes, J., and Sweeney, S. (1995). "Structural Damping with Shape Memory Alloys: One Class of Devices." Smart Structures and Materials: Passive Damping, Proceedings of SPIE, 2445, 225-240.

Li, H., Liu, Z., and Ou, J. (2007). "Study on reinforced concrete beams strengthened using shape memory alloy wires in combination with carbon-fiber-reinforced polymer plates." Smart Materials and Structures, 16(6), 2550-2559.

Liang, C., and Rogers, C.A. (1990). "One-Dimensional Thermomechanical Constitutive Relations for Shape Memory Materials." Collection of Technical Papers

AIAA/ASME/ASCE/AHS Structures, Structural Dynamics & Materials Conference, 16-28.

Maji, A. K., and Negret, I. (1998). "Smart Prestressing with Shape-Memory Alloy." Journal of Engineering Mechanics, 124(10), 1121-1128.

Mazzolani, F. M., Corte, G. D. And Faggiano, B. (2004). "Seismic Upgrading of RC Building y Means of Advanced Techniques: The ILVA-IDEM Project." The proceeding of the 13th World Conference on Earthquake Engineering, Paper no. 2703, Canada.

Ocel, J., DesRoches, R., Leon, R. T., Hess, W. G., Krumme, R., Hayes, J. R., Sweeney, S. (2004). "Steel Beam-Column Connections using Shape Memory Alloys." ASCE, Journal of Structural Engineering, 130(5), 732-740.

Otsuka, K. and Wayman, C. M. (1998). Mechanism of Shape Memory Effect and Superelasticity, Shape Memory Materials, Cambridge University Press Cambridge, U.K., 27-48.

Saadat, S., Salichs, J., Duval, L., Noori, M.N., Hou, Z., Bar-on., I. And Davoodi, H. (1999). "Utilization of Shape Memory Alloys for Structural Vibration Control." A Summary Review fr Presentation at US-Japan Workshop on Smart Materials and New Technologies for Improvement of Seismic Performance of Urban Structures, Disaster Prevention Research Institute, Kyoto University, Japan.

Saiidi, M.S., and Wang, H. (2006). "Exploratory Study of Seismic Response of Concrete Columns with Shape Memory Alloys Reinforcement." ACI Structural Journal, 103(3), 436-443

Saiidi, M.S., Sadrossadat-Zadeh, M., Ayoub, C., Itani, A. (2007). "Pilot Study of Behavior of Concrete Beams Reinforced with Shape Memory Alloys." ASCE, Journal of Materials in Civil Engineering, 19(6), 454-461.

Sakai, Y., Kitagawa, Y., Fukuta, T., and Iiba, M. (2003). "Experimental Study on Enhancement of Self-Restoration of Concrete Beams Using SMA Wire." Proceedings of SPIE - The International Society for Optical Engineering, 5057, 178-186.

SeismoStruct Help file (2008). Version 4.0.0, available at http://www.seismosoft.com/SeismoStruct/index.htm.

Tamai, H., Miura, K., Kitagawa, Y., Fukuta, T. (2003). "Application of SMA Rod to Exposed-Type Column Base in Smart Structural System." Proceedings, Smart Structures and Materials: Smart Systems and Nondestructive Evaluation for Civil Infrastructures, The International Society for Optical Engineering, 169-177.

Tanaka, K., and Nagaki, S. (1982). "Thermomechanical Description of Materials with Internal Variables in the Process of Phase Transitions." Ingenieur-Archiv, 51(5), 287-299.

Youssef MA, Alam MS, Nehdi M. (In-press). "Experimental investigation on the seismic behaviour of beam-column joints reinforced with superelastic shape memory alloys." Journal of Earthquake Engineering, accepted January 2008.

Chapter 3 Flexural Behaviour of Concrete Members Reinforced with Shape Memory Alloys

3.1 Introduction

Although SMAs have many applications in different fields, they are considered relatively new to the civil engineering field. The shape memory effect, superelasticity, and performance under cyclic loading are unique properties that distinguish SMAs from other metals and alloys and make them attractive for various civil engineering applications. Some of these applications have been discussed in Chapter 2. Other applications are discussed by Wilson and Wesolowsky (2005), DesRoches and Smith (2004), Song et al. (2006), and Alam et al. (2007). This chapter focuses particularly on one of these applications in which SMA bars are used to reinforce concrete structures.

The unique stress-strain relationship of SMA bars is expected to affect the moment-curvature (M-Φ) relationship of concrete sections. Thus values of α_1, β_1, and $\varepsilon_{c\text{-}max}$ that are used to evaluate the average concrete compressive stress and the location of the centroid of the compressive force are expected to be different for SMA RC sections. A23.3 (2004) specifies a value of 0.0035 for $\varepsilon_{c\text{-}max}$ and provides Equation [3-1] to calculate α_1 and β_1. f'_c is the concrete compressive strength. Moment capacity of a concrete section supporting an axial load P can be evaluated using plane section assumption and utilizing equilibrium as shown in Figure 3-1.

$$\alpha_1 = 0.85 - 0.0015 f_c' \qquad \geq 0.67 \qquad [3\text{-}1a]$$

$$\beta_1 = 0.97 - 0.0025 f_c' \qquad \geq 0.67 \qquad [3\text{-}1b]$$

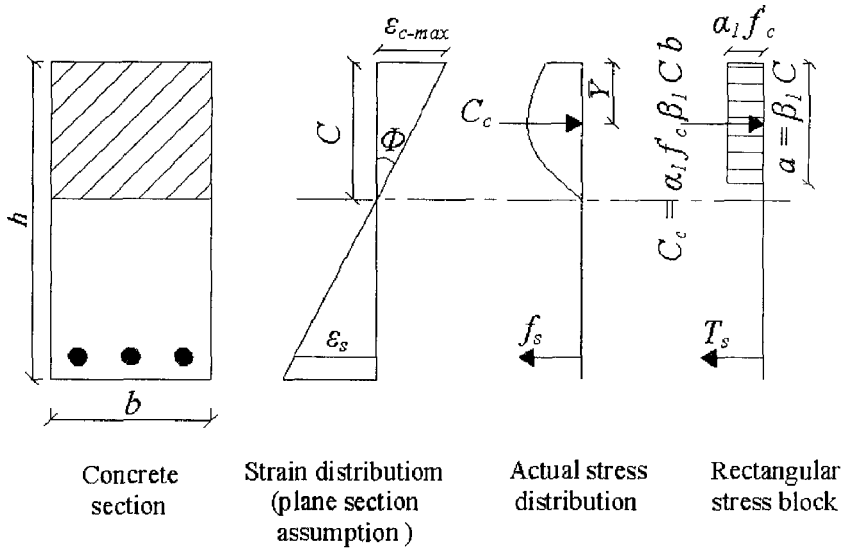

Figure 3-1: Stress block parameters for rectangular sections

M-Φ analysis utilizing non-linear material constitutive models, Figure 3-2, can accurately determine the moment M_f and ultimate curvature Φ_u corresponding to ultimate concrete strain ε_{cu}, and $\varepsilon_{c\text{-}max}$ and Φ_{max} corresponding to the ultimate moment capacity M_u for a steel RC section (Ozbakkalogln and Saatcioglu 2004). In this chapter, a parametric study is conducted on concrete sections reinforced with either SMA or steel bars. The sections have different reinforcement ratio, dimensions, Axial Load Level $\left[ALI = \frac{P}{f_c' \text{ x } A_g} \text{, where } A_g \text{ is the area of the concrete section} \right]$, and f_c'. The main features of the *M-Φ* relationship and normal force-moment interaction diagram for SMA RC sections are identified. Based on the results of this study, A23.3 (2004) values for $\varepsilon_{c\text{-}}$

$_{max}$, α_1, and β_1 are judged and new values are proposed for both steel and SMA RC sections.

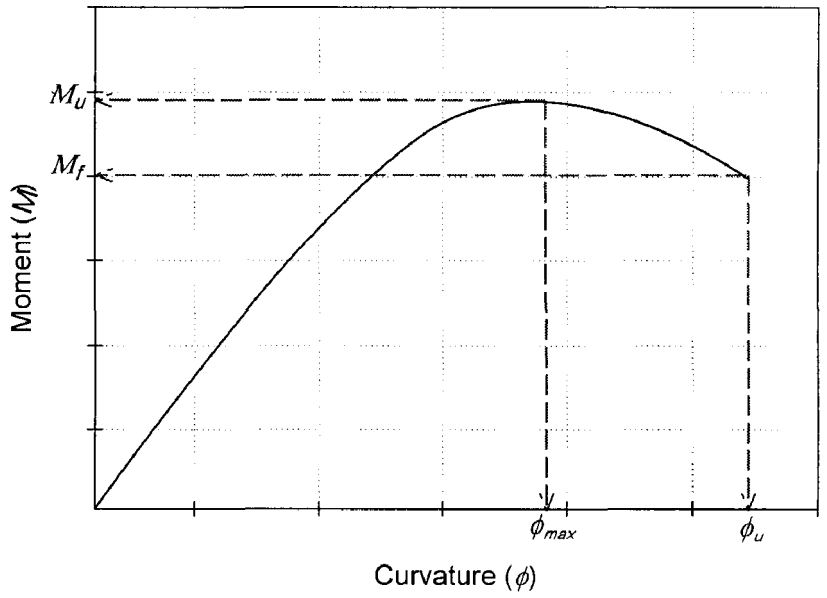

Figure 3-2: Typical *M-Φ* relationship

3.2 Material properties

3.2.1 Concrete stress-strain model

The model of Scott et al. (1982) given by Equation [3-2] and shown in Figure 3-3, is used to model the stress-strain behaviour of concrete in compression. Concrete is assumed to crush when ε_{cu} reaches 0.0035 (A23.3 2004). This value lies within the known range for unconfined concrete (Park and Paulay 1975). Concrete tensile resistance is ignored.

$$f_c = f_c'\left[2.0\left(\frac{\varepsilon_c}{0.002}\right)-\left(\frac{\varepsilon_c}{0.002}\right)^2\right] \qquad 0 \le \varepsilon_c \le 0.002 \qquad \text{[3-2a]}$$

$$f_c = f_c'[1 - Z(\varepsilon_c - 0.002)] \qquad \varepsilon_c \ge 0.002 \quad \textit{and} \quad f_c \ge 0.2f_c' \qquad \text{[3-2b]}$$

$$Z = \frac{0.5}{\frac{3+0.29f_c'(\text{MPa})}{145f_c'(\text{MPa})-1000} - 0.002} \qquad \text{[3-2c]}$$

Where: f_c = concrete compressive stress, Z = slope of compressive strain softening branch, ε_c = concrete compressive strain.

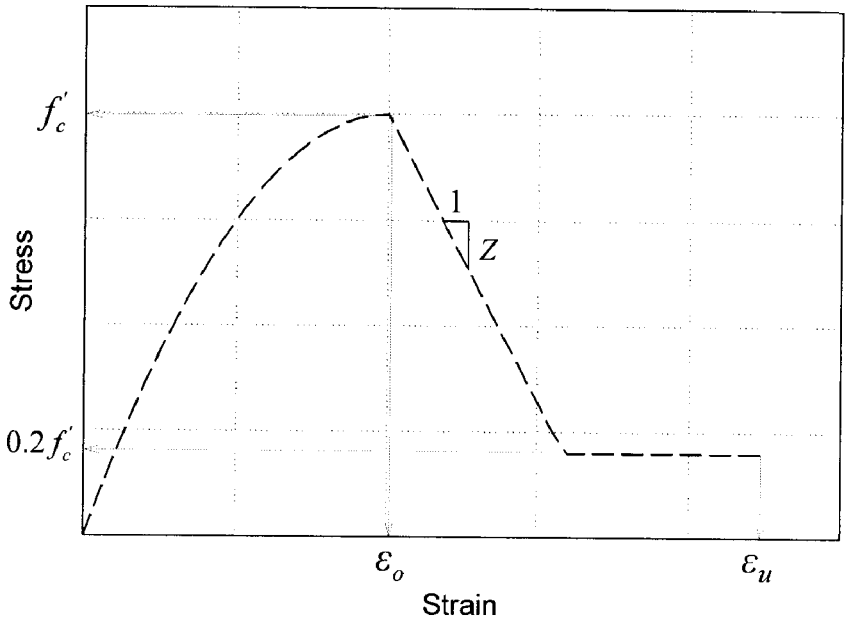

Figure 3-3: Stress-strain model for concrete in compression

3.2.2 Steel stress-strain model

The stress-strain relationship for steel is assumed to be bilinear as shown in Figure 3-4. The material behaves elastically with a modulus of elasticity $E_{y\text{-}s}$ until the strain reaches $\varepsilon_{y\text{-}s}$. As the strain exceeds $\varepsilon_{y\text{-}s}$, the modulus of elasticity $E_{u\text{-}s}$ is significantly reduced to about 1 to 2% of $E_{y\text{-}s}$. The equations used to represent the model are as follow:

$$f_s = E_{y\text{-}s}\,\varepsilon_s \qquad 0 \le \varepsilon_s \le \varepsilon_{y\text{-}s} \qquad \text{[3-3a]}$$

$$f_s = f_{y\text{-}s} + E_{u\text{-}s}\left(\varepsilon_s - \varepsilon_{y\text{-}s}\right) \qquad \varepsilon_{y\text{-}s} \le \varepsilon_s \le \varepsilon_{u\text{-}s} \qquad \text{[3-3b]}$$

Where: f_s = steel stress, $f_{y\text{-}s}$ = steel yielding stress, $f_{u\text{-}s}$ = steel ultimate stress, ε_s = steel strain, $\varepsilon_{y\text{-}s}$ = steel yielding strain, $\varepsilon_{u\text{-}s}$ = steel strain at failure, $E_{y\text{-}s}$ = steel elastic modulus of elasticity, and $E_{u\text{-}s}$ = steel plastic modulus of elasticity.

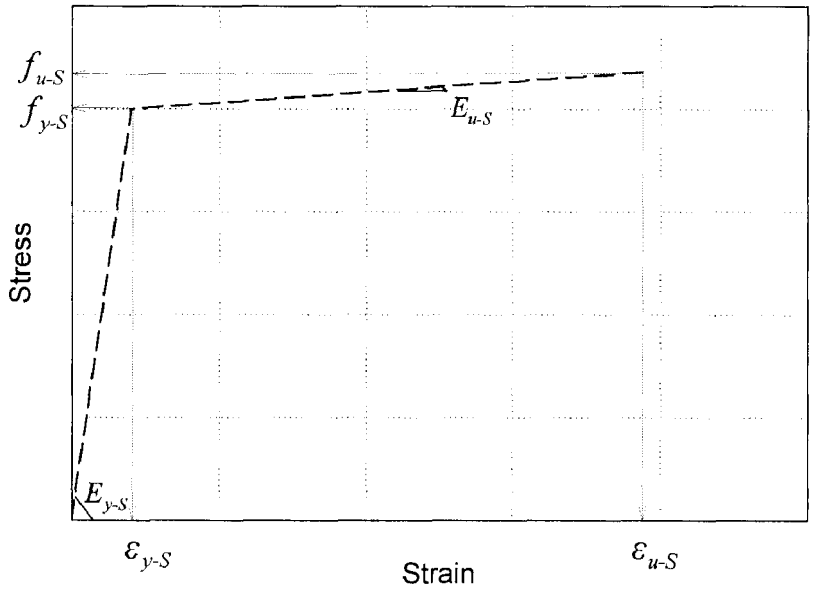

Figure 3-4: Stress-strain model for steel

3.2.3 SMA stress-strain model

Ni-Ti alloys are the most suitable SMA for structural applications because of their high recoverable strain and durability (Alam et al. 2007, Manach and Favier 1997, Zak et al. 2003, DesRoches et al. 2004, Ostuka and Wayman 1999, Liu et al. 1998, Orgeas and Favier 1995). Their stress-strain relationship consists of four linear branches that are connected by smooth curves. As a simplification, the smooth curves are ignored and the linear branches are assumed to intersect as shown in Figure 3-5. Although SMA does not yield, the points at which the modulus of elasticity is significantly reduced will be defined as yield points. The alloy behaves elastically with a modulus of elasticity $E_{y\text{-}SMA}$ until reaching the yield stress $f_{y\text{-}SMA}$. As the strain ε_{SMA} exceeds the yield strain $\varepsilon_{y\text{-}SMA}$, the modulus of elasticity E_{p1} becomes 10% to 15% of $E_{y\text{-}SMA}$. For strains above the maximum recovery strain ε_{p1}, the material becomes stiffer and the modulus of elasticity E_{p2} reaches about 50 to 60% of $E_{y\text{-}SMA}$. The final linear branch starts at another yield point with a modulus of elasticity $E_{u\text{-}SMA}$ that is 3 to 8% of $E_{y\text{-}SMA}$. The following equations represent the model:

$$f_{SMA} = E_{y\text{-}SMA}\ \varepsilon_{SMA} \qquad o \le \varepsilon_{SMA} \le \varepsilon_{y\text{-}SMA} \qquad [3\text{-}4a]$$

$$f_{SMA} = f_{y\text{-}SMA} + E_{p1}\left(\varepsilon_{SMA} - \varepsilon_{y\text{-}SMA}\right) \qquad \varepsilon_{y\text{-}SMA} \le \varepsilon_{SMA} \le \varepsilon_{p1} \qquad [3\text{-}4b]$$

$$f_{SMA} = f_{p1} + E_{p2}\left(\varepsilon_{SMA} - \varepsilon_{p1}\right) \qquad \varepsilon_{p1} \le \varepsilon_{SMA} \le \varepsilon_{p2} \qquad [3\text{-}4c]$$

$$f_{SMA} = f_{p2} + E_{u\text{-}SMA}\left(\varepsilon_{SMA} - \varepsilon_{p2}\right) \qquad \varepsilon_{p2} \le \varepsilon_{SMA} \le \varepsilon_{u\text{-}SMA} \qquad [3\text{-}4d]$$

Where: f_{SMA} = SMA stress, f_{p1} = maximum recovery stress, f_{p2} = second SMA yielding stress, ε_{p2} = second SMA yielding strain, and $\varepsilon_{u\text{-}SMA}$ = SMA strain at failure.

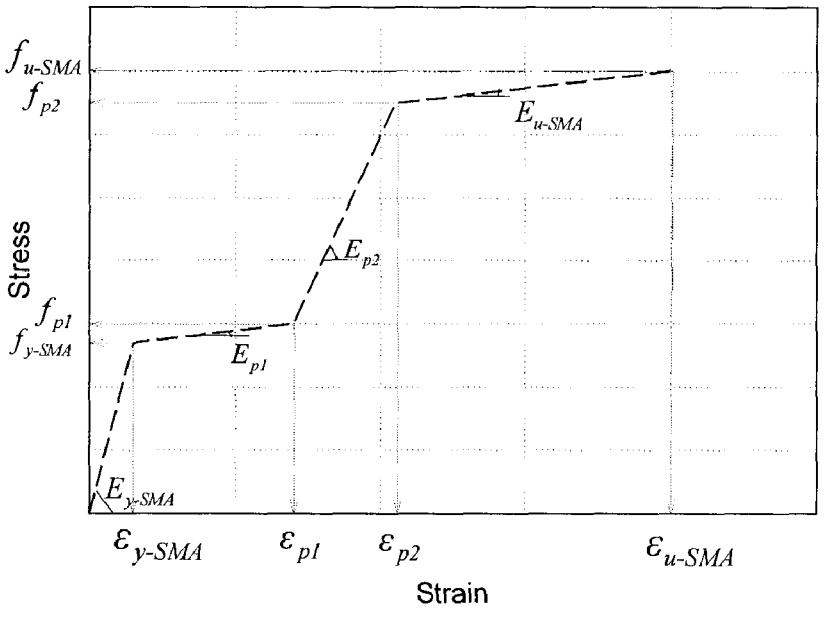

Figure 3-5: Stress-strain model for SMA

3.3 Sectional analysis

Moment-curvature analysis was conducted based on the fibre model methodology (Youssef and Rahman 2007). This methodology depends on dividing the section into a finite number of layers as shown in Figure 3-6. Using the defined stress-strain models for the materials and taking into considerations section equilibrium and kinematics, the mechanical behaviour of the section is analyzed. The relationship between the axial strain, the curvature, the applied moment, and the axial force can be written as:

$$\begin{pmatrix} \Delta M \\ \Delta P \end{pmatrix} = \begin{pmatrix} \sum E_i A_i y_i^2 & -\sum E_i A_i y_i \\ -\sum E_i A_i y_i & \sum E_i A_i \end{pmatrix} X \begin{pmatrix} \Delta\phi \\ \Delta\varepsilon_c \end{pmatrix} \quad [3\text{-}5]$$

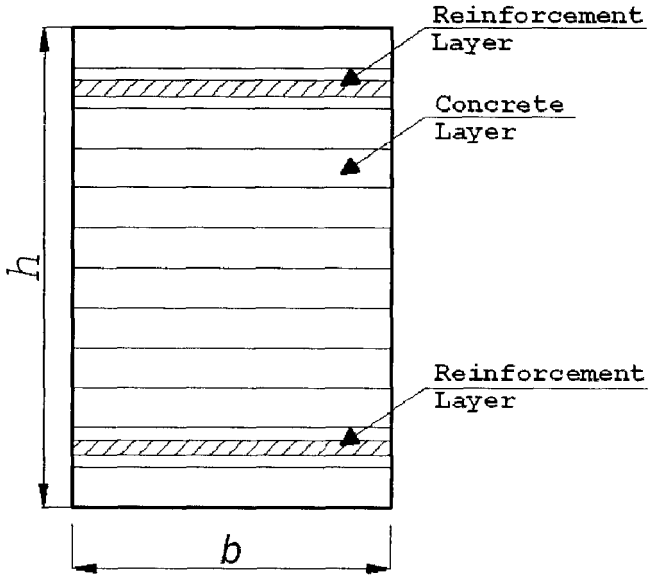

Figure 3-6: Fibre model for a concrete section

Assumptions applicable to steel RC sections and included in the analysis are summarized below. The assumptions are:

1) Plane sections remain plane, so strain distribution is linear,
2) Perfect bond exists between concrete and reinforcement, and
3) The tensile strength of concrete is ignored.

The load is applied into two different stages. In the first stage (Figure 3-7-(a)), the axial load is applied in an incremental way while the moment is kept equal to zero. After reaching the specified axial load, stage *II* (Figure 3-7-(b)) starts by applying displacement

load (curvature) in an incremental way while keeping the axial load equal to the specified value. The steps involved in these stages can be summarized as follows.

3.3.1 Stage I:

1) The initial axial load, concrete strain, and curvature are set to zero,
2) The initial E_i values for the concrete and steel layers are calculated,
3) A suitable load increment ΔP is chosen and applied to the cross section,
4) The incremental increase in the strain $\Delta\varepsilon_c$ is calculated using Equation [3-5],
5) The modified E_i values are calculated using the modified axial strain ($\varepsilon_c = \varepsilon_{c,previous} + \Delta\varepsilon_c$),
6) If the axial load is equal to the specified load, the values of ε_c and E_i are recorded and analysis of stage *II* starts, and
7) Analysis proceeds by repeating steps 4 to 6.

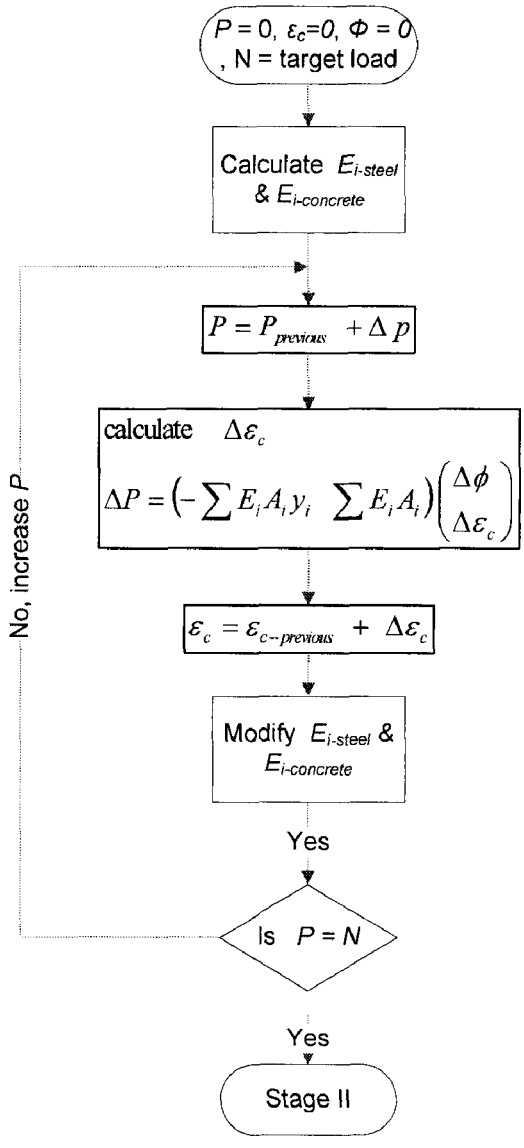

(a) Stage I

Figure 3-7: Flow chart for the fibre model analysis

3.3.2 Stage II:

The axial load is kept constant at the desired value recorded in stage *I* and the applied curvature is increased from zero to a specified value. A displacement approach is selected to capture the sectional behaviour after reaching the maximum compressive strength. The

steps involved in this stage have to be conducted twice to define the sectional behaviour when subjected to positive and negative curvatures and are summarized below:

1) The values of ε_c and E_i are set equal to those recorded in step 6 of analysis stage *I*,
2) A suitable curvature increment $\Delta\Phi$ is chosen and applied to the section,
3) The modified E_i values are calculated using the axial strain of each layer ($\varepsilon_{ci} = \varepsilon_{c\text{-}previous} \pm \Delta\Phi\, y_i$),
4) $\Delta\varepsilon_{ci}$ is calculated from Equation [3-5], such that ΔP is equal to zero ($\varepsilon_c = \varepsilon_{c\text{-}previous} + \Delta\varepsilon_c$),
5) $\Delta\varepsilon_c$ is checked against a predefined tolerance. If the error is higher than the tolerance, steps 3 and 4 are repeated,
6) The value of ΔM is calculated from Equation [3-5]. The total moment on the section is $M = M_{Previous} + \Delta M$. At this moment stage, the total concrete compressive forces, the forces in the steel layer and the centre of gravity of these forces are recorded, and
7) The analysis is repeated by applying a curvature increment $\Delta\Phi$ and repeating steps 3 to 6.

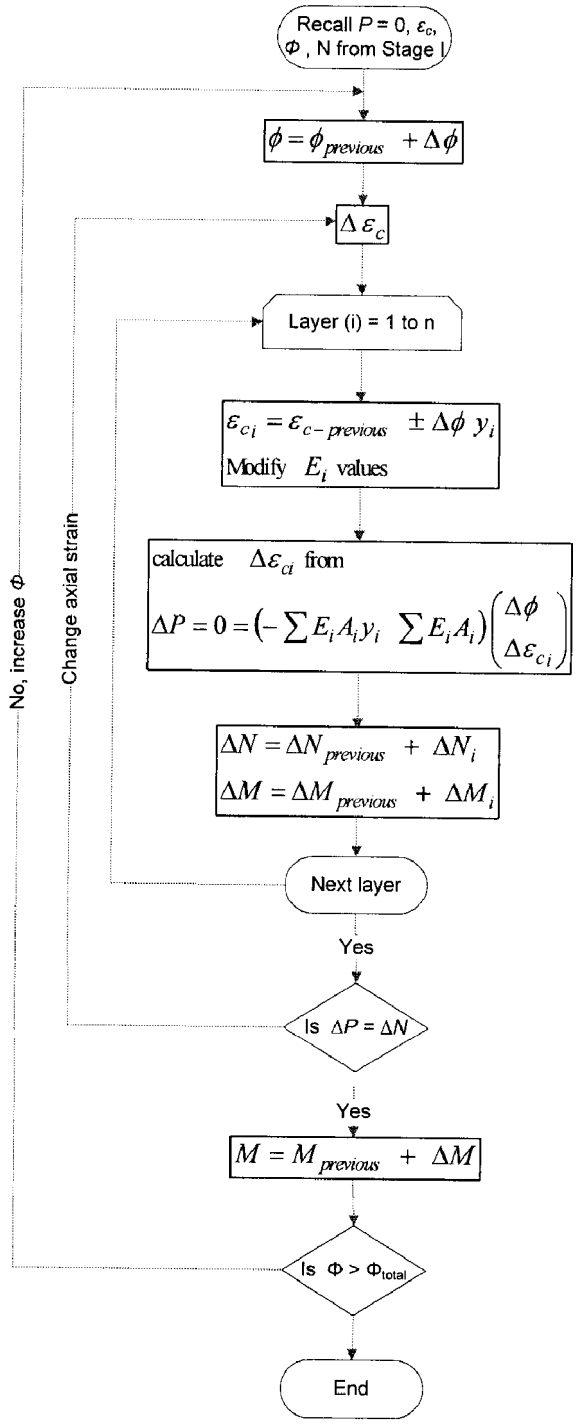

(b) Stage II

Figure 3-7: Flow chart for the fibre model analysis

3.4 Experimental validation

To validate the applicability of using sectional analysis for SMA RC sections, the behaviour of three small-scale SMA reinforced concrete beams tested by Saiidi et al. (2007) was predicted numerically. The beams have the same dimensions but differ in their reinforcement ratio. All the beams have a span of 1270 mm, cross-section width of 127 mm, midspan cross-section height of 152 mm, and end cross-section height of 305 mm. Details of the SMA reinforcement are given in Table 3-1.

Table 3-1: Properties of tested beams

Specimen	Midspan SMA reinforcement	$\varepsilon_{y\text{-}SMA}$ (mm/mm)	$f_{y\text{-}SMA}$ (MPa)	$E_{y\text{-}SMA}$ (MPa)
BNL2	2 Φ 6.40 mm	0.013	400	34078
BNH1	1 Φ 9.50 mm	0.013	510	39245
BNH2	2 Φ 9.50 mm	0.013	510	39245

Figure 3-8 shows the test setup. The beams were externally reinforced with SMA bars between the loading points and with regular steel reinforcing bars elsewhere. Figure 3-9 shows a typical SMA bar used in the beams. Saiidi et al. (2007) indicated that their analytical predictions deviated from the experimental results because of the lack of bond between the concrete and the reinforcing bars and due to the variation of the diameter of the SMA bars. In this chapter, the sectional analysis explained earlier is modified to account for the actual test setup.

Figure 3-10 shows a flow chart for the modified procedure. The procedure starts by assuming an average SMA bar strain $\varepsilon_{SMA\text{-}avg}$. Based on the length and cross-sectional area of the middle and two end parts of the SMA bar, their strains (ε_{mid}, and ε_{end}) are calculated. The force in the SMA bar is constant along its length and can be evaluated using ε_{mid} or ε_{end}. To satisfy section equilibrium, the compressive force in the concrete should be equal to the assumed tensile force. For a specific top compressive strain ε_{top}, the curvature Φ is iterated until equilibrium is satisfied. The corresponding moment is then calculated. The analysis is repeated for a range of top compressive strains ε_{top}. The relationship between the moment and the concrete strain at the location of the bar is established. The moment corresponding to the assumed $\varepsilon_{SMA\text{-}avg}$ is then obtained. This procedure is repeated for different values of $\varepsilon_{SMA\text{-}avg}$, which allows defining the M-Φ relationship. Analysis is terminated when ε_{top} reaches 0.0035.

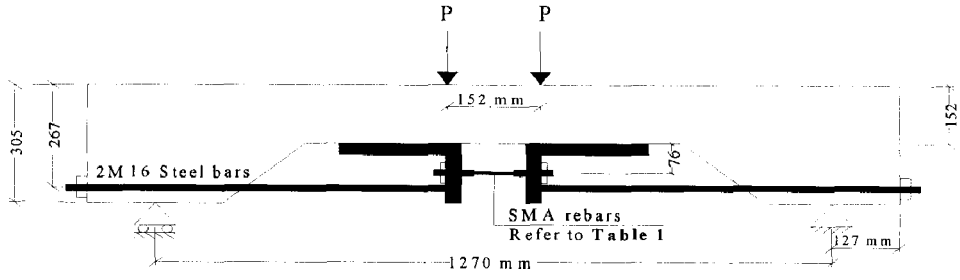

Figure 3-8: Test setup

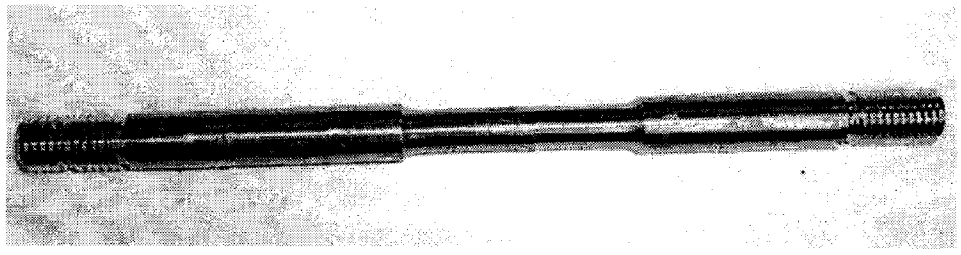

Figure 3-9: SMA typical bar (Saiidi et al. 2007)

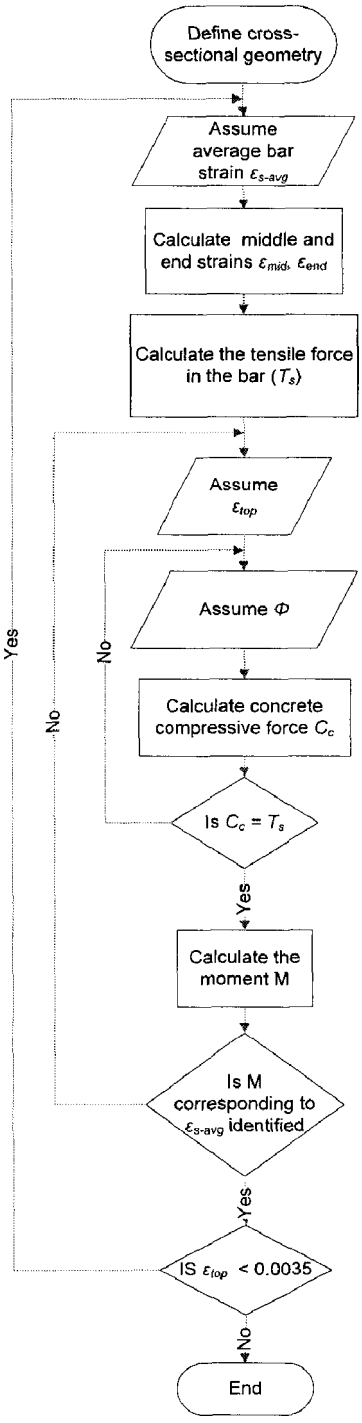

Figure 3-10: Flow chart of the modified analysis procedure

It was clear from the load-average bar strain relationship reported by Ayoub et al. (2003) that the strain in BNH2 exceeded ε_{pl}. As the stress-strain relationship for the Ni-Ti bars

provided by Saiidi et al. (2007) was bilinear, ε_{p1} and E_{p2} were assumed equal to 0.05 mm/mm, 22463 MPa, respectively. Figure 3-11 shows the comparison between the analytical and experimental *M-Φ* diagrams for SMA reinforced beams. Very good agreement was observed for all specimens.

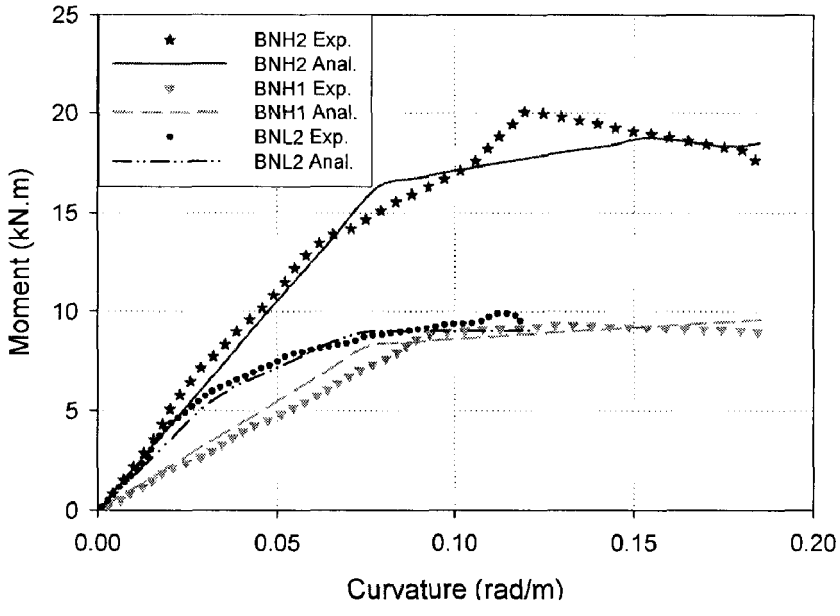

Figure 3-11: Experimental versus analytical moment-curvature for SMA reinforced beams

3.5 Parametric study

A parametric study is conducted for typical concrete sections with different *h* (500 mm, 700 mm, and 900 mm), *b* (200 mm, 300 mm, and 400 mm), tensile reinforcement ratios ρ (0.25%, 0.50%, and 0.75%), compressive reinforcement ratios ρ' (0%, 0.125%, and 0.25%), f'_c (20 MPa, 40 MPa, and 60 MPa), and axial load levels (*ALI* ranges from 0 to 1). Table 3-2 shows details of the analyzed sections. Each section is analyzed twice

assuming that reinforcing bars are either SMA or steel with the mechanical properties given in Table 3-3.

Table 3-2: Details of analyzed sections

Section	Studied variables	h (mm)	b (mm)	A_s (mm^2)	A'_s (mm^2)	f'_c (MPa)
C_1	h	500	300	655	0	40
C_2	b, h	700	300	655	0	40
C_3	h	900	300	655	0	40
C_4	b	700	200	655	0	40
C_5	b	700	400	655	0	40
C_6	ρ, ρ', f'_c	700	300	525	0	40
C_7	ρ	700	300	1050	0	40
C_8	ρ	700	300	1575	0	40
C_9	ρ'	700	300	525	262.5	40
C_{10}	ρ'	700	300	525	525.0	40
C_{11}	f'_c	700	300	525	0	20
C_{12}	f'_c	700	300	525	0	60

Because of the high value of $\varepsilon_{y\text{-}SMA}$ (0.015 mm/mm), SMA bars did not exhibit tensile yielding at *ALI* higher than 0.2. In this chapter, *ALI* = 0 and 0.3 were chosen to present the behaviour of SMA RC sections in details. The results obtained for other *ALI* values were used to develop normal force-moment interaction diagrams. These diagrams were developed for both types of reinforcement, i.e. steel and SMA.

Table 3-3: Mechanical properties of SMA and steel bars

Material	Property	E_y (GPa)	f_y (MPa)	f_{pl} (MPa)	f_u (MPa)	ε_{pl} (%)	ε_u (%)
SMA	Tension	36	540	600	1400	7.0	20
	Compression	60	650	735	1500	4.5	20
Steel	Tension or Compression	200	438	NA	615	NA	3.5

3.6 Moment-curvature response

Due to the difference in the modulus of elasticity of steel and SMA, the curvature Φ_y corresponding to f_y for SMA RC sections was found to be higher than that for similar steel RC sections. The failure of SMA RC sections was initiated by crushing of concrete. Rupture of SMA bars did not govern failure because of the high ultimate tensile strain of the SMA bars (0.2 mm/mm). For steel RC sections, the failure type varied between concrete crushing and rupture of steel bars depending on section dimensions, reinforcement ratio, and axial load level. The effect of the different parameters on the *M-Φ* relationship is shown in Figures 3-12 to 3-21. In these figures, the point at which the bars reach f_y is marked by (y), while the point at which the strain in the SMA bars exceeds ε_{pl} is defined by an (*H*). The two types of failure are defined by (*cc*) for concrete crushing and (*r*) for rupture of reinforcing bars.

3.6.1 Effect of section height *h*

Figure 3-12 and Figure 3-13 show the effect of varying h on the M-Φ relationship at two levels of axial load (ALI=0 and 0.3). At ALI=0, increasing h increased the section capacity for both types of reinforcement. Yielding of SMA RC sections occurred at higher curvature values (400% to 500%) than that for the steel RC sections. The ultimate curvature Φ_u of steel RC sections was found to decrease by 50% as h increased by 80%. This decrease is attributed to the failure type as it occurred by rupture of steel rather than crushing of concrete. The section ultimate curvature, Φ_u for SMA RC sections was not significantly affected by a similar increase in h since failure is governed by crushing of concrete.

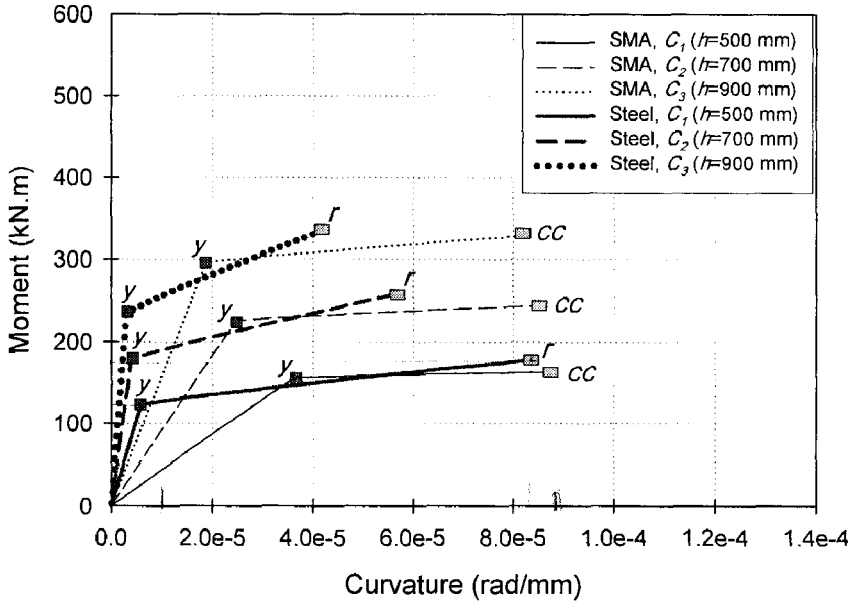

Figure 3-12: Effect of varying h on the M-Φ relationship (ALI=0)

Increasing the axial load level from 0 to 0.3 resulted in a significant increase (315%) in the cracking moment for both steel and SMA RC sections. Although the yielding moment M_y for steel RC sections increased with axial load increase, SMA RC sections did not exhibit yielding. The amount of dissipated energy calculated by integrating the area under the M-Φ relationship increased with the increase in h for both cases of reinforcement. At ALI of 0.3, SMA RC sections have similar initial stiffness and dissipated comparable energy as steel RC sections.

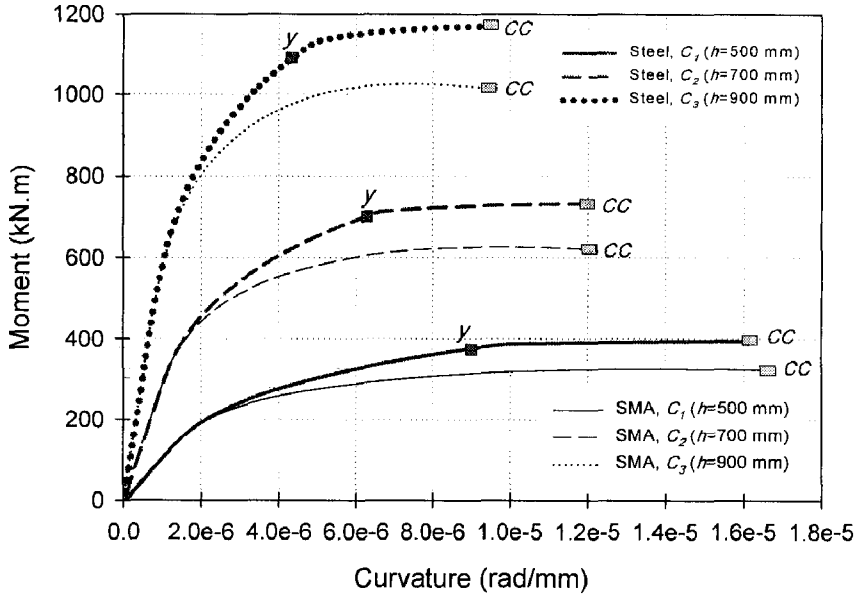

Figure 3-13: Effect of varying h on the M-Φ relationship (ALI=0.3)

3.6.2 Effect of section width b

The effect of varying b on the M-Φ analysis is illustrated in Figure 3-14 and Figure 3-15. At ALI=0, increasing b had a minor effect on M_y and M_u for both steel and SMA reinforcement. Although Φ_u was not affected for steel RC sections, Φ_u for SMA RC

sections increased by 90% as b increased by 100%. This increase in Φ_u resulted in 125% increase in the dissipated energy.

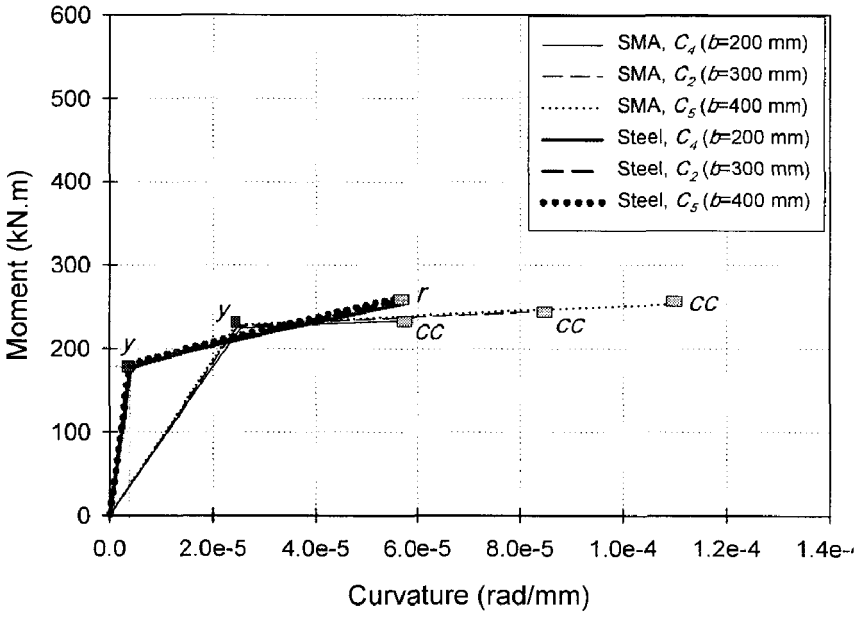

Figure 3-14: Effect of varying *b* on the *M-Φ* relationship (*ALI*=0)

At higher axial load level (*ALI*=0.3), Figure 3-15, the curves for SMA and steel RC sections coincided prior to cracking. For both types of RC sections, Φ_u was not affected by changing *b* and a significant increase, about 80%, in section capacity was achieved by increasing *b* by 100%. Although SMA bars did not exhibit any yielding for the studied sections, they dissipated large amount of energy, 4848 N.rad to 9665 N.rad. M_y for steel RC sections increased by 200% to 400% due to the increase in the axial load level. The increase in the axial load level decreased the dissipated energy by about 60% for both types of reinforcement.

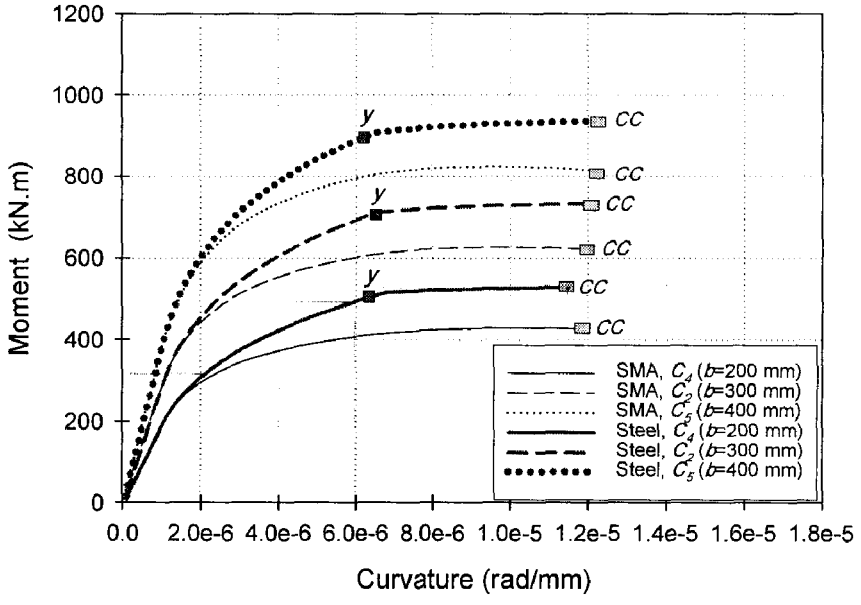

Figure 3-15: Effect of varying *b* on the *M-Φ* relationship (*ALI=0.3*)

3.6.3 Effect of tensile reinforcement ratio ρ

As shown in Figure 3-16 (*ALI*=0), a 200% increase in ρ increases the section capacity by 160% for both types of reinforcement. Although M_y increased with increasing ρ, the yielding curvature was slightly affected. The increase in ρ resulted in decreasing Φ_u. For lower reinforcement ratio (ρ=0.25%), the dissipated energy for SMA RC sections was 45% higher than that of steel RC sections since SMA bars exhibited extensive yielding. As ρ increased, the dissipated energy became higher for steel RC sections.

At higher levels of axial load, *ALI*=0.3, the effect of increasing ρ on increasing the section capacity is higher for steel RC sections, Figure 3-17. Increasing *ALI* from 0 to 0.3 increased the cracking moment by 320%. Failure occurred by crushing of concrete and

thus Φ_u was not affected. The dissipated energy for steel RC sections was 11% higher than SMA RC sections.

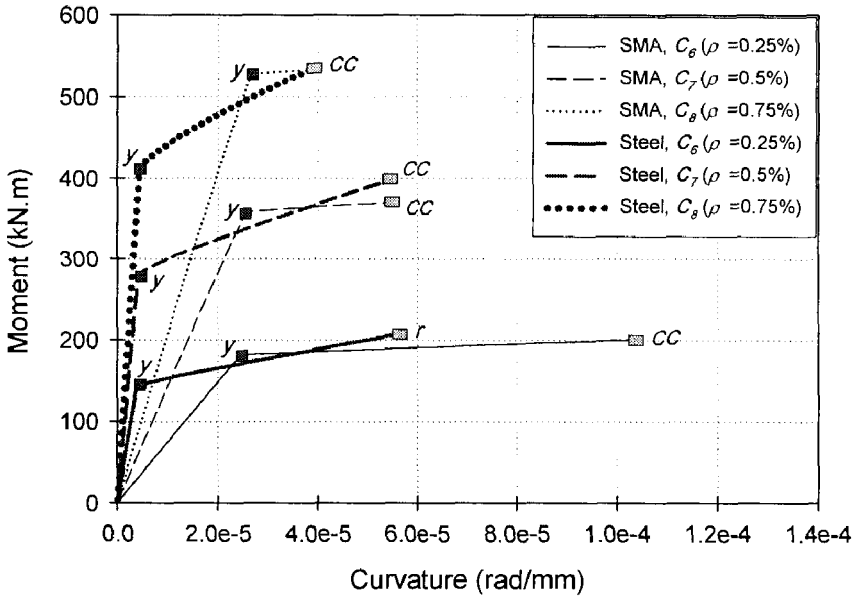

Figure 3-16: Effect of varying ρ on the *M-Φ* relationship (*ALI=0*)

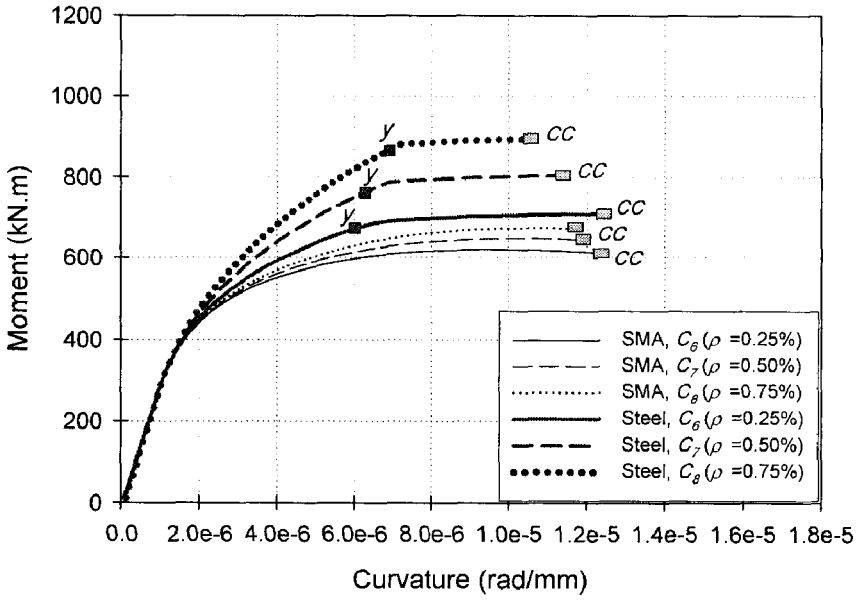

Figure 3-17: Effect of varying ρ on the *M-Φ* relationship (*ALI=0.3*)

3.6.4 Effect of compressive reinforcement ratio ρ'

Figure 3-18 represents the M-Φ relationship for SMA and steel RC sections for different values of ρ'. At ALI=0, ρ' has no effect on M_y, Φ_u, and M_u. Failure of steel RC sections occurred by rupture of steel. As the SMA bars exhibited higher yielding than that of the steel bars, the dissipated energy and section ultimate curvature Φ_u were higher for SMA RC sections than for steel RC ones.

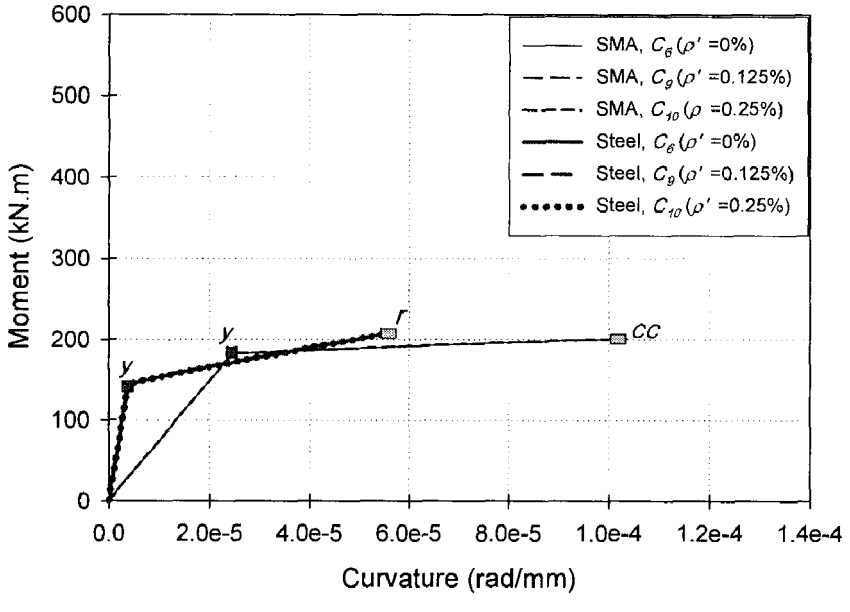

Figure 3-18: Effect of varying ρ' on the M-Φ relationship (ALI=0)

Increasing ALI from 0 to 0.3 resulted in higher section capacity for both types of reinforcement, Figure 3-19. ρ' was found to slightly affect the section capacity. M_y was also slightly affected for steel RC sections. SMA RC sections did not exhibit yielding at this level of axial load. Failure occurred by crushing of concrete for both SMA and steel RC sections. This type of failure resulted in almost equal Φ_u for the analyzed sections.

The dissipated energy for steel RC sections was 12% to 23% higher than SMA RC sections.

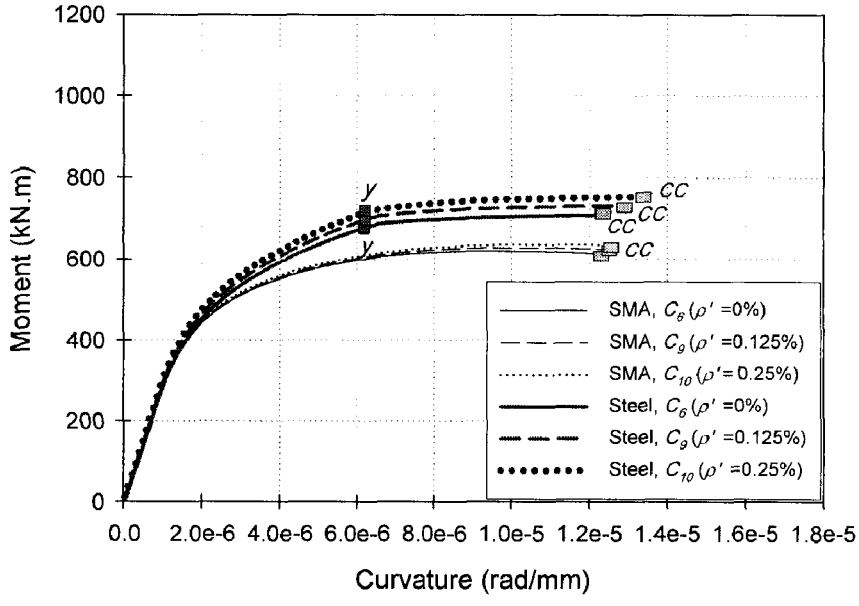

Figure 3-19: Effect of varying ρ' on the *M-Φ* relationship (*ALI=0.3*)

3.6.5 Effect of concrete compressive strength f_c'

At *ALI*=0, Figure 3-20, increasing f_c' from 20 to 40 MPa did not notably affect M_y or M_u for both types of reinforcement. For steel RC sections, failure occurred by rupture of steel bars and thus Φ_u was almost constant. However, for SMA RC sections, Φ_u increased by 90% with the increase of f_c' . At f_c'=60 MPa, the yielding plateau of SMA bars was followed by a strain hardening behaviour resulting in a substantial increase in section capacity and ductility.

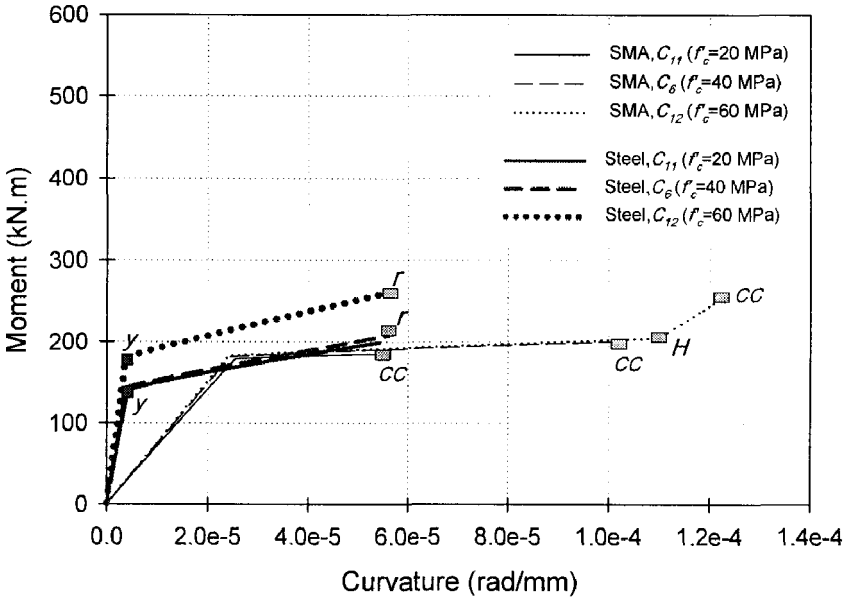

Figure 3-20: Effect of varying f_c' on the *M-Φ* relationship (*ALI=0*)

At *ALI*=0.3, Figure 3-21, the cracking and ultimate moments for both types of reinforcement increased by 160% to 180%. Increasing f_c' from 20 MPa to 60 MPa resulted in an increase of 155% in the yielding moment of steel RC sections. SMA bars did not yield at this level of axial load. Φ_u was comparable for SMA and steel RC sections since failure occurred by crushing of concrete.

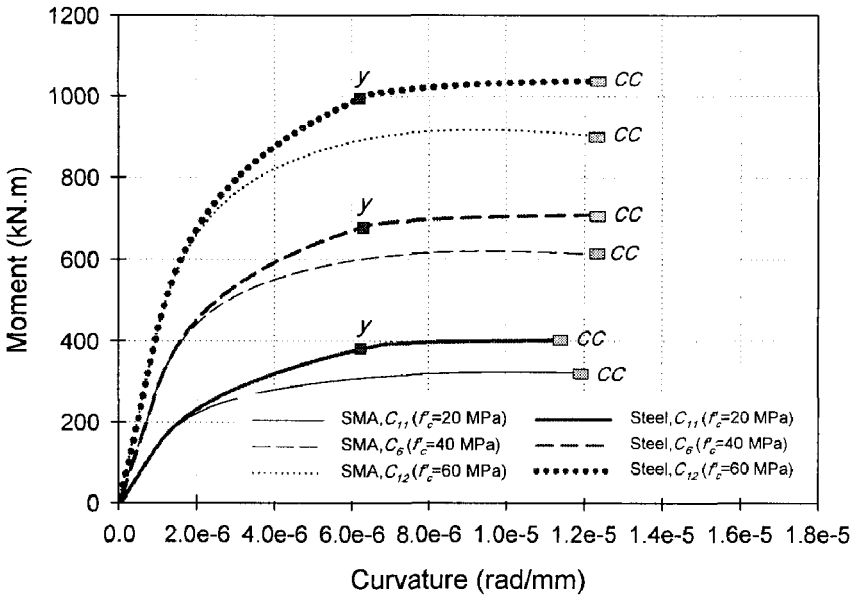

Figure 3-21: Effect of varying f_c' on the M-Φ relationship (ALI=0.3)

3.7 Normalized interaction diagrams

As mentioned earlier, the M-Φ analysis was conducted at different ALI. The obtained values for M_u at different ALI were used to develop the axial load-moment interaction diagrams that are shown in Figures 3-22 to 3-26. For each analyzed section, $\varepsilon_{c\text{-}max}$ and Φ_{max} corresponding to the peak moment M_u were identified.

The point at which the interaction diagrams of steel RC sections change the sign of their slope is known as the balance point. It is the point at which steel yields ($\varepsilon_{y\text{-}s}$=0.0022) simultaneously with concrete reaching its crushing strain (ε_{cu}=0.0035). For the analyzed sections, the balance point occurred at an axial load level ALI ranging from 0.3 to 0.5. The difference in the stress-strain relationship between steel and SMA resulted in a different behaviour for SMA RC sections. The point at which the curve changed the sign

of its slope was not related to yielding of SMA bars. It occurred at an axial load level close to that for steel RC sections (*ALI*=0.3 to 0.5). At this point, SMA bars did not yield and $\varepsilon_{c\text{-}max}$ varied from 0.00261 to 0.0031.

3.7.1 Effect of section height *h*

Figure 3-22 illustrates the effect of varying *h* on the interaction diagrams. The pure flexural capacity $\left[\frac{P}{A_g} = 0\right]$ was the most affected point. As the axial load level increased on the section, the effect of varying *h* on section capacity decreased. The pure axial capacity was slightly higher (3%) for SMA RC sections than for the steel ones because of the higher yielding stress of the SMA bars. This increase was noticed for all other cases.

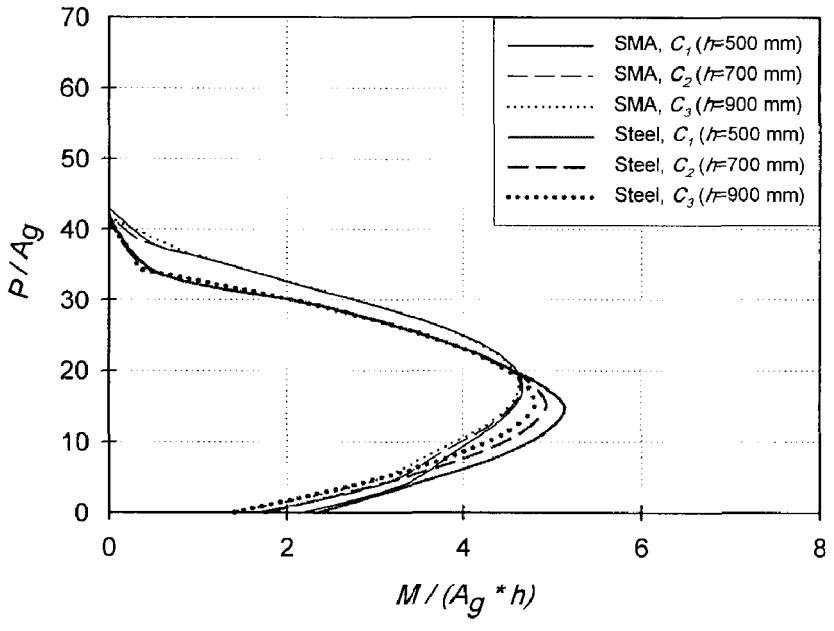

Figure 3-22: Effect of varying *h* on the normalized interaction diagram

3.7.2 Effect of section width *b*

As shown in Figure 3-23, varying *b* has a clear effect on the interaction diagram for both steel and SMA reinforcement. The pure flexural capacity, where the axial load is zero, changed by about 50% when *b* increased from 200 mm to 400 mm. Varying *b* from 200 mm to 300 mm did not affect the interaction diagrams at high levels of axial load (*ALI* > 0.5). However, increasing *b* from 300 mm to 400 mm results in a clear effect on section capacity at all levels of axial load.

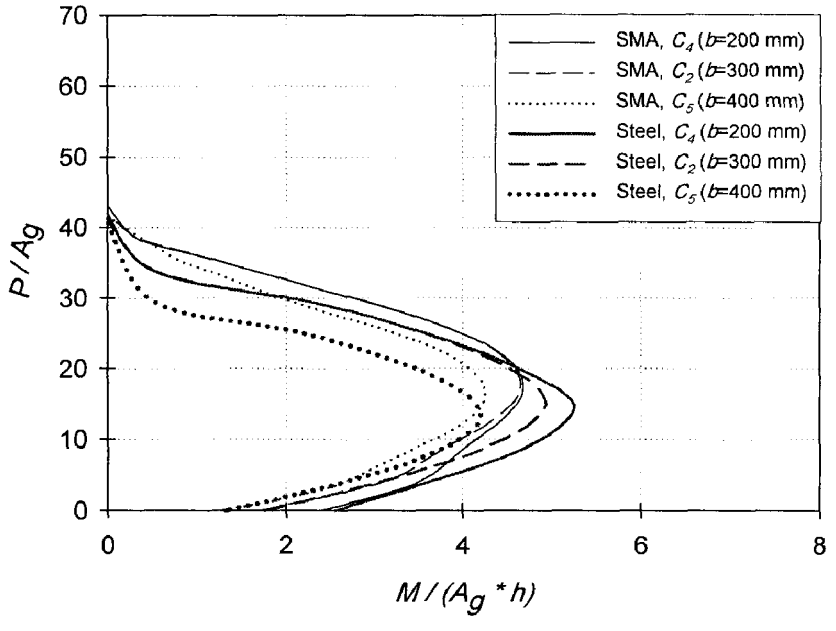

Figure 3-23: Effect of varying *b* on the normalized interaction diagram

3.7.3 Effect of tensile reinforcement ratio ρ

The interaction diagrams shown in Figure 3-24 represent the effect of varying ρ on the section capacity. At low levels of axial loads (*ALI* < 0.4), increasing the reinforcement

ratio ρ from 0.25% to 0.75% resulted in a significant increase (140% for steel- 165% for SMA) in section capacity. For $ALI > 0.4$, the effect of increasing ρ was reduced as failure was governed by crushing of concrete rather than rupture of steel.

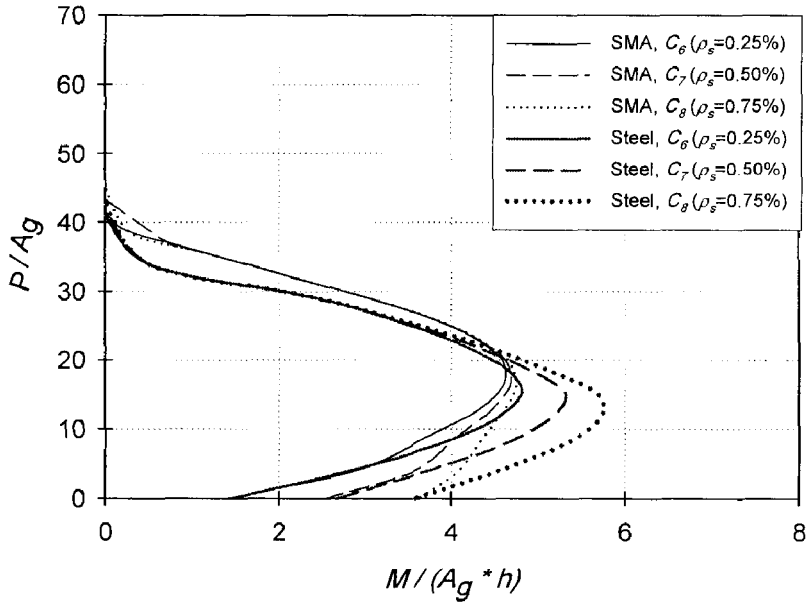

Figure 3-24: Effect of varying ρ on the normalized interaction diagram

3.7.4 Effect of compressive reinforcement ratio ρ'

As shown in Figure 3-25, the interaction diagrams for steel RC sections were affected more by varying ρ' than SMA RC sections. The pure flexural capacity was not affected significantly by varying the reinforcement ratio ρ' for both steel and SMA reinforcement. At $ALI = 0.4$, the capacity of steel RC sections increased by 11% as ρ' increased from 0 to 0.25%.

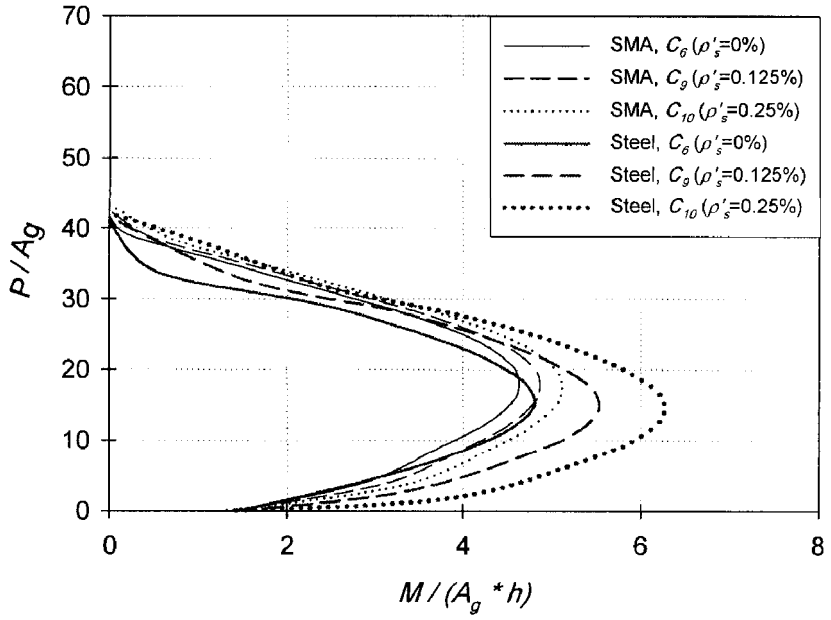

Figure 3-25: Effect of varying ρ' on the normalized interaction diagram

3.7.5 Effect of concrete compressive strength f_c'

It can be observed from Figure 3-26 that increasing f_c' significantly increases the section capacity. The pure flexural capacity increased by 35% by changing f_c' from 20 MPa to 60 MPa, and the section capacity at higher axial load levels (i.e. ALI = 0.4) drastically increased (195%). The pure axial capacity (M=0) also increased significantly (185%) with increase in f_c' of 200%.

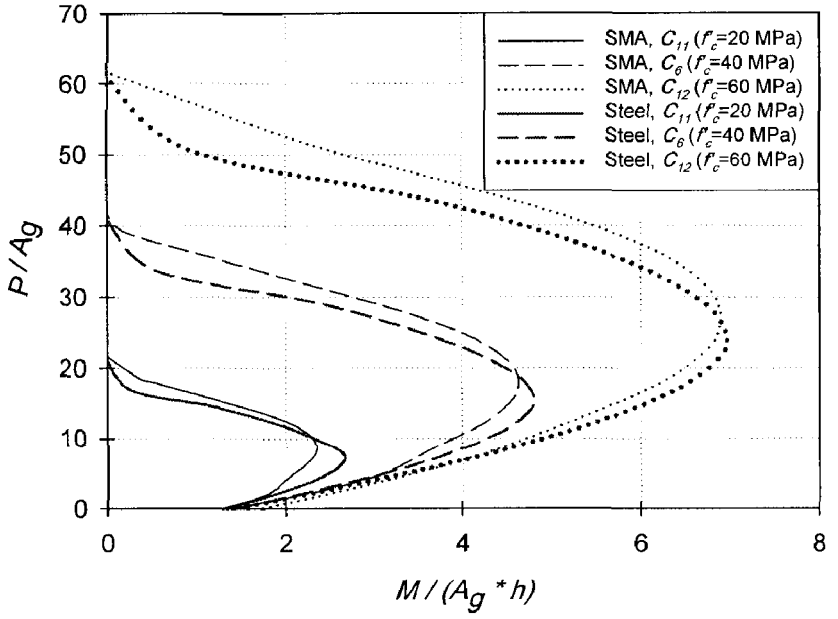

Figure 3-26: Effect of varying f_c' on the normalized interaction diagram

3.8 Rectangular stress block parameters

Building codes provide engineers with equivalent stress block parameters α_1 and β_1 to simplify the design process. The use of α_1, and β_1 allows calculating the concrete compressive force and its location. A23.3 (2004) equations for calculating α_1, and β_1, Equation [3-1], are dependent on f_c' to account for the difference in behaviour of high strength concrete (f_c' > 60 MPa).

In this section, and for each of the analyzed sections, α_1 and β_1 were calculated from the known strain distribution at the peak moments. Figure 3-27 shows a flow chart for the developed program for α_1 and β_1 calculations. As shown in the figure, the compressive force in concrete C_c and its point of application are evaluated by calculating the area under the stress-strain relationship of concrete corresponding to the known $\varepsilon_{c\text{-}max}$, and

Φ_{max}, and its centroid. The stress block parameters are then found such that they result in the same area and same location of the centroid. In addition, the Canadian code recommended values have been judged for steel RC sections.

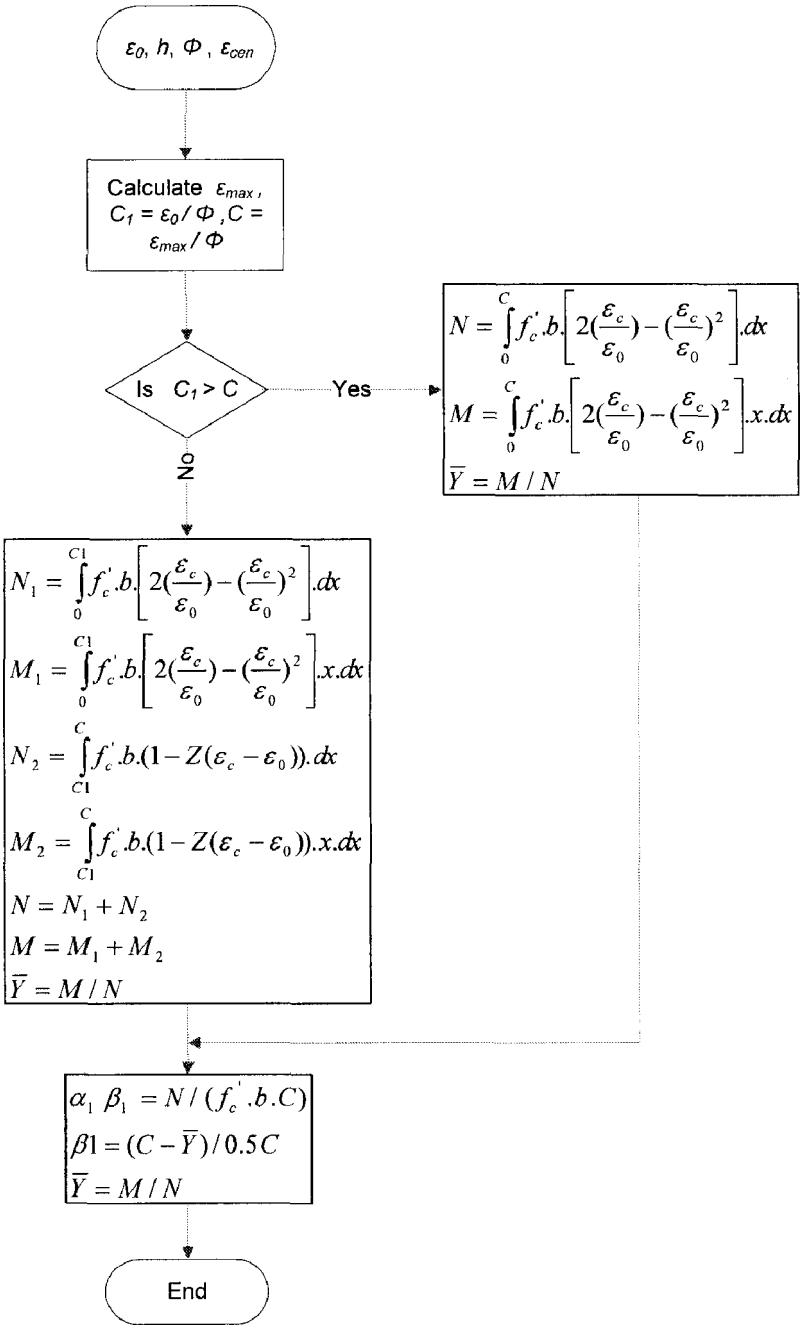

Figure 3-27: Flow chart for the stress block parameters calculations

3.8.1 Steel RC sections

Figure 3-28 shows the variation of $\varepsilon_{c\text{-}max}$ with the axial load level for steel RC sections. At $ALI = 0$, failure occurred in some of the considered sections by rupture of the reinforcement, before $\varepsilon_{c\text{-}max}$ reaches its limit of 0.0035. As a result, $\varepsilon_{c\text{-}max}$ varied between 0.0020 and 0.0035. For $ALI \leq 0.1$, the failure occurred at $\varepsilon_{c\text{-}max} = 0.0035$. $\varepsilon_{c\text{-}max}$ started to decrease with ALI increase approaching a value of 0.002 at $ALI = 1.0$. This behaviour is similar to the recommendation of the Eurocode (Beeby and Narayanan 2005) where the value for the limiting concrete compressive strain is a function of the load eccentricity. A value of 0.0035 is recommended for flexural and for combined bending and axial load where the neutral axis remains within the section. For other sections (neutral axis outside the section), a value between 0.0035 and 0.002 is to be used.

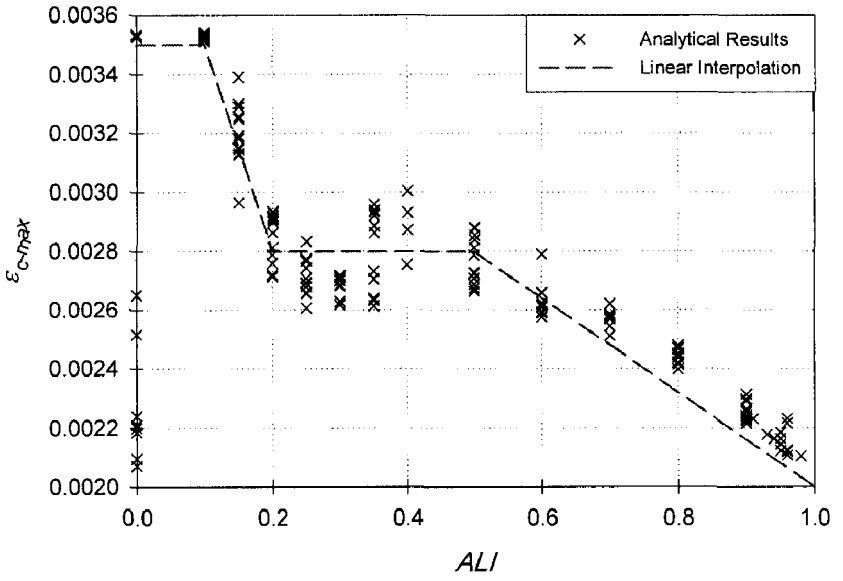

Figure 3-28: $\varepsilon_{c\text{-}max} - ALI$ relationship for Steel RC sections

From the parametric study conducted in this chapter, it is recommended to calculate $\varepsilon_{c\text{-}max}$ as a function of *ALI*. $\varepsilon_{c\text{-}max}$ can be assumed equal to 0.0035 for $ALI \leq 0.1$, 0.0028 for $0.2 \leq ALI \leq 0.5$, and 0.002 for $ALI = 1.0$. A linear interpolation can be used for different *ALI* values. The recommended values for $\varepsilon_{c\text{-}max}$ are shown on Figure 3-28.

Figure 3-29 and Figure 3-30 show the variation of α_1 and β_1 with $\varepsilon_{c\text{-}max}$. α_1 is found to approach a value of 1.0 at $\varepsilon_{c\text{-}max}$ of 0.002 (pure axial load). Based on the analytical results, two Equations [3-6] and [3-7] were developed to calculate α_1, and β_1 based on $\varepsilon_{c\text{-}max}$. The predictions of these equations are shown in Figure 3-29 and Figure 3-30.

$$\alpha_1 = 88.36\times10^{3}\ \varepsilon_{c-\max}^{2} - 552.4\ \varepsilon_{c-\max} + 1.750 \qquad 0.002 \leq \varepsilon_{c-\max} \leq 0.00275 \quad [3\text{-}6a]$$

$$\alpha_1 = -33.54\times10^{3}\ \varepsilon_{c-\max}^{2} + 150.7\ \varepsilon_{c-\max} + 750.0\times10^{-3} \qquad 0.00275 \leq \varepsilon_{c-\max} \leq 0.0035 \quad [3\text{-}6b]$$

$$\beta_1 = -1630\times10^{3}\ \varepsilon_{c-\max}^{2} + 8388\ \varepsilon_{c-\max} - 10.00 \qquad 0.002 \leq \varepsilon_{c-\max} \leq 0.00275 \quad [3\text{-}7a]$$

$$\beta_1 = -5513\ \varepsilon_{c-\max}^{2} + 114.1\ \varepsilon_{c-\max} + 540.0\times10^{-3} \qquad 0.00275 \leq \varepsilon_{c-\max} \leq 0.0035 \quad [3\text{-}7b]$$

The capacity of the analyzed sections were calculated based on the values of $\varepsilon_{c\text{-}max}$, α_1, and β_1 recommended in the previous sections and based on A23.3 (2004) recommended values. Figure 3-31 shows a comparison of the calculated values and the exact values obtained using the *M-Φ* analysis. The proposed values resulted in very good agreement, maximum error equal to 5%. The recommended values by A23.3 (2004) were found to significantly underestimate the section capacity at high levels of axial load.

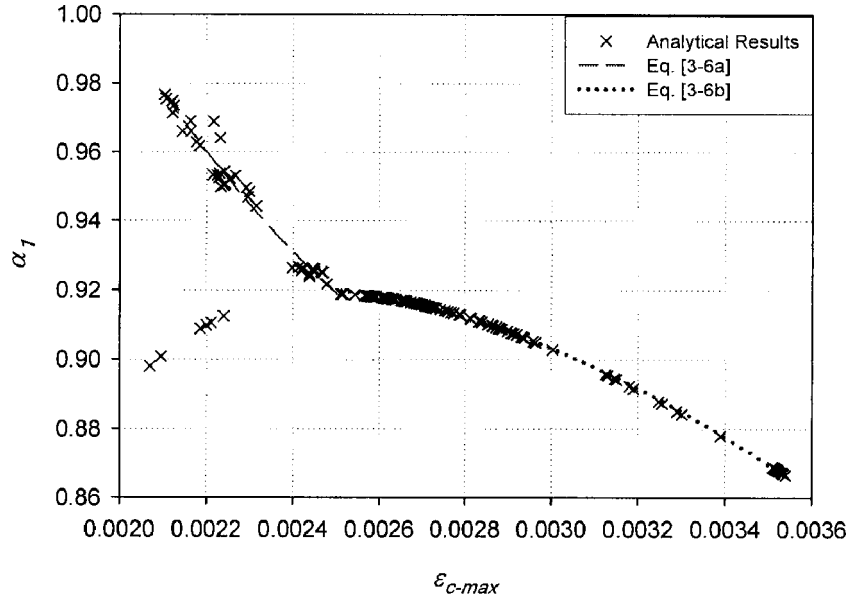

Figure 3-29: $\alpha_1 - \varepsilon_{c\text{-}max}$ relationship for Steel RC sections

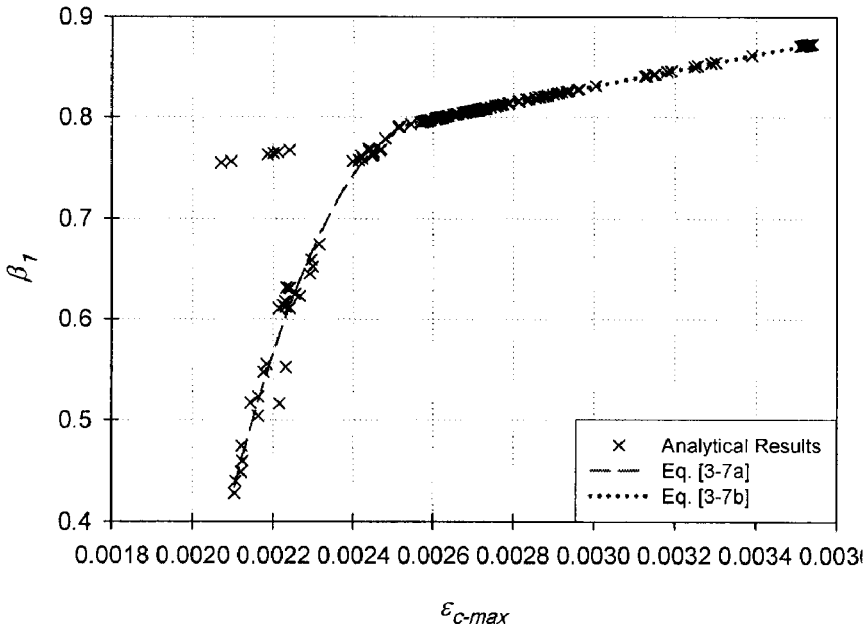

Figure 3-30: $\beta_1 - \varepsilon_{c\text{-}max}$ relationship for Steel RC sections

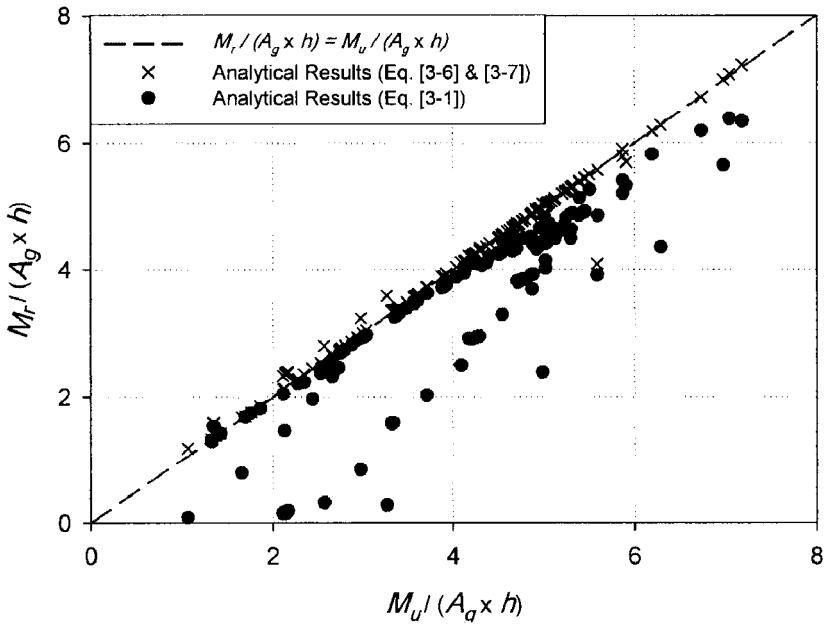

Figure 3-31: $M_r / (A_g \times h) - M_u / (A_g \times h)$ relationship for Steel RC sections

3.8.2 SMA RC sections

For SMA RC sections, $\varepsilon_{c\text{-}max}$ is found to be dependent on the axial load level *ALI* as shown in Figure 3-32. It is recommended to assume $\varepsilon_{c\text{-}max}$ equal to 0.0035 for $ALI \leq 0.2$, 0.00275 for $ALI = 0.4$, 0.00255 for $ALI = 0.6$, and 0.002 for $ALI = 1.0$. A linear interpolation can be used for different *ALI* values.

Figure 3-33 and Figure 3-34 show the variation of α_1 and β_1 with $\varepsilon_{c\text{-}max}$. Based on these figures, Equations [3-8] and [3-9] were developed to calculate α_1 and β_1. The square value of the coefficient of determination, R^2, corresponding to these equations ranges between 0.9922 and 0.9999.

$$\alpha_1 = 182.7\times10^3\ \varepsilon_{c-\max}^2 - 982.1\,\varepsilon_{c-\max} + 2.240 \qquad 0.002 \le \varepsilon_{c-\max} \le 0.00275 \quad [3\text{-}8a]$$

$$\alpha_1 = -24.62\times10^3\ \varepsilon_{c-\max}^2 + 94.05\,\varepsilon_{c-\max} + 840.0\times10^{-3} \qquad 0.00275 \le \varepsilon_{c-\max} \le 0.0035 \quad [3\text{-}8b]$$

$$\beta_1 = -1477\times10^3\ \varepsilon_{c-\max}^2 + 7719\,\varepsilon_{c-\max} - 9.280 \qquad 0.002 \le \varepsilon_{c-\max} \le 0.00275 \quad [3\text{-}9a]$$

$$\beta_1 = -5867\,\varepsilon_{c-\max}^2 + 116.4\,\varepsilon_{c-\max} + 540.0\times10^{-3} \qquad 0.00275 \le \varepsilon_{c-\max} \le 0.0035 \quad [3\text{-}9b]$$

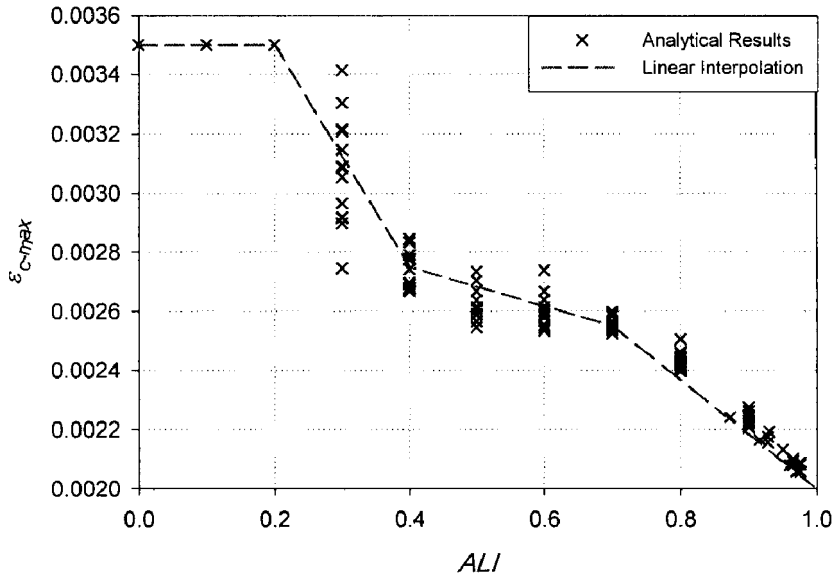

Figure 3-32: $\varepsilon_{c\text{-}max} - ALI$ relationship for SMA RC sections

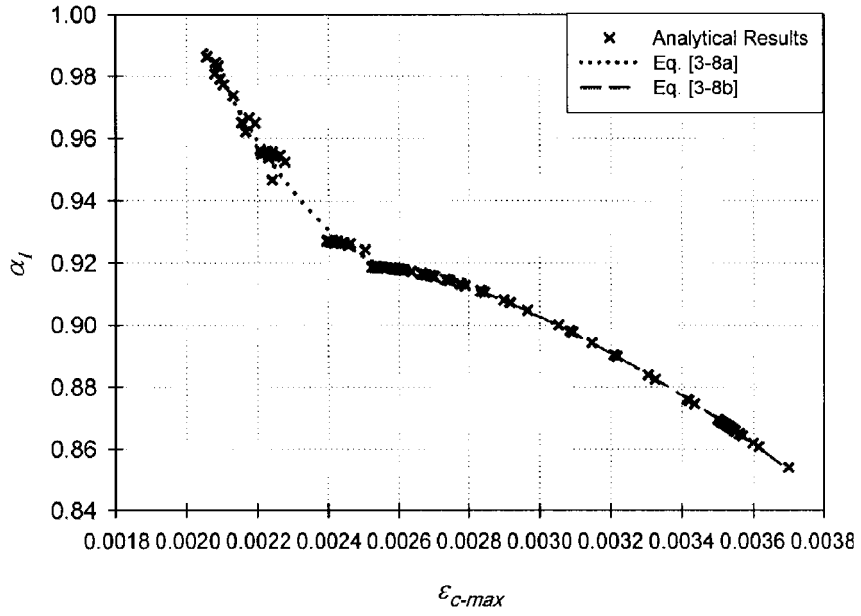

Figure 3-33: $\alpha_1 - \varepsilon_{c\text{-}max}$ relationship for SMA RC sections

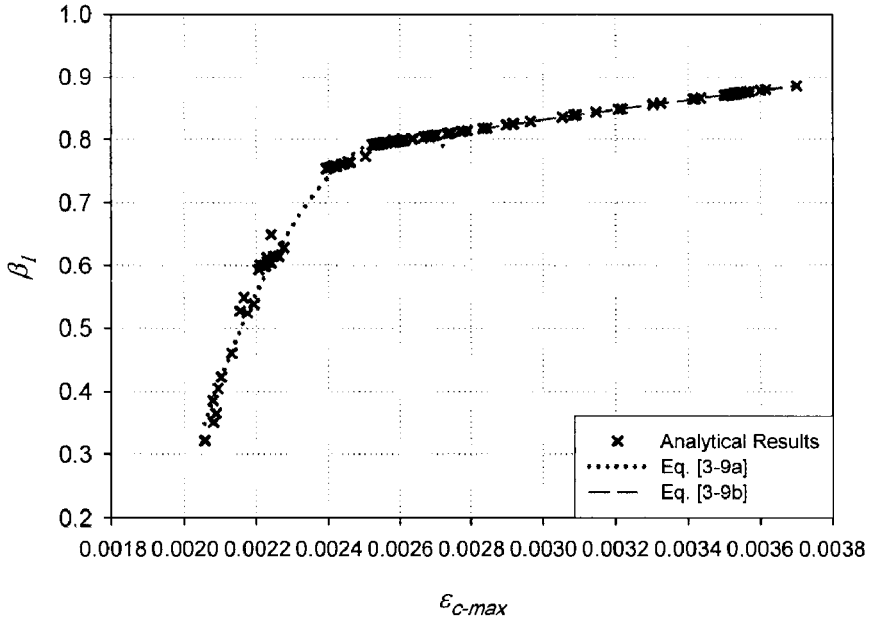

Figure 3-34: $\beta_1 - \varepsilon_{c\text{-}max}$ relationship for SMA RC sections

The accuracy of the estimated values for $\varepsilon_{c\text{-}max}$, α_1, and β_1 was checked by calculating the capacity based on the proposed values (Equations [3-8] and [3-9]). Figure 3-35 shows the relationship between the normalized ultimate moment M_u obtained from the M-Φ analysis versus the normalized moment M_r obtained based on the recommended values of $\varepsilon_{c\text{-}max}$, α_1, and β_1. The maximum error in M_r is 2% for $ALI < 0.5$, and 6% for $0.6 \leq ALI \leq 0.9$. The error for sections with compression reinforcement was higher. The normalized moment M_{code} calculated based on the recommended values by A23.3 (2004) were also plotted versus the normalized ultimate moment M_u obtained from the M-Φ analysis, Figure 3-35. A23.3 (2004) recommended values were found to be conservative in calculating the section capacity at all levels of axial load. At high ALI, A23.3 (2004) recommended values were found to significantly underestimate the section capacity.

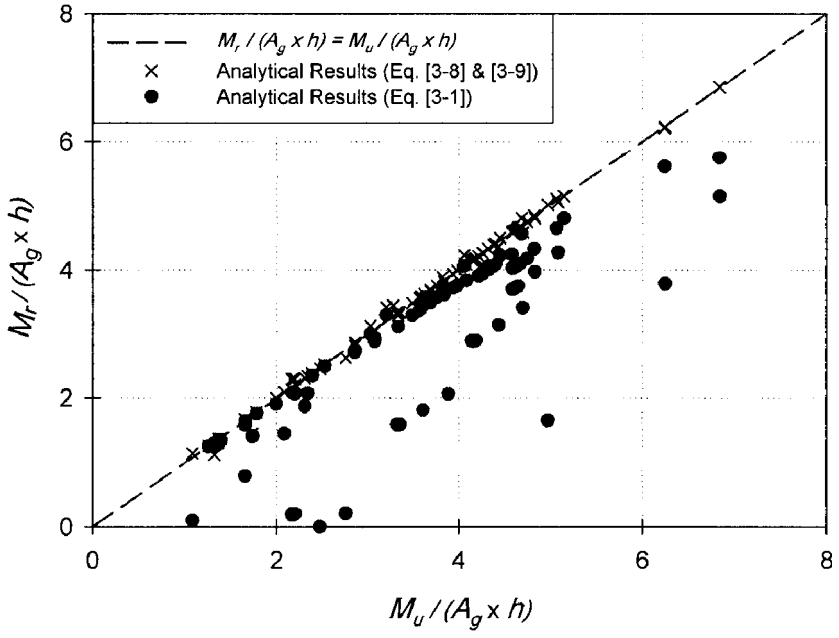

Figure 3-35: $M_r / (A_g \times h) - M_u / (A_g \times h)$ relationship for SMA RC sections

3.9 Summary and conclusions

This study investigates the flexural behaviour of SMA RC sections as compared to steel RC sections. The accuracy of using sectional analysis for SMA RC sections was validated by comparing analytical predictions and experimental results for three simply supported beams. Sectional analysis was modified to account for the test setup that included using external unbonded SMA bars.

A number of steel and SMA RC sections were then chosen. Variables were section height and width, tensile and compressive reinforcement ratios, concrete compressive strength, and axial load level. For each section, the M-Φ relationship was established and used to evaluate the moment capacity M_u and the corresponding curvature Φ_{max} and maximum concrete strain $\varepsilon_{c\text{-}max}$. Based on the obtained results, the following conclusions can be drawn.

3.9.1 Moment-curvature relationship

At $ALI = 0$, SMA RC sections have lower initial stiffness than steel RC sections. The difference in the initial stiffness vanishes for higher ALI as the axial load delays cracking of the section. Although SMA bars did not yield at $ALI > 0.2$, SMA RC sections dissipated comparable energy to steel RC sections. Upon cracking of concrete, the reduced stiffness of SMA sections enabled dissipating this energy.

Steel RC sections failed by rupture of steel bars or concrete crushing at low axial load levels and by concrete crushing at high ALI. SMA RC sections failed by concrete

crushing rather than rupture of SMA bars because of their high tensile strain. For higher concrete compressive strength, sections with low area of SMA bars exhibited a strain hardening following the initial yielding. This behaviour might not be acceptable as the strain in the SMA bars exceeded their recovery strain, which defeat the purpose of using them.

3.9.2 Normal force-moment interaction diagrams

The change in the sign of the slope of steel RC interaction diagrams happens at the balanced moment. This point is defined as the point at which the steel yields in tension and the concrete crushes in compression. For SMA RC sections, the point at which the sign of the slope changes is not related to yielding of SMA bars. It happens as a result of the change in the maximum concrete strain and the compression zone height. It was also observed that the pure axial capacity of SMA RC sections is higher than that of steel RC sections due to the higher yield stress for SMA bars.

3.9.3 Stress block parameters

The maximum concrete strain $\varepsilon_{c\text{-}max}$ for steel RC sections was found to be equal to 0.0035 for *ALI* between 0 and 0.1. This correlates well with the Canadian standards. However, for *ALI* = 0, $\varepsilon_{c\text{-}max}$ was found to deviate from this value because of the change in the failure mode from compression failure to reinforcement rupture. This change was discussed by other researchers and found to have minor effect on the calculations of the moment capacity. Another deviation was observed at *ALI* exceeding 0.1. It is proposed to

assume $\varepsilon_{c\text{-}max}$ equal to 0.0035 for $ALI \leq 0.1$, 0.0028 for $0.2 \leq ALI \leq 0.5$, and 0.002 for $ALI = 1.0$. A linear interpolation can be used for different ALI values. The corresponding values for α_1, and β_1 are proposed.

For SMA RC sections, it was found that $\varepsilon_{c\text{-}max}$ can be assumed 0.0035 for $ALI \leq 0.2$, 0.00275 for $ALI = 0.4$, 0.00255 for $ALI = 0.6$, and 0.002 for $ALI = 1.0$. For other ALI values, $\varepsilon_{c\text{-}max}$ is proposed to be evaluated by linear interpolation. Two equations were developed to calculate α_1, and β_1 for SMA RC sections.

The accuracy of the proposed values of $\varepsilon_{c\text{-}max}$, α_1, and β_1 for steel and SMA RC sections was validated by comparing the moment capacity calculated based on these parameters and that obtained from the moment-curvature relationships. The equations provided good estimates of the moment capacity and were found to be superior to the equations proposed by the Canadian code.

3.10 References

Alam M.S., Youssef M.A., Nehdi, M. (2007). "Utilizing shape memory alloys to enhance the performance and safety of civil infrastructure: a review." Canadian Journal of Civil Engineering, 34(9), 1075-1086.

Ayoub, C., Saiidi, M., and Itani, A. A study of shape-memory alloy-reinforced beams and cubes. *Rep. No. CCEER-03-7*, Center for Civil Engineering Earthquake Research, Dept. of Civil Engineering, Univ. of Nevada, Reno, Nevada.

Beeby, A.W., and Narayanan, R.S. (2005). Designers' guide to EN 1992-1-1 and EN 1992-1-2 : Eurocode 2: design of concrete structures : general rules and rules for buildings and structural fire design. Thomas Telford, London.

CSA A23.3 (2004). Design of concrete structures. Canadian Standards Association, Rexdale, Ontario, Canada, 240 pages.

DesRoches, R., and Smith, B. (2004). "Shape memory alloys in seismic resistant design and retrofit: a critical review of their potential and limitations." Journal of Earthquake Engineering, 8, 415-429.

DesRoches, R., McCormick, J., and Delemont, M. (2004). "Cyclic properties of superelastic shape memory alloy wires and bars." ASCE, Journal of Structural Engineering, 130(1), 38-46.

Liu, Y., Xie, Z., Humbeeck, J.V. and Delaey, L. (1998). "Asymmetry of stress–strain curves under tension and compression for NiTi shape memory alloys." Acta Materialia, 46(12), 4325-4338.

Manach, P.-Y., and Favier, D. (1997). "Shear and tensile thermomechanical behavior of near equiatomic NiTi alloy." Materials Science & Engineering A: Structural Materials: Properties, Microstructure and Processing, A222: 45-57.

Orgeas, L., and Favier, D. (1995). "Non-symmetric tension-compression behavior of NiTi alloy." Journal De Physique, IV: JP 5(8), 605-610.

Otsuka, K. and Wayman, C.M. (1999). Shape memory materials. 1st Paperback Edition, Cambridge University Press, Cambridge.

Ozbakkalogln T., and Saatcioglu M. (2004). "Rectangular Stress Block for High-Strength Concrete." ACI Structural Journal, 101(4), 475 - 483.

Park R., Paulay T. (1975). Reinforced concrete structures. John Wiley & sons, New York.

Saiidi, M. S., Sadrossadat-Zadeh, M., Ayoub, C., Itani, A. (2007). "Pilot Study of Behavior of Concrete Beams Reinforced with Shape Memory Alloys." ASCE, Journal of Materials in Civil Engineering, 19(6), 454-461.

Scott, B.D.; Park, R.; and Priestley, M.J.N. (1982). "Stress-strain behavior of concrete confined by overlapping hoops at low and high strain rates." ACI journal, 79(1), 13-27.

Song, G., Ma, N., and Li, H.-N. (2006). "Application of shape memory alloys in civil structures." Engineering Structures, 28, 1266-1274.

Wilson, J.C. and Wesolowsky, M.J. (2005). "Shape memory alloys for seismic response modification: A state-of-the-art review." Earthquake Spectra, 21, 569-601.

Youssef, M.A., and Rahman, M. (2007). "Simplified seismic modeling of reinforced concrete flexural members." Magazine of Concrete Research, 59(9), 639-649.

Zak, A.J., Cartmell, M.P., Ostachowicz, W.M. and Wiercigroch, M. (2003). "One-dimensional shape memory alloy models for use with reinforced composite structures." Smart Materials and Structures, 12(3), 338-346.

Chapter 4 Deflection of Shape Memory Alloy Reinforced Concrete Beams: Assessment of Existing Models

4.1 Introduction

The unique properties of shape memory alloys (SMAs) can be utilized to achieve smart structures that can adjust their properties according to the applied loading. The potential of using SMA in civil engineering applications is increasing. These applications include using SMA as bracing members in frames (Mazzolani et al. 2004), prestressing tendons for concrete elements (Maji and Negret 1998, El-Tawil and Ortega-Rosales 2004), anchors for columns (Tamai et al. 2003), damping devices (Clark et al. 1995, Krumme et al. 1995), bridge restrainers (DesRoches and Delemont 2002), and primary reinforcement for concrete structures (Elbahy et al. 2008, Saiidi et al. 2007).

The design of any structure must generally satisfy two basic design criteria; strength and serviceability. While the strength criteria allow the structure to safely support the design loads for its specified service life, serviceability requirements ensure satisfactory operation during its service life. These serviceability requirements include limits on allowable deflection. Excessive deflection is often perceived usually as failure. In addition, excessive deflection in concrete beams and slabs can lead to cracking of structural and non-structural elements.

In this chapter, moment-curvature analysis will be utilized to calculate the deflection of SMA-reinforced concrete (RC) members. The effect of cross-section dimensions, reinforcement ratio, concrete compressive strength, and modulus of elasticity of SMA are evaluated. This parametric study is also used to check the validity of available models for predicting the deflection of SMA RC elements.

4.2 Deflection of steel-reinforced concrete members

The availability of high-strength materials (e.g. concrete and steel) resulted in the development of structural elements having small cross-sections and design being controlled by deflection. Two methodologies are available in design standards to control the deflection of structural elements; (1) limiting the member span-to-depth ratio, and (2) ensuring that the calculated deflections do not exceed specified limits. The Canadian standards CSA-A23.3-04 (2004) use the equation proposed by Branson (1963), Equation [4-1], to estimate the effective moment of inertia, I_e, of structural members. This equation represents a gradual transition from the un-cracked cross-section inertia, I_g, to the cracked moment of inertia, I_{cr}, based on the ratio of the applied moment, M_a, to the cracking moment, M_{cr}.

$$I_e = \left(\frac{M_{cr}}{M_a}\right)^3 I_g + \left[1 - \left(\frac{M_{cr}}{M_a}\right)^3\right] I_{cr} \qquad \leq I_g \qquad [4\text{-}1]$$

Branson's equation is empirical and is based on test results for steel RC beams having a reinforcement ratio between 1% and 2%. Scanlon et al. (2001) and Gilbert (2006) have

shown that this equation underestimates the deflection of lightly reinforced concrete members.

The validity of using Branson's Equation for SMA RC members needs to be assessed. The relatively low modulus of elasticity of SMA when compared to steel and its characteristic stress-strain relationship are expected to significantly affect the section stiffness after cracking. The experimental work done by Youssef et al. (2008) illustrating the advantages of using SMAs in critical regions of beam-column joints is utilized in this chapter to validate the adopted calculation method.

4.3 Materials models and sectional analysis

4.3.1 Concrete stress-strain model

The behaviour of concrete in compression was assumed to follow the stress-strain model of Kent and Park (1971) that was later extended by Scott et al. (1982). Although relatively more accurate and complex models have been introduced (for instance Stevens et al. (1987), Sittipunt and Wood (1993)), the Scott et al. (1982) model offers a good balance between simplicity and accuracy. The model (Equation [4-2]) describes the concrete behaviour in compression by three stages as shown in Figure 4-1-(a). A value of 0.0035 was assigned to the ultimate concrete strain, ε_{cu}, where the concrete is assumed to disintegrate (CSA-A23.3-04 2004).

$$f_c = f_c'\left[2.0\left(\frac{\varepsilon_c}{0.002}\right)-\left(\frac{\varepsilon_c}{0.002}\right)^2\right] \qquad 0 \le \varepsilon_c \le 0.002 \qquad \text{[4-2a]}$$

$$f_c = f_c'[1 - Z(\varepsilon_c - 0.002)] \qquad \varepsilon_c \geq 0.002 \quad and \quad f_c \geq 0.2 f_c' \qquad [4\text{-}2b]$$

$$Z = \frac{0.5}{\frac{3 + 0.29 f_c'(\text{MPa})}{145 f_c'(\text{MPa}) - 1000} - 0.002} \qquad [4\text{-}2c]$$

Where: f_c = concrete compressive stress, Z = slope of compressive strain softening branch, ε_c = concrete compressive strain.

The model of Stevens et al. (1987) was utilized to describe the concrete tensile behaviour. As shown in Figure 4-1-(b), the concrete is assumed to behave linearly until reaching the cracking stress, f_{cr}. Once the concrete cracks, the softening branch given by Stevens et al. (1987), Equation [4-3], is used to describe the post-cracking behaviour of concrete. The simplification proposed by Youssef and Ghobarah (1999) involving eliminating the effect of the amount of reinforcement and its inclination is adopted.

$$f_t = f_{cr}\left[0.95 \text{ x } e^{-1000 \text{ x } (\varepsilon_c - \varepsilon_{cr})} + 0.05\right] \qquad \varepsilon_c \geq \varepsilon_{cr} \qquad [4\text{-}3]$$

4.3.2 SMA stress-strain model

The stress-strain relationship of Ni-Ti (Nickel-Titanium based SMA) consists of four linear branches that are connected by smooth curves (Alam et al. 2007). To simplify the modeling process, these smooth curves are ignored and the linear branches are assumed to intersect, Figure 4-1-(c). The Ni-Ti alloy behaves elastically with a modulus of elasticity $E_{y\text{-}SMA}$ until reaching the first yielding stress $f_{y\text{-}SMA}$, which represents the start of

the martensite stress induced transformation. Once the strain, ε_{SMA} exceeds the first yielding strain, $\varepsilon_{y\text{-}SMA}$, the modulus of elasticity is significantly reduced to about 10% to 15% of $E_{y\text{-}SMA}$. For strains above that induced by the maximum recovery stress ε_{p1}, the material regains part of its stiffness because of the phase transformation. The new modulus of elasticity, E_{p2} reaches about 50% to 60% of $E_{y\text{-}SMA}$. The last linear branch starts at the real yielding of the Ni-Ti. The material softens again and the modulus of elasticity $E_{u\text{-}SMA}$ reaches a value as low as 3% to 8% of $E_{y\text{-}SMA}$. The model is represented by Equation [4-4].

$$f_{SMA} = E_{y-SMA}\ \varepsilon_{SMA} \qquad \varepsilon_{y-SMA} \leq \varepsilon_{SMA} \leq \varepsilon_{p1} \qquad [4\text{-}4a]$$

$$f_{SMA} = f_{y-SMA} + E_{p1}\left(\varepsilon_{SMA} - \varepsilon_{y-SMA}\right) \qquad \varepsilon_{y-SMA} \leq \varepsilon_{SMA} \leq \varepsilon_{p1} \qquad [4\text{-}4b]$$

$$f_{SMA} = f_{p1} + E_{p2}\left(\varepsilon_{SMA} - \varepsilon_{p1}\right) \qquad \varepsilon_{p1} \leq \varepsilon_{SMA} \leq \varepsilon_{p2} \qquad [4\text{-}4c]$$

$$f_{SMA} = f_{p2} + E_{u-SMA}\left(\varepsilon_{SMA} - \varepsilon_{p2}\right) \qquad \varepsilon_{p2} \leq \varepsilon_{SMA} \leq \varepsilon_{u-SMA} \qquad [4\text{-}4d]$$

Where: f_{SMA} = SMA stress, f_{p1} = maximum recovery stress, $f_{y\text{-}SMA}$ = first SMA yielding stress, $\varepsilon_{y\text{-}SMA}$ = first SMA yielding strain, and $\varepsilon_{u\text{-}SMA}$ = SMA strain at failure.

4.3.3 Sectional analysis

Moment-curvature analysis was conducted based on the fibre model methodology (Youssef and Rahman 2007). This methodology depends on dividing the section into a finite number of layers as shown in Figure 4-1-(d). Using the defined stress-strain models for the materials and taking into consideration section equilibrium and kinematics, the

mechanical behaviour of the section can be analyzed. The relationship between the axial strain, the curvature, the applied moment, and the axial force can be written as:

$$\begin{pmatrix} \Delta M \\ \Delta P \end{pmatrix} = \begin{pmatrix} \sum E_i\, A_i\, y_i^2 & -\sum E_i\, A_i\, y_i \\ -\sum E_i\, A_i\, y_i & \sum E_i\, A_i \end{pmatrix} X \begin{pmatrix} \Delta\phi \\ \Delta\varepsilon_c \end{pmatrix} \qquad [4\text{-}5]$$

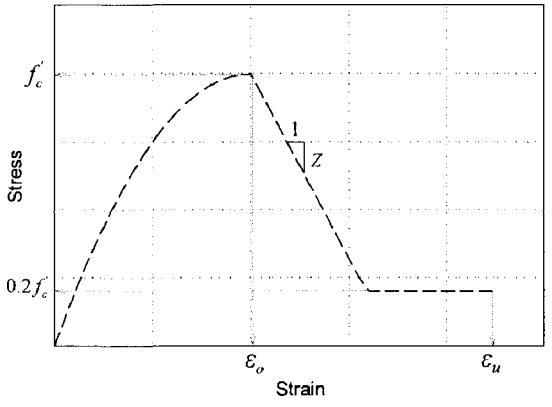

(a) Stress-strain model for concrete in compression

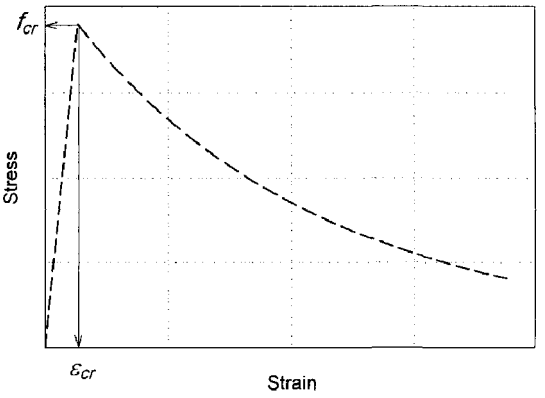

(b) Stress-strain model for concrete in tension

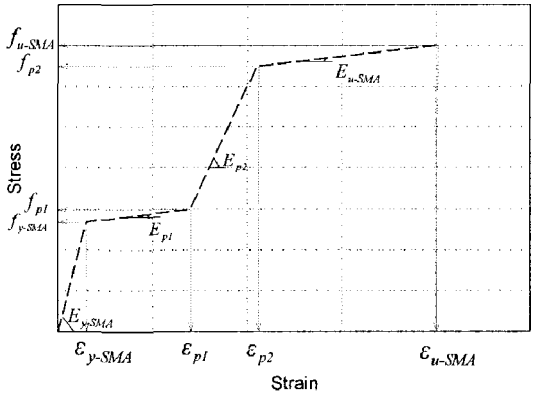

(c) Stress-strain model for SMA

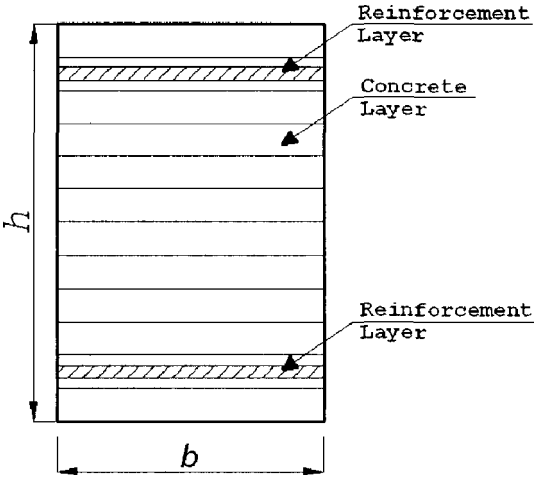

(d) Fibre model for a concrete section

Figure 4-1: Stress-strain models for sectional analysis.

Assumptions applicable to steel RC sections and included in the analysis are: (1) plane sections remain plane so that strain distribution is linear, and (2) perfect bond exists between concrete and reinforcement.

The load is applied in two different stages. In the first stage, the axial load is applied in an incremental way while the moment is kept equal to zero. After reaching the specified axial load, the second stage starts by applying a displacement load (curvature) in an incremental way while keeping the axial load equal to the specified value.

4.4 Deflection calculation using moment-area method

One of the most accurate methods for estimating flexural deformations of RC members is based on integrating the curvature distribution using the moment-area method. The analysis starts by drawing the bending moment diagram of the studied beam, and evaluating the corresponding curvature distribution. Rotations can be calculated by integrating the area under the curvature diagram, while deflections can be computed by calculating the first moment of area of the integrated area.

To check the accuracy of using the moment-area method in the deflection calculations of SMA RC members, the two beam-column joint specimens tested by Youssef et al. (2008) were utilized. One of the joints was reinforced with regular steel reinforcement (JBC1), while the other (JBC2) was reinforced with steel in conjunction with SMA in the plastic hinge region of the beam.

The columns of the two joints have the same cross-section dimensions (250 mm x 400 mm) and reinforcement (4-M20 longitudinal bars and M10 stirrups spaced at 80 mm in the joint region and 115 mm elsewhere). The beams of the two joints, JBC1 and JBC2, had similar cross-section dimensions (250 mm x 400 mm) and amount of transverse reinforcement (M10 spaced at 80 mm in the plastic hinge region and 110 mm in the remaining length of the beam). Figure 4-2-(a) illustrates the elevation and cross-sections of JBC1 and JBC2. The Ni-Ti SMA bars had a length of 450 mm and were connected to steel bars using mechanical couplers. Figure 4-2-(b) shows the stress-strain relationship of the used Ni-Ti alloy. It has a yield stress of 401 MPa and a yield strain of 0.75%. The properties of the used concrete, longitudinal steel, and transverse steel are summarized in Table 4-1. A constant axial load of 350 kN was applied at the top of the column for both specimens. The bottom of the columns was hinged. Roller support was used at the top of the columns. A reversed quasi-static cyclic loading was applied at the beam tip. Youssef et al. (2008) indicated that the deformations were mainly due to the rotation of the beam and that the rotation of the column and the beam-column joint were minimum.

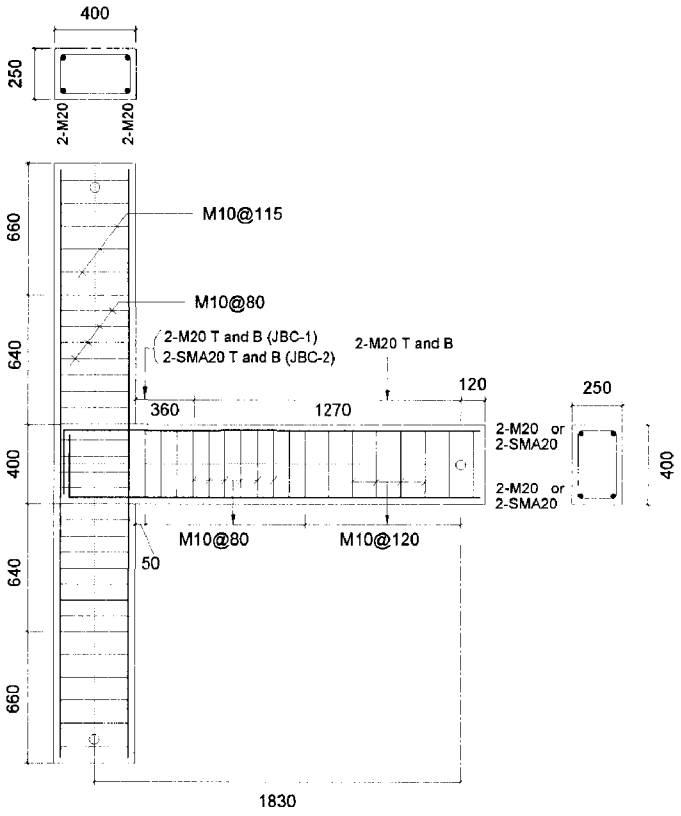

(a)

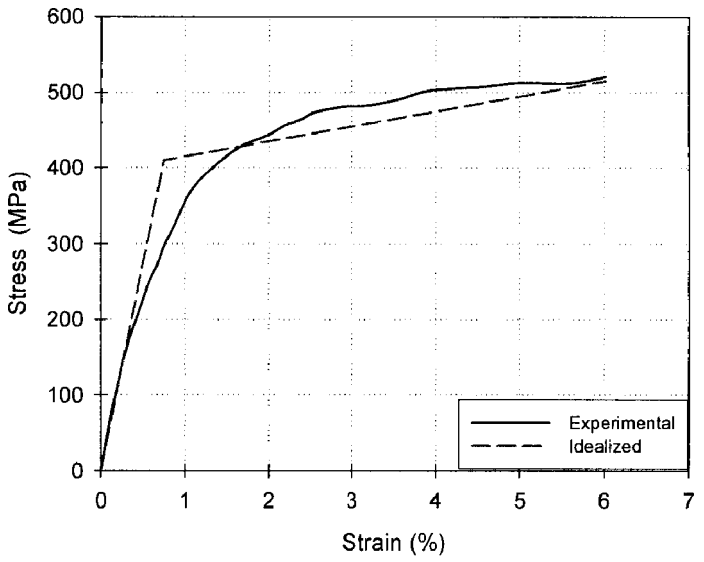

(b)

Figure 4-2: (a) Reinforcement details of specimens JBC-1 and JBC-2 (Youssef et al. 2008), and (b) Ni-Ti stress-strain relationship

Table 4-1: Materials properties

Material	Property	JBC1	JBC2
Concrete	Compressive Strength	53.5	53.7
	Tensile Strength	3.5	2.8
Longitudinal Steel	Yielding Stress	520	450
	Ultimate Strength	630	650
Transverse Steel	Yielding Stress	422	422
	Ultimate Strength	682	682

Moment-curvature analysis is performed using the sectional analysis methodology. The beam is modelled as cantilever fixed at the joint. The rotations of the column and beam-column joint were neglected based on the observations of Youssef et al. (2008). Confinement was accounted for in the concrete models. Figure 4-3-(a) illustrates the moment-curvature relationships for the SMA and steel RC sections assuming a stirrups spacing of 80 mm. The curvature distribution is drawn along the beam length based on the load level and the reinforcement type. The deflection is calculated by calculating the first moment of the integrated areas under the curvature diagram. Figure 4-3-(b) shows

the load-deflection relationships obtained from the moment area method for both JBC1 and JBC2. Good agreement between experimental and analytical results can be observed.

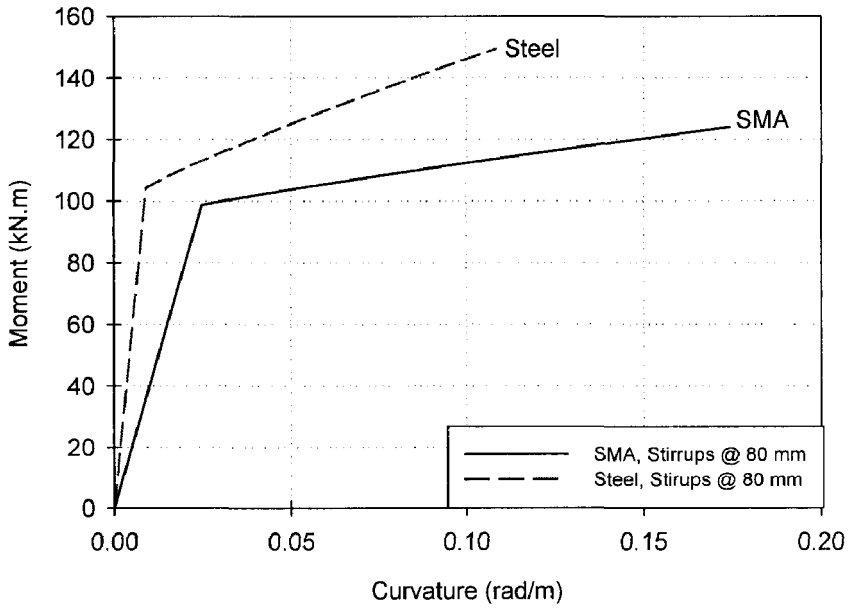

(a)

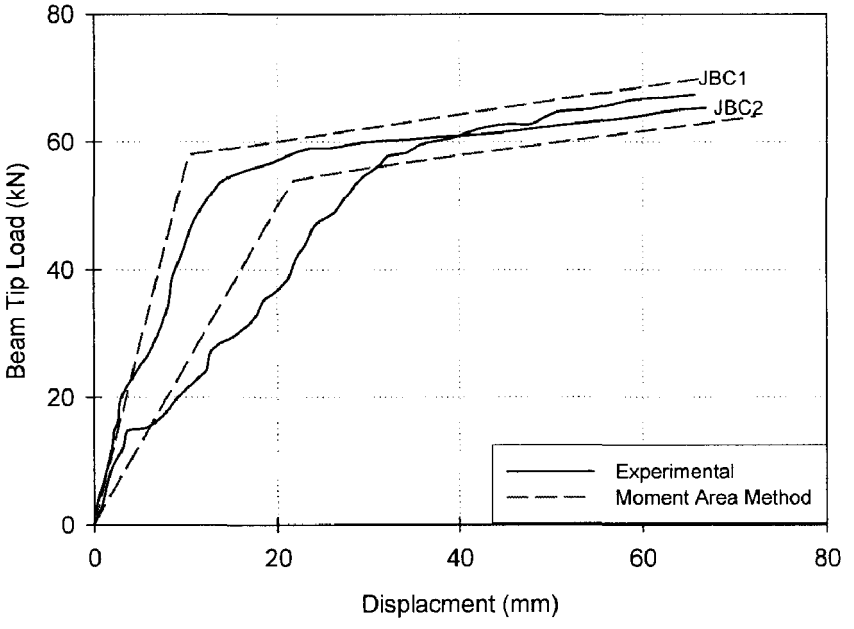

(b)

Figure 4-3: (a) moment-curvature analysis for SMA and steel RC sections (JBC2), and (b) Load-displacement behaviour of JBC1 and JBC2

4.5 Parametric study

A parametric study is conducted to study the deflection behaviour of flexural concrete members reinforced with SMA. The studied parameters are the cross-section dimensions, reinforcement ratio, concrete compressive strength, and the modulus of elasticity of SMA. Details of the analyzed sections are summarized in Table 4-2. The moment-area method is used to calculate the deflection of the studied members. All sections showed a high reduction in the section stiffness after concrete cracking. The results of the parametric study are used to evaluate the applicability of available models for estimating the deflection of SMA RC sections.

Table 4-2: Details of analyzed sections

Section	Studied variables	h (mm)	b (mm)	A_s (mm^2)	E (MPa)	f'_c (MPa)	L (mm)
C_1	h	400	300	1,200	40,000	45	6000
C_2	h	600	300	1,200	40,000	45	6000
C_3	h	800	300	1,200	40,000	45	6000
C_4	b	500	250	950	40,000	40	5000
C_5	b	500	400	950	40,000	40	5000
C_6	b	500	600	950	40,000	40	5000
C_9	ρ	500	250	460	40,000	40	5000
C_{10}	ρ	500	250	920	40,000	40	5000
C_{11}	ρ	500	250	1,380	40,000	40	5000
C_{12}	ρ	500	250	2,050	40,000	40	5000
C_{13}	E	500	250	800	30,000	40	5000
C_{14}	E	500	250	800	45,000	40	5000
C_{15}	E	500	250	800	65,000	40	5000
C_{16}	f'_c	600	300	1,100	40,000	20	6000
C_{17}	f'_c	600	300	1,100	40,000	35	6000
C_{18}	f'_c	600	300	1,100	40,000	55	6000

4.6 Effective moment of inertia

Deflection calculation of concrete flexural members is dependent on the section moment of inertia, concrete tensile stiffening, and load level. At a crack location, the moment of inertia of the section equals the cracked moment of inertia, I_{cr}. The average inertia

considering the cracked and un-cracked sections is the effective moment of inertia (I_e). Figure 4-4 shows the variation of the section moment of inertia versus loading. The effective moment of inertia decreased rapidly compared to the un-cracked moment of inertia as the load level increases, approaching the cracked moment of inertia, I_{cr}. There are a number of methods in the literature to calculate the effective moment of inertia. The Canadian Standards (A23.3-04 2004) use the equation proposed by Branson (1963), Equation [4-1], for this purpose.

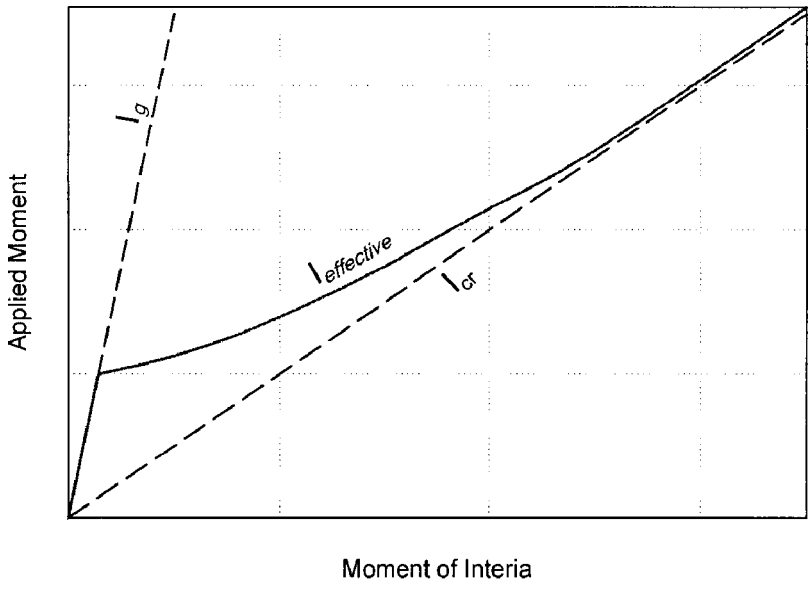

Figure 4-4: Variation of section stiffness with loading.

Branson's equation gives a reasonable estimate of the bending stiffness provided that the reinforcement ratio is greater than 0.5% (Rangan and Sarker 2001). For lower reinforcement ratios, it was found that Branson's equation highly overestimates the section stiffness, and thus significantly underestimates the member deflection (Benmokrane et al. 1996, Brown and Bartholomew 1996, Tountanji and Saafi 2000,

Bischoff 2007a). To overcome this problem, the Australian Standards (AS 3600 2001) proposed limiting the value of I_e to 0.6 I_g if the reinforcement ratio is less than 0.5%.

Replacing the conventional steel reinforcement with new materials having different mechanical properties such as SMA requires checking the validity of Equation [4-1]. Similar studies have been conducted for FRP RC members (ACI 440.1R-03 2003, ACI 440.1R-03 2004, Bischoff 2007a). Since the modulus of elasticity of FRP is lower than that of steel and comparable to that of SMA in the pre-yielding region of the stress-strain relationship, the models developed for predicting the deflection of FRP RC members are summarized below.

Benmokrane et al. (1996) proposed modifying Branson's equation by multiplying it by two constants, Equation [4-6]. These constants were proposed based on load-deflection results obtained from four experimentally tested FRP RC beams. The beams had reinforcement ratios varying between 0.56% and 1.10%, and modulus of elasticity varying between 40,000 MPa and 45,000 MPa.

$$I_e = \frac{1}{7}\left(\frac{M_{cr}}{M_a}\right)^3 I_g + 0.84\left[1-\left(\frac{M_{cr}}{M_a}\right)^3\right] I_{cr} \qquad \leq I_g \qquad [4\text{-}6]$$

Brown and Bartholomew (1996) proposed to replace Branson's equation with Equation [4-7]. The proposed equation was developed based on regression analysis of experimental results that included testing eight GFRP RC beams. The beams had different

reinforcement ratios ($0.38\% \leq \rho \leq 1.38\%$) and different modulus of elasticity values ($40{,}000$ MPa $\leq \rho \leq 45{,}000$ MPa).

$$I_e = \left(\frac{M_{cr}}{M_a}\right)^5 I_g + \left[1 - \left(\frac{M_{cr}}{M_a}\right)^5\right] I_{cr} \qquad \leq I_g \qquad [4\text{-}7]$$

Tountanji and Saafi (2000) modified the equation of Brown and Bartholomew (1996) making it a function of the modulus of elasticity of FRP and the reinforcement ratio, Equation [4-8]. These modifications were based on test results of six FRP RC beams. The beams had reinforcement ratios varying between 0.52% and 1.10% and a constant modulus of elasticity of 40,000 MPa.

$$I_e = \left(\frac{M_{cr}}{M_a}\right)^m I_g + \left[1 - \left(\frac{M_{cr}}{M_a}\right)^m\right] I_{cr} \qquad \leq I_g \qquad [4\text{-}8a]$$

$$\text{where} \quad m = 6 - 10\frac{E_{FRP}}{E_s}\rho, \qquad \frac{E_{FRP}}{E_s}\rho_{FRP} < 0.3$$
$$m = 3.0 \qquad \frac{E_{FRP}}{E_s}\rho_{FRP} \geq 0.3 \qquad [4\text{-}8b]$$

The ISIS design manual (2001) suggested an effective moment of inertia, Equation [4-9], which is quite different in form compared to the previous equations. It is based on equations given by CEB-FIP (1990) and validated by Ghali et al. (2001) through analytical verification of the experimental programs conducted by Hall (2000), and Hall and Ghali (1997).

$$I_e = \frac{I_T\, I_{cr}}{I_{cr} + \left[1 - 0.5\left(\frac{M_{cr}}{M_a}\right)^2\right](I_T - I_{cr})} \leq I_g \qquad [4\text{-}9]$$

Where: I_T is the un-cracked moment of inertia of the transformed section.

ACI 440.1R-03 (2003) used as similar form to Branson's equation. However, a reduction factor (β) was used to reduce the effective moment of inertia, Equation [4-10]. This reduction factor was dependent on the modulus of elasticity of FRP.

$$I_e = \left(\frac{M_{cr}}{M_a}\right)^3 \beta\, I_g + \left[1 - \left(\frac{M_{cr}}{M_a}\right)^3\right] I_{cr} \leq I_g \qquad [4\text{-}10a]$$

$$\text{where} \quad \beta = \alpha \left(1 + \frac{E_{FRP}}{E_s}\right) \qquad [4\text{-}10b]$$

Where: α is a bond dependent coefficient. It can be taken as 0.5.

Several attempts have been made to modify Equation [4-10], as it was found that it underestimates the deflection of FRP RC members. Yost et al. (2003) argued that the accuracy of the I_e equation given by ACI 440.1R-03 (2003) is mainly dependent on the reinforcement ratio. A modification to the bond dependent coefficient α was proposed, Equation [4-11].

$$\alpha = 0.064\left(\frac{\rho_{FRP}}{\rho_b}\right) + 0.13 \qquad [4\text{-}11]$$

ACI 440.1R-04 (2004) proposed a new expression for β, Equation [4-12]. The new value for β is mainly dependent on the section reinforcement ratio ρ.

$$\beta = \frac{1}{5}\left(\frac{\rho_{FRP}}{\rho_b}\right) \qquad \leq 1.0 \qquad [4\text{-}12]$$

Bischoff (2007a) argued that Branson's equation gives a weighted average of the gross and cracked moments of inertia at any given load level. This formulation is similar to springs of the un-cracked and cracked moments of inertia arranged in parallel. Having a low value for the reinforcement ratio or the modulus of elasticity significantly increases the ratio between the un-cracked moment of inertia, I_g, and the cracked moment of inertia, I_{cr}. Such cases are not represented by springs in parallel. Bischoff (2007a) proposed arranging the springs in series to properly model the tension stiffening of concrete. The proposed model by Bischoff (2007b), Equation [4-13], was calibrated for beams having $\frac{I_g}{I_{cr}}$ equal to 2.2. The model is shown to be appropriate for steel RC members having a low value of the reinforcement ratio, and for FRP RC members.

$$\frac{1}{I_e} = \left(\frac{M_{cr}}{M_a}\right)^2 \frac{1}{I_g} + \left[1 - \left(\frac{M_{cr}}{M_a}\right)^2\right] \frac{1}{I_{cr}} \qquad \geq \frac{1}{I_g} \qquad [4\text{-}13]$$

4.7 Results and discussion

The results of the parametric study are discussed in this section. A number of deflection points representing the expected service load level were chosen. The chosen load levels correspond to 1.1 M_{cr}, 1.5 M_{cr}, 2.0 M_{cr}, and 3.0 M_{cr}. Figure 4-5 shows the analytically evaluated deflection values for each of the studied cases at the chosen load levels plotted versus the deflection predicted using the models given in Section 4.6. A noticeable difference between the predictions of the different models can be observed. The effects of the studied parameters on the load-deflection behaviour of SMA RC members is discussed in this section.

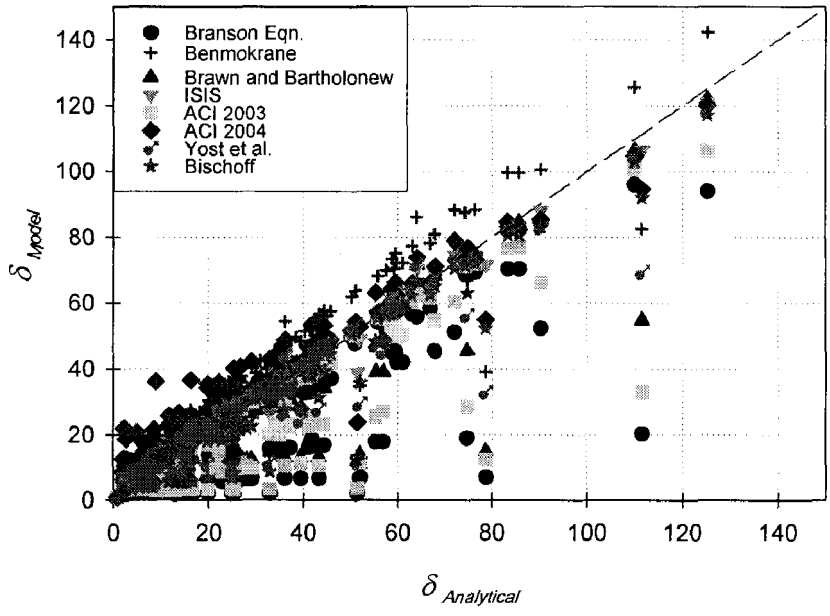

Figure 4-5: Moment-area method versus different models deflections.

Figure 4-6-(a) illustrates the load-deflection relationship for the chosen cross-section heights. Upon cracking, a noticeable decrease in I_e was observed for all studied sections.

Branson's equation was found to overestimate the flexural stiffness resulting in an underestimation of the deflection. The model proposed by Bischoff (2007b) was found to underestimate the deflection for one of the members (h = 800 mm). For the other two members, good agreement was observed between Bischoff's model and the moment-area results.

The effect of varying the cross-section width on the load-deflection relationships is illustrated in Figure 4-6-(b). After cracking of concrete, varying the cross-section width did not have a significant effect on I_e. Bischoff's model was found to result in an acceptable load-deflection for b = 250 mm. However, the model did not predict the deflection well for the 400 mm and 600 mm wide members. Branson's equation was found to significantly underestimate the deflection of all the studied members.

The difference between the effective moment of inertia values obtained from Branson's equation and those obtained from the moment-curvature analysis was found to significantly decrease with the increase in the reinforcement ratio, Figure 4-6-(c). Good agreement between the deflections obtained from Branson's equation and those obtained from the moment-area method was observed for ρ = 1.20% and ρ = 1.77%. In the case of ρ = 0.4% or ρ = 0.8%, Branson's equation was unable to accurately predict the deflection. Bischoff's model was found to slightly underestimate the member deflection for ρ = 0.4%. For other reinforcement ratios, Bischoff's model gave good estimates of the deflection.

The effect of the modulus of elasticity of SMA on the load-deflection behaviour was found to be significant, Figure 4-6-(d). Branson's equation predicted the effective moment of inertia well for members having relatively high modulus of elasticity value (E = 65,000 MPa). For relatively low modulus of elasticity values, a notable difference between the deflections predicted using Branson's equation and those obtained from the moment-area method was observed. Bischoff's model provided conservative predictions for E = 45,000 MPa and E = 65,000 MPa. However, for E = 30,000 MPa, the model was found to underestimate the beam deflection, especially for load levels close to the cracking load.

Varying the concrete compressive strength within the normal concrete strength range did not have significant effect on the load-deflection behaviour of SMA RC members, Figure 4-6-(e). Branson's equation significantly overestimated the flexural stiffness of the studied members. Bischoff's model was found to have poor agreement with the moment-area method at loads close to the cracking load.

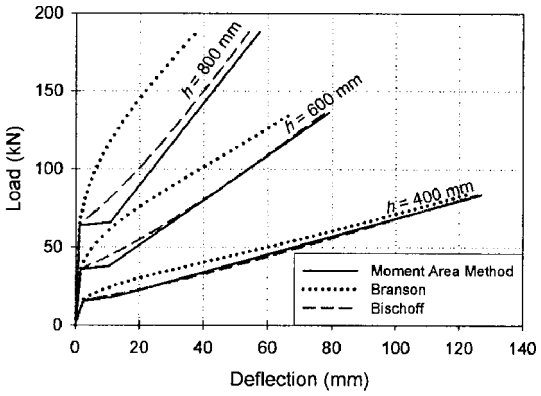

(a) Effect of cross-section height

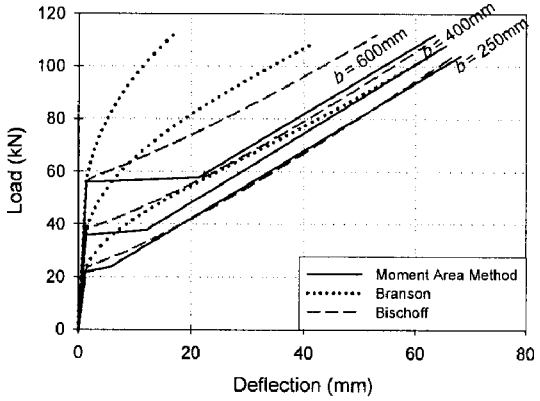

(b) Effect of cross-section width

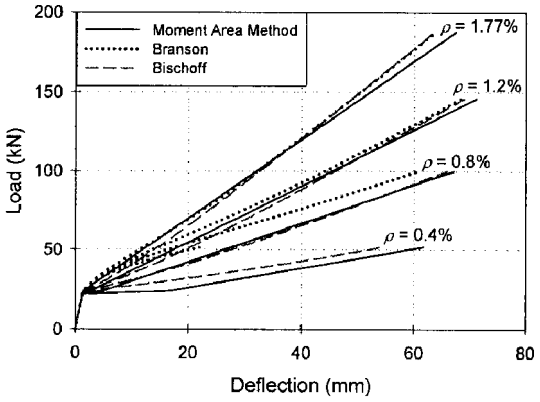

(c) Effect of reinforcement ratio

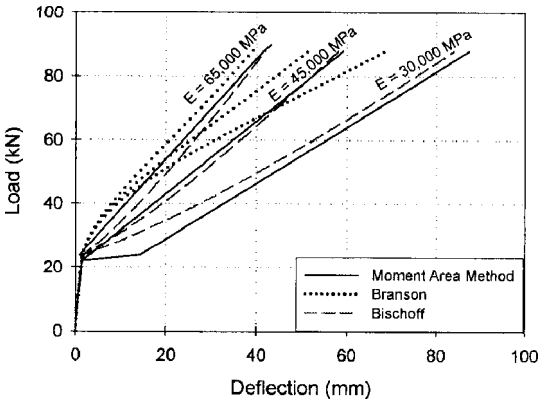

(d) Effect of reinforcement modulus of elasticity

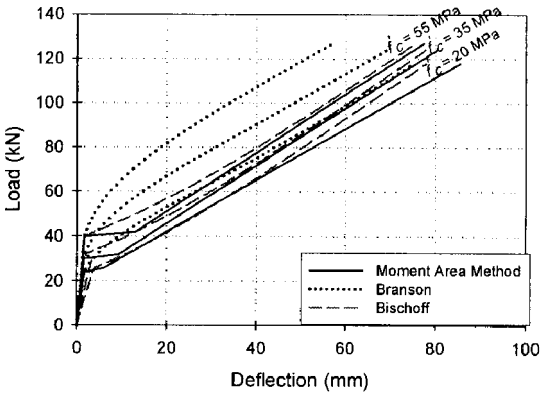

(e) Effect of concrete compressive strength

Figure 4-6: Load-deflection relationship for SMA RC members.

4.8 Accuracy of deflection models

The accuracy of the previously described models in predicting the deflection of SMA RC members is evaluated in this section. Figure 4-7 shows the deflection calculated using the moment-area method plotted versus the deflection obtained from the different models at load levels corresponding to 1.1 M_{cr}, 1.5 M_{cr}, 2.0 M_{cr}, and 3.0 M_{cr}. The reliability and accuracy of each model was evaluated using the root mean square error (*RMSE*), Equation [4-14], and the average algebraic error (*AGE*), Equation [4-15]. The *RMSE* and *AGE* results for all models are summarized in Figure 4-8.

$$RMSE = \frac{1}{n}\sum_{i=1}^{n}\sqrt{(\delta_{\text{Analtical}} - \delta_{\text{Model}})^2} \qquad [4\text{-}14]$$

$$AGE = \frac{1}{n}\sum_{i=1}^{n}\frac{(\delta_{\text{Analtical}} - \delta_{\text{Model}})}{\delta_{\text{Analtical}}} \qquad [4\text{-}15]$$

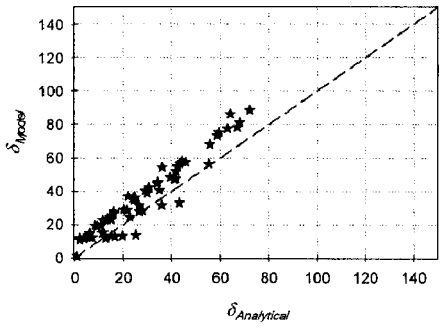

(a) Benmokrane's Equation

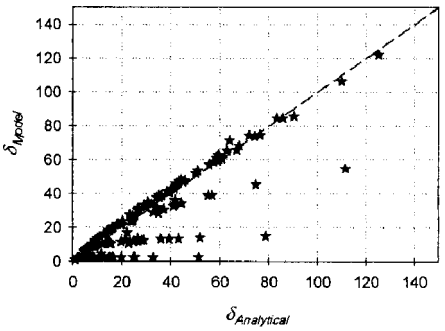

(b) Brown and Bartholomew's Equation

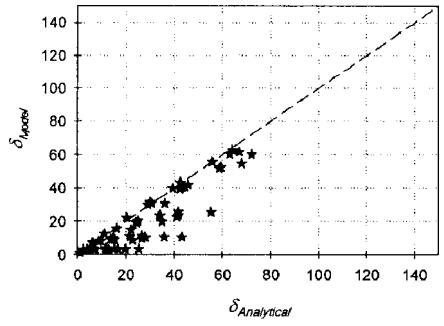

(c) ACI 440.1R-03 Equation

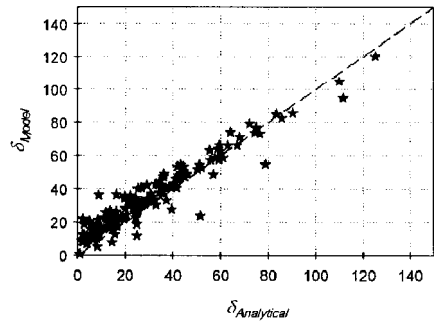

(d) ACI 440.1R-04 Equation

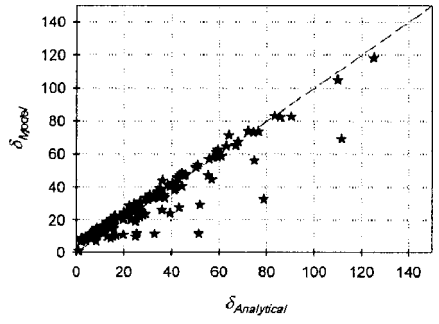

(e) Yost et al.'s Equation

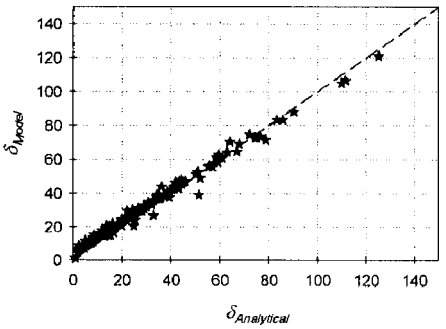

(f) ISIS Equation

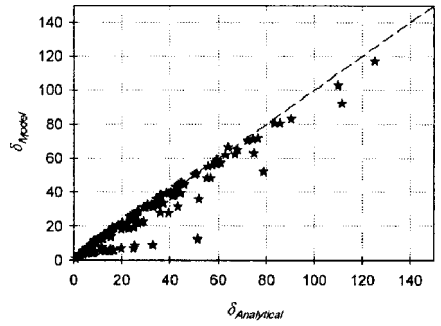

(g) Bischoff's Equation

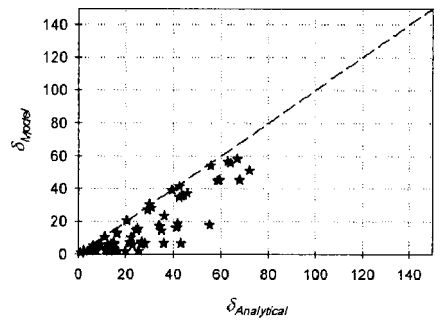

(h) Branson's Equation

Figure 4-7: Moment-area method versus different equations deflections.

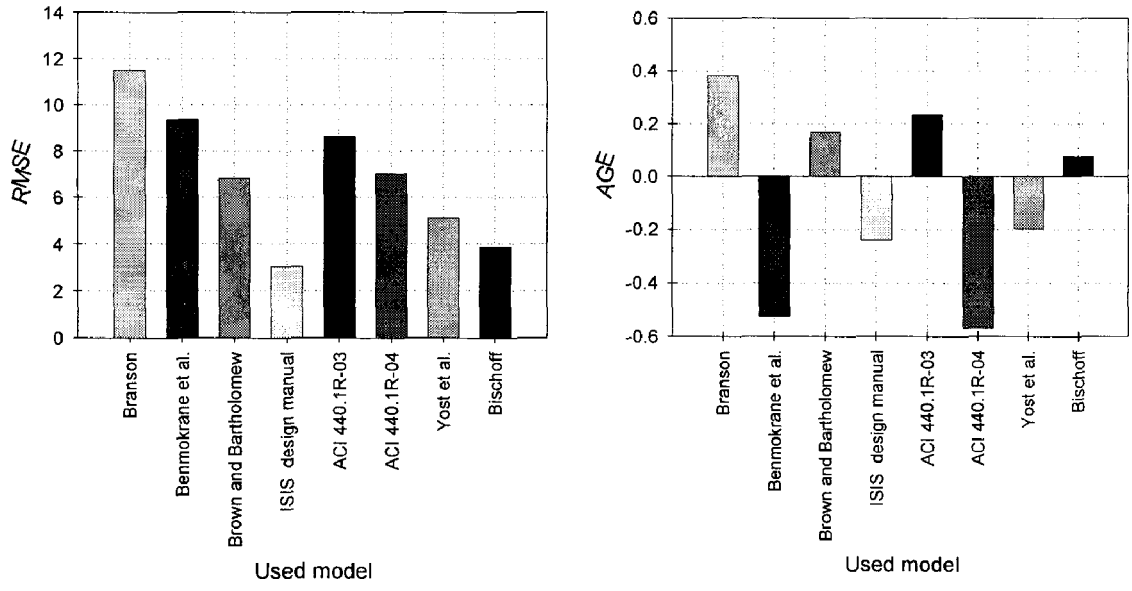

(a) *RMSE* for predicted deflections using different models

(b) *AGE* for predicted deflections using different models

Figure 4-8: Evaluation of different models accuracy.

Figure 4-7 shows that the model proposed by Benmokrane et al. (1996) is not conservative for cases corresponding to low reinforcement ratio ($\rho \leq 0.4\%$). For other reinforcement ratios, the model was conservative. *RMSE* of 9.36 and *AGE* of -0.52 were obtained for this model. The model proposed by Brown and Bartholomew (1996) was found to underestimate the deflection for members having reinforcement ratios up to 0.80%. The *RMSE* was found to be 6.80 for this model.

The model proposed by ACI 440.1R-03 (2003), which is mainly dependent on the reinforcement modulus of elasticity was found to be in poor agreement with the deflections obtained using the moment-area method for reinforcement ratios up to 1.20%. *RMSE* of 8.64 was obtained for this model. The deflections calculated using the ACI 440.1R-04 (2004) were found to be significantly higher than those obtained from the

moment-area method (*AGE* = 0.57). *RMSE* for the results obtained using this model was 7.00. The model proposed by Yost et al. (2003) was found to be conservative except for members with low reinforcement ratio ($\rho \leq 0.4\%$) or low modulus of elasticity (E = 30,000 MPa). An *AGE* of -0.20 was observed for this model while the *RMSE* was found to be 5.11.

The ISIS design manual (2001) showed the minimum *RMSE* with a value of 3.03. It generally overestimated the members' deflection with *AGE* value of -0.24. Bischoff's model showed comparable *RMSE* to that of the ISIS design manual (2001), *RMSE* = 3.85. However, the model was found to slightly underestimate the members deflection (*AGE* = 0.0763). The highest *RMSE* was obtained for Branson's equation (*RMSE* = 11.5) as a result of the significant overestimation of the members flexural stiffness. An *AGE* of 0.38 was observed in the case of Branson's equation, which indicates the general underestimation of the members deflection.

Based on the observed deflection values for different parameters, *RMSE*, and *AGE*, Bischoff's model provided the best predictions among the eight models considered herein for members having reinforcement ratios greater than 0.6%. For lightly reinforced concrete members ($\rho \leq 0.6\%$), the ISIS design manual (2001) gave the best predictions.

4.9 Conclusions

This parametric study investigates the load-deflection behaviour of SMA RC members. The effects of the cross-section height and width, reinforcement ratio, reinforcement

modulus of elasticity, and concrete compressive strength were evaluated. Deflections were calculated based on the moment-area method. The accuracy of using this method with SMA RC members was validated in comparison with available experimental results. The equation provided by the Canadian Standards Association, A23.3-04 (2004), for deflection calculation was found to significantly overestimate the flexural stiffness of SMA RC members, and thus significantly underestimates their deflection. This is expected because of the significant difference between the modulus of elasticity of SMA and that of steel. This was observed earlier for FRP RC members. Different models available in the literature for the deflection calculation of steel and FRP RC members were examined.

The effect of varying the cross-section dimensions (height and width), reinforcement ratio, reinforcement modulus of elasticity, and concrete compressive strength on the load deflection behaviour of SMA RC members was discussed. Varying the concrete compressive strength and the cross-section width was found to have a minor effect on the I_e value. The parametric study results indicated that the reinforcement ratio and reinforcement modulus of elasticity have a significant effect on I_e. Moreover, the accuracy of the reviewed models was found to mainly depend on these two parameters.

The results from the parametric study were used to check the applicability and accuracy of existing models to predict the deflection of SMA RC members. Statistical tools, such as *RMSE* and *AGE*, were used to evaluate the accuracy of each model. *RMSE* and *AGE* showed that the model proposed by Bischoff (2007b) had the best performance for members having reinforcement ratios greater than 0.6%. For lightly reinforced concrete

members (ρ < 0.6%), the Bischoff model was un-conservative, and the ISIS design manual (2001) was found to be conservative and relatively accurate in predicting the deflection of SMA RC members.

4.10 References

ACI 440 (2003). Guide for the Design and Construction of Concrete Reinforced with FRP Bars, American Concrete Institute, Farmington Hills, Michigan, 42 p.

ACI 440 (2004). Guide for the Design and Construction of Concrete Reinforced with FRP Bars, Proposed Revision, American Concrete Institute, Farmington Hills, Michigan, 35 p.

Alam, M.S., Youssef, M.A., Nehdi, M. (2007). "Utilizing Shape Memory Alloys to Enhance the Performance and Safety of Civil Infrastructure: a Review." Canadian Journal of Civil Engineering, 34(9), 1075-1086.

AS3600 (2001). Australian Standard for Concrete Structures, Standards Australia (SA), Sydney, Australia.

Benmokrane, B., Chaallal, O., and Masmoudi, R. (1996). "Flexural Response of Concrete Beams Reinforced with FRP Reinforcing Bars." ACI Structural Journal, 91(2), 46 55.

Bischoff, P.H. (2007a). "Rational Model for Calculating Deflection of Reinforced Concrete Beams and Slabs." Canadian Journal of Civil Engineering, 34(8), 992-1002.

Bischoff, P.H. (2007b). "Effective Moment of Inertia for Calculating Deflections of Concrete Members Containing Steel Reinforcement and Fiber-Reinforced Polymer Reinforcement." ACI Structural Journal, 104(1), 68-75.

Branson, D.E. (1963). "Instantaneous and Time-Dependent Deflections of Simple and Continuous Reinforced Beams." HPR Rep. No. 7, Part 1, Alabama Highway Department, Bureau of Public Roads, Montgomery, Ala, 78 p.

Brown, V.L., and Bartholomew, C.L. (1996). "Long-Term Deflections of GFRP-Reinforced Concrete Beams." Proceedings, ICCI, Tucson, Ariz., 389 400.

CEB-FIP (1990). Model Code for Concrete Structures, Comité Euro-International du Béton, Thomas Telford, London, UK.

Clark, P.W., Aiken, I.D., Kelly, J.M., Higashino, M. and Krumme, R.C. (1995). "Experimental and Analytical Studies of Shape Memory Alloy Dampers for Structural Control." Smart Structures and Materials: Passive Damping, Proceedings of SPIE, 2445, 241-251.

CSA A23.3-04 (2004). Design of Concrete Structures, Canadian Standards Association, Rexdale, Ontario, Canada, 240 p.

DesRoches, R. and Delemont, R. (2002). "Seismic Retrofit of Bridges Using Shape Memory Alloys." Engineering Structures, 24(3), 325-332.

Elbahy, Y.I., Youssef, M.A., Nehdi, M. (2008). "Flexural Behaviour of Concrete Memebers Reinforced with Shape Memory Alloys." 2nd Canadian Conference on Effective Design of Structures, McMaster University, Hamilton, Ontario, Canada, 477-486.

El-Tawil, S., and Ortega-Rosales, J. (2004). "Prestressing Concrete Using Shape Memory Alloy Tendons." ACI Structural Journal, 101(6), 846-851.

Ghali, A., Hall, T., and Bobey, W. (2001). "Minimum Thickness of Concrete Members Reinforced with Fibre Reinforced Polymer Bars." Canadian Journal of Civil Engineering, 28, 583 592.

Gilbert, R.I. (2006). "Discussion of 'Reevaluation of Deflection Prediction for Concrete Beams Reinforced with Steel and Fiber Reinforced Polymer Bars.' by Peter H. Bischoff." Journal of Structural Engineering, 132(8), 1328 1330.

Hall, T., and Ghali, A. (1997). "Prediction of the Flexural Behaviour of Concrete Members Reinforced with GFRP Bars." Society for the Advancement of Material and Process Engineering (SAMPE), Proceedings of the 42nd International SAMPE Symposium and Exhibition, Anaheim, California, 1, 298-310.

Hall, T.S. (2000). "Deflections of Concrete Members Reinforced with Fibre Reinforced Polymer (FRP) Bars." M.Sc. Thesis, Department of Civil Engineering, The University of Calgary, Calgary, Alberta, 293 p.

ISIS Canada (2001). Reinforcing Concrete Structures with Fibre Reinforced Polymers, Design Manual 3, Winnipeg, Manitoba.

Kent, D.C., and Park, R. (1971). "Flexural Members with Confined Concrete." Journal of the Structural Division, ASCE, 97(7), 1969-1990.

Krumme, R., Hayes, J., and Sweeney, S. (1995). "Structural Damping with Shape Memory Alloys: One Class of Devices." Smart Structures and Materials: Passive Damping, Proceedings of SPIE, 2445, 225-240.

Maji, A.K., and Negret, I. (1998). "Smart Prestressing with Shape-Memory Alloy." Journal of Engineering Mechanics, 124(10), 1121-1128.

Mazzolani, F.M., Corte, G.D., and Faggiano, B. (2004). "Seismic Upgrading of RC Building by Means of Advanced Techniques: The ILVA-IDEM Project." The proceedings of the 13th World Conference on Earthquake Engineering, Paper No. 2703, Vancouver, British Columbia, Canada.

Rangan, B.V. and Sarker, P.K. (2001). "Bending Stiffness of Concrete Flexural Members Reinforced with High Strength Steel." Code Provisions for Deflection Control in Concrete Structures, American Concrete Institute, SP203-09, 203, 143-156.

Saiidi, M.S., Sadrossadat-Zadeh, M., Ayoub, C., Itani, A. (2007). "Pilot Study of Behavior of Concrete Beams Reinforced with Shape Memory Alloys." ASCE, Journal of Materials in Civil Engineering, 19(6), 454-461.

Scanlon, A., Cagley Orsak, D.R., and Buettner, D.R. (2001). "ACI Code Requirements for Deflection Control: a Critical Review. In Code Provisions for Deflection Control in Concrete Structures." Edited by E.G. Nawy and A. Scanlon, American Concrete Institute, Farmington Hills, Mich, SP-203, 1-14

Scott, B.D.; Park, R.; and Priestley, M.J.N. (1982). "Stress-Strain Behavior of Concrete Confined by Overlapping Hoops at Low and High Strain Rates." ACI journal, 79(1), 13-27.

Sittipunt, C., and Wood, S.L. (1993). "Finite Element Analysis of Reinforced Concrete Shear Walls." Report No. UILU-ENG-93-2015, University of ILLiois at Urbana, Ill, 401 p.

Stevens, N.J., Uzumeri, S.M., and Collins, M.P. (1987). "Analytical Modeling of Reinforced Concrete Subjected to Monotonic and Reversed Loading." Publication No. 87-1, University of Toronto, 3634 p.

Tamai, H., Miura, K., Kitagawa, Y., Fukuta, T. (2003). "Application of SMA Rod to Exposed-Type Column Base in Smart Structural System." Proceedings, Smart Structures and Materials: Smart Systems and Nondestructive Evaluation for Civil Infrastructures, The International Society for Optical Engineering, 169-177.

Toutanji, H.A., and Saafi, M. (2000). "Flexural Behavior of Concrete Beams Reinforced with Glass Fiber-Reinforced Polymer GFRP Bars." ACI Structural Journal, 97(5), 712 719.

Yost, J.R., Gross, S.P., and Dinehart, D.W. (2003). "Effective Moment of Inertia for Glass Fiber-Reinforced Polymer-Reinforced Concrete Beams." ACI Structural Journal, 100(6), 732 739.

Youssef, M.A., Alam, M.S., Nehdi, M. "Experimental Investigation on the Seismic Behaviour of Beam-Column Joints Reinforced with Superelastic Shape Memory Alloys." In-press, Journal of Earthquake Engineering, accepted January 2008.

Youssef, M., and Ghobarah, A. (1999). "Strength Deterioration due to Bond Slip and Concrete Crushing in Modeling of Reinforced Concrete Members." ACI Structural Journal, 96(6), 956-967.

Youssef, M.A., and Rahman, M. (2007). "Simplified Seismic Modeling of Reinforced Concrete Flexural Members." Magazine of Concrete Research, 59(9), 639-649.

Chapter 5 Deflection of Shape memory Alloy Reinforced Concrete Beams: New Model Based on Artificial Neural Networks

5.1 Introduction

The term shape memory alloys (SMAs) refers to certain types of alloys with the ability to undergo large deformations, and return to their undeformed shape upon unloading or heating. Four properties of SMAs have motivated researchers to utilize them in civil engineering. These properties are: (i) absorption of large amounts of strain energy under cyclic loading (Dolce and Cardone 2001, Piedboeuf and Gauvin 1998, Grandhi and Wolons 1999), (ii) large recoverable strain approaching a value of 10% (Alam et al. 2007), (iii) extraordinary fatigue resistance under repeated large strain cycles (Eggeler et al. 2004, Hornbogen 2004), and (iv) very good durability (Janke et al. 2005). These unique properties have motivated researches to utilize SMAs as primary reinforcement for reinforced concrete structures (Elbahy et al. 2008, Saiidi et al. 2007).

Deflection calculation of concrete flexural members depends on the flexural stiffness, which varies along the structural member because of the presence of flexural cracks in it. An effective moment of inertia, I_e which has an average value between the gross moment of inertia, I_g and the cracked moment of inertia, I_{cr} should be used for deflection calculations. The ACI 318-05 (2005) and CSA-A23.3-04 (2004) design standards use the

equation proposed by Branson (1963) for calculating effective moment of inertia for steel-reinforced concrete (RC) sections, Equation [5-1].

$$I_e = \left(\frac{M_{cr}}{M_a}\right)^3 I_g + \left[1 - \left(\frac{M_{cr}}{M_a}\right)^3\right] I_{cr} \qquad \leq I_g \qquad [5\text{-}1]$$

Using different types of reinforcement having different mechanical properties requires assessing the applicability of such an equation. For instance, using Equation [5-1] for calculating the effective moment of inertia of Fibre-Reinforced Polymers (FRP) RC members may result in a significant overestimation of the member moment of inertia (Bischoff 2005, Bischoff and Scanlon 2007). This overestimation is attributed to the difference between the modulus of elasticity of steel and FRP bars. To overcome this problem, the ACI 440.1R-03 (2003) committee proposed a reduction factor β that is mainly dependent on the value of the modulus of elasticity of the FRP to be multiplied by the gross moment of inertia term in Branson's equation in the case of FRP reinforcement. The ACI 440.1R-04 (2004) committee modified the equation proposed by ACI 440.1R-03 (2003) for the reduction factor β to an equation that is mainly dependent on the reinforcement ratio ρ, rather than the modulus of elasticity E.

Since the modulus of elasticity of FRP is generally close to that of SMA in the pre-yielding zone of the stress-strain model, the ability of the models proposed by the ACI 440.1-R-03 (2003) and ACI 440.1-R-04 (2004) committees to accurately predict the deflection of SMA RC members was evaluated in Chapter 4. The models gave good

predictions for members having high reinforcement ratios (ρ > 1.0%). However, for lightly reinforced members (ρ < 0.5%), the models gave poor predictions.

Artificial intelligence (AI) is the study of mental processes through the use of computational models (Charniak and McDermott 1985). It attempts to simulate the human mental faculties through computing. It can also be defined by as the science concerned with understanding the intelligence behaviour and how it can be artificially created (Smithers et al. 1990). The use of AI in solving problems and modeling applications in civil engineering has increased over the last decades (Nehdi et al. 2001, El-Chabib and Nehdi 2006).

This chapter focuses on utilizing the artificial neural network technique in predicting the deflection of SMA RC members. A new model is developed to predict the effective moment of inertia of SMA RC members.

5.2 Artificial neural networks

Artificial neural network modeling is inspired by the understanding and abstraction of the biological structure of neurons and the internal operations of the human brain (Haykin 1994). It is a highly non-linear system offering a substantial ability to solve complex computational tasks. For instance, ANN is capable to perform self-organizing, pattern recognition, and functional approximation.

Neural networks are built of neurons (or processing units) that are usually arranged in layers and are often connected to neurons in other layers. The function of these neurons is performing simple computations. Based on the activation level, each processing unit sends signals to other units in the network. Through propagation, the network learns and adapts to new data examples and stores information about the weights of the connections between neurons. Thus, a neural network has the ability to learn the relationship between a set of inputs and the corresponding outputs. This gives the network the ability to produce appropriate output values when unfamiliar inputs are provided.

The basic features of an artificial neural network include: (i) Processing unit, (ii) Pattern of connectivity between these processing units, (iii) State of activation for each processing unit, (iv) Propagation rules, (v) Activation functions for each processing unit, and (vi) Rule of learning.

Figure 5-1 shows a simplified model for an artificial neuron (processing unit). Generally, each neuron j in layer l receives one or more inputs X_i^{l-1} from neurons in the previous layer (l-1) to which it is connected (Nehdi et al. 2001b). Then, the neuron j performs a simple computation to form a single net input U_j^l given by Equation [5-2].

$$U_{ji}^{l} = \sum_{i=1}^{n} W_{ji}^{l} \, X_i^{l-1} + \theta_j^{l} \qquad [5\text{-}2]$$

Where: W_{ji}^{l} is the connection weight (strength) connecting the neuron j in layer l to neuron i in layer (l-1), n is the number of neurons in layer (l-1), θ_j^{l} is a threshold value

assigned to neuron j in layer l, and X_i^{l-1} is the input coming from neuron i in layer l-1 to neuron j in layer l.

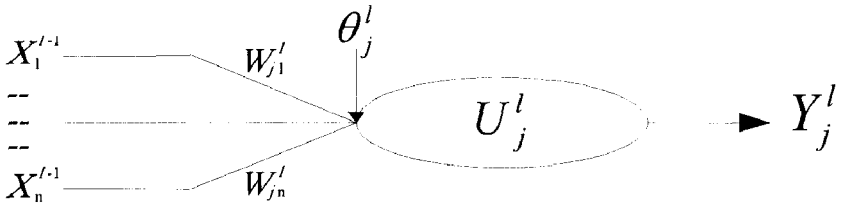

Figure 5-1: Simplified model of artificial neuron.

The net input U_j^l is then modified using an activation function f to generate an output value Y_j^l (Equation [5-3]).

$$Y_j^l = f(U_j^l) \qquad [5\text{-}3]$$

Where: f is a nonlinear activation function assigned to each neuron in the network. A commonly used transfer function is the continuous nonlinear sigmoid function. The advantage of this function lies in its ability to meet the differentiability requirements needed in the back propagation algorithm. The activation function can be represented by Equation [5-4].

$$f_j^l = \frac{1}{1 + e^{-(u_j^l - \theta_j^l)}} \qquad [5\text{-}4]$$

The features explained by Rumelhart et al. (1986) can vary from one network to another. As a result, different types of networks can be obtained. These include the Hopfield

network (Hopfield 1982), Bolzmann machines (Ackaly et al. 1985), the Kohonen network (Kohonen 1982), and the multi-layer back-propagation neural networks (Rumelhart et al. 1986). Among these different types of networks, the multi-layer back-propagation network is the most commonly used in engineering applications. The concept and methodology of ANNs are discussed in more details by Haykin (1994).

5.3 Feed-forward back-propagation neural networks

Feed-forward back-propagation (FFBP) or multi-layer perceptron (MLP) networks are the most widely used neural networks in engineering applications. They have the ability to perform non-linear transformations for functional approximation problems, recognize logic functions, and subdivide the pattern space for classification. MLP networks have multiple layers and each layer may contain perceptrons or processing units. The perceptron is similar to the artificial neuron and was first introduced by Rosenblatt (1958).

A feed-forward multi-layer perceptron network structure consists of an input layer, an output layer, and a number of hidden layers. Figure 5-2 shows a typical architecture of the feed-forward networks. Some researchers do not consider the input layer as an integral layer in the network architecture. However, it is agreed that the processing units in the input layer do not perform any computations. They only serve as a link between the input vector and processing units in the first hidden layer. Each layer may contain several processing units (neurons). The neurons in one layer are fully or partially connected to the neurons in the subsequent layer with different weights. No backward connections

exist between neurons and no connections between neurons in the same layer are allowed in FFBP.

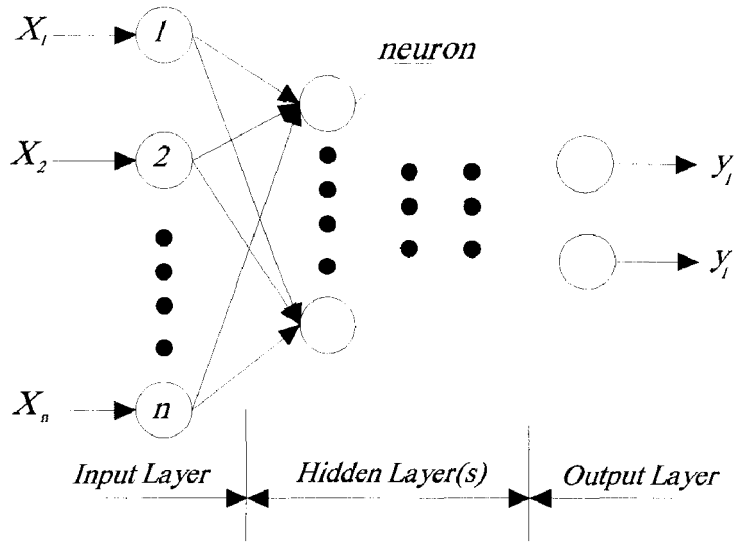

Figure 5-2: General Feed-Forward multilayer network.

Based on the number of input and output parameters, the number of neurons in the input and output layers can be determined. However, there are no rules to decide on the optimum number of hidden layers or the optimum number of processing units (neurons) in the hidden layers. More research is still needed in this area. On the other hand, it is known that the number of hidden layers and neurons is dependent on the complexity of the problem. Although there are few recommendations in the literature to determine the suitable number of hidden neurons, the numbers of hidden layers and corresponding neurons is usually obtained by trial and error and usually depends on the experience of the user.

The performance of a trained MLP network depends on the final weights (strengths) of connections between the processing units (neurons) in the different layers. Choosing a number of neurons smaller than the optimum number results in a smaller number of connections and their associated weights. Thus, the ability of the network to implement non-linear transformations for functional approximation problems is reduced. Choosing a number of neurons higher than the optimum number will result in a much higher number of connections and their associated weights. This will slow down the training process and reduce the ability of the network to generalize.

Generally, there are three important steps that should be carefully considered and addressed while constructing an effective ANN model (El-Chabib et al. 2003). These steps are: (i) Database selection, (ii) Network architecture selection, and (iii) Network training and validation.

5.4 Database selection

The selection of the database to train a neural network is very critical. The generated database for the training process should contain the necessary information to teach the network the relationships between the inputs and outputs. Two important principles must be considered in the generated database: (i) the database should contain complete information about the relationships between the inputs and outputs, and (ii) the training data should be large enough and continuous for the training process.

The results from the parametric study conducted in Chapter 4 were used in constructing the used database. The main parameters in the parametric study were the basic factors that affect the effective moment of moment of inertia I_e, cross-section dimensions (h and b), reinforcement ratio ρ, modulus of elasticity of the reinforcement E, concrete compressive strength $f_c^{'}$, and the applied load level M_a. The parametric study was carried out for simply supported beams loaded with two point loads at third span. The deflection values were calculated using the moment-area method. The corresponding β values were then obtained.

The database was compiled in a patterned format. Each pattern consists of an input vector containing the main inputs, and an output vector containing the corresponding β value for this input. The input vector contains six inputs which are the cross-section height to width ratio h/b, beam slenderness ratio L/h, the ratio between the reinforcement ratio and the balanced reinforcement ratio ρ_s/ρ_b, reinforcement modulus of elasticity E_{SMA}, concrete compressive strength $f_c^{'}$, and the ratio of the applied moment to the cracking moment M_a/M_{cr}.

The database comprised with more than 900 patterns, 750 training pattern and 150 cross-validation pattern, so that it provides the network with sufficient data to capture the relations between each input pattern and the corresponding output value. An additional 150 patterns within the same range of the training data were used to test the network's ability to predict the output when unfamiliar input data is presented. The database contains sections with reinforcement ratios as low as 0.4%, and modulus of elasticity as low as 20,000 MPa. The load range started from the cracking load and extended till the

load causing yielding of the reinforcement. Table 5-3 shows the ranges, mean values and standard deviations of all input and output variables in the final database. Figure 5-3 shows a graphical representation of the selected range of reinforcement ratios versus the corresponding β values.

Table 5-3: Range, average and standard deviation of measured input and output variables

Variable	Training data			Testing data		
	Range	Average	Standard deviation	Range	Average	Standard deviation
h/b	0.83 to 2.67	1.97	0.27	0.83 to 2.67	1.98	0.28
L/h	7.50 to 15.00	10.01	0.97	7.50 to 15.00	9.96	0.97
ρ_s/ρ_b	0.17 to 1.74	0.62	0.34	0.17 to 1.74	0.62	0.35
E_{SMA} (MPa)	20,000 to 65,000	42200	13052	20,000 to 65,000	41454	13168
f'_c (MPa)	20 to 55	40.36	4.79	20 to 55	40.45	4.40
M_a/M_{cr}	1.00 to 7.42	2.84	1.36	1.04 to 6.49	2.75	1.22
β	0.01 to 2.13	0.52	0.47	0.01 to 2.13	0.52	0.42

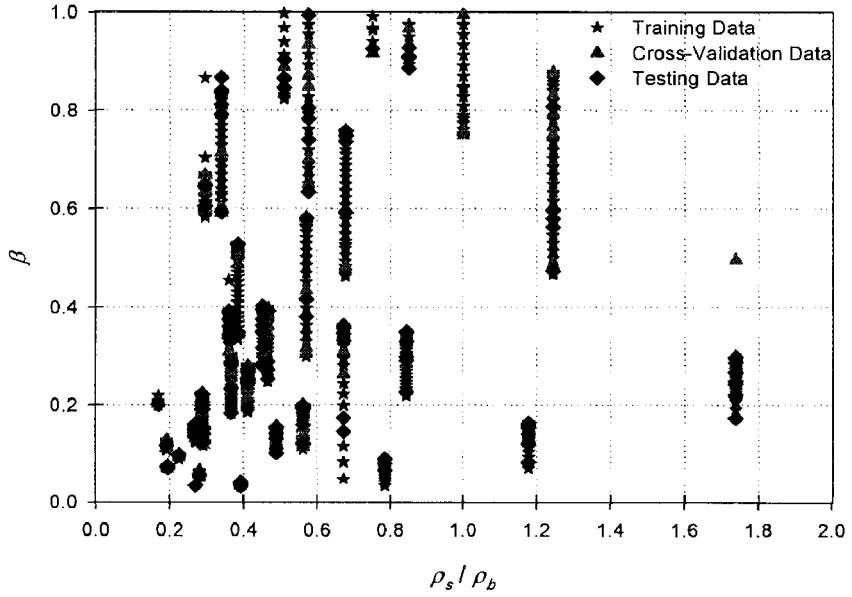

Figure 5-3: Graphical representation of the selected reinforcement ratios and the corresponding β values.

5.5 Selection of network architecture

As mentioned earlier, the feed-forward back-propagation neural networks are believed to be most suited for engineering applications. Therefore, it was used in this study to predict the reduction factor β. As there is no rules to determine the architecture of a neural network that would result in best performance, a trial and error approach was adopted. Many network architectures were tested. Some of these architectures had one, two, or three hidden layers. It should be noted that it is possible to obtain different network architectures that result in satisfactory performance. A network architecture that consists of an input layer, an output layer, and three hidden layers was found to offer best performance in the present study, Figure 5-4.

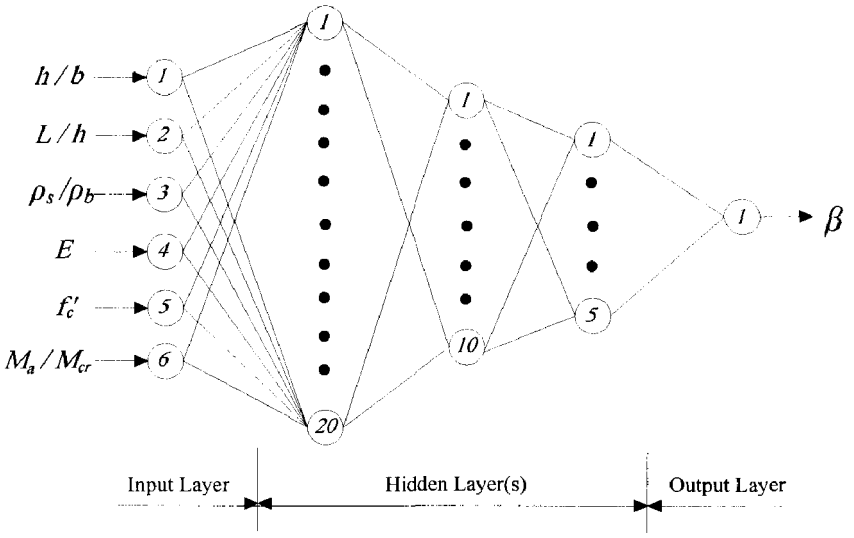

Figure 5-4: Schematic diagram for the selected network architecture.

The input layer consists of six processing units (neurons) that represent the parameters affecting the reduction factor β value. The output layer contains one processing unit which represents the reduction factor β. The first hidden layer consists of 20 neurons; the second hidden layer consists of 10 neurons, while the third layer contains 5 neurons. Connections between the neurons in the different layers were adopted. A sigmoid function was used as the transfer (activation) function for all of the processing units in the hidden and output layers.

The learning algorithm used in this study is the Levenberg-Marquardt algorithm (Demuth and Beal 1998). The main advantage of this learning algorithm is simplifying the learning process and reducing the time required for training. The Levenberg-Marquardt algorithm propagates the error computed at the output layer back to the network. However, this propagation is based on the Jacobian matrix J that contains the first derivatives of the

network errors with respect to weights and biases (Nehdi et al. 2001b). One iteration of the Levenberg-Marquardt algorithm is given by Equation [5-5].

$$W_{k+1} = W_k - \left[J^T J + \mu I\right]^{-1} J^T e \qquad [5\text{-}5]$$

Where: W_k is a vector of current weights and biases, μ is a learning rate, J is the Jacobian matrix, J_T is the transpose of the Jacobian matrix, I is the identity matrix, and e is a vector of the network errors.

5.6 Network training and validation

Training a MLP network is basically teaching it the embedded relationships between the inputs and outputs. However, the learning process is usually complex. It depends on several undefined parameters. During the training process, the MLP searches for the optimum connections' weights (strengths) between the processing units to predict accurate values of the outputs.

The training process can be performed in either a supervised or unsupervised manner. In a supervised training, the network is provided with patterns of data which contains the input data and the corresponding output values. Thus, the network is told what to learn. In an unsupervised training, there are no target outputs. The network is provided only with the input data. Therefore, the network must modify its weights and biases based on the input data only by categorizing the input patterns into a finite number of classes. Once the network is successfully trained, it should not only successfully predict the output of the

training data, but it should also be able to accurately predict the output of unfamiliar sets of input data located within the range of the training data (Nehdi et al. 2001b).

The training process of a MLP network is usually done in two stages: (i) Feed – forward, and (ii) Back – propagation. During the feed-forward stage, the data flow from the input processing units to predict the desired network output, β. Then, the obtained output is compared to a predefined output. If the difference is greater than a predefined tolerance, the error is propagated backward from the output layer to modify the network connections weights (back-propagation stage). The back propagation of the error is performed in the present model based on the Levenberg-Marquardt algorithm as explained earlier. Figure 5-5 shows a flow chart of the training process.

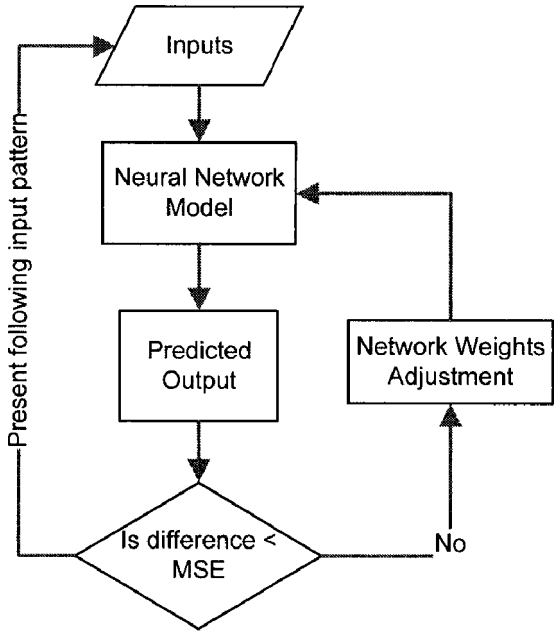

Figure 5-5: Flow chart of the training process.

The training process of the selected network to predict the reduction factor β is an iterative process, which includes feeding the selected network with data as pairs (input/output). The input data includes (h/b, L/h, ρ_s/ρ_b, E, f'_c, M_a/M_{cr}), while the output includes the target value of β. Based on these pairs of data, the network modifies its weights based on the Levenberg-Marquardt algorithm. The network receives the first input vector, carries out the appropriate computations and activation through the processing units in the hidden layers, and produces an output value for β. The network compares its output to the corresponding target provided in the training pair (the predefined output value for this input vector). The difference between the network output and target value is then calculated and stored. After the first training pattern is completed, the network is provided with a second training pair, and so on until the network goes through all data available for training. This completes the first epoch. After each epoch, the mean squared of all errors is calculated and stored. Then, the network back-propagates the error using the assigned learning algorithm to adjust the weights and biases for all processing units in the network (Nehdi et al. 2001b).

The training process continues till either the network converges, or it reaches an acceptable tolerance between the predicted value of β and the desired target value provided for training, or the maximum number of epochs provided for early stopping is reached. The desired error at the output layer was selected as 1E-05, while the maximum number of epochs was selected as 10,000 epochs. It was observed that for all of the analysis cases, the training process stopped because of reaching the desired tolerance rather than reaching the maximum number of epochs.

5.7 Results and discussion

The acceptance/rejection of an ANN model for predicting the reduction factor β for the deflection calculations of SMA RC members depends on its ability to generalize its predictions to new input patterns not previously used in network training. Good generalization mainly depends on the final set up of weights and biases, and the degree of success of the training process. In other words, before testing the model's ability to generalize, the success of the training process must first be evaluated. In addition, the model response to training patterns should be evaluated.

5.7.1 Performance of ANN using training data

The selected network architecture (Figure 5-4) was trained to predict the reduction factor β that can be used to predict the deflection of SMA RC members. As there is no clear trend in neural predictions for either over- or underestimating the reduction factor, the reliability of its predictions was evaluated using the average absolute error (AAE) given by Equation [5-6].

$$AAE = \frac{1}{n}\sum_{i=1}^{n}\frac{|\beta_{\text{Analytical}} - \beta_{\text{Predicted}}|}{\beta_{\text{Predicted}}} \qquad [5\text{-}6]$$

Where: n is the number of the data patterns.

The network was trained using 900 training patterns selected from the results of the parametric study conducted in Chapter 4 to predict the reduction factor β. These patterns

were divided into two sets. The first set is the training set (750 patterns), while the other is the cross-validation set (150 patterns). Each training pattern consists of an input vector of six elements representing the factors affecting the β value, and a target representing the corresponding value of β. After completing the training process, the performance of the network was first checked using the input patterns used in the training process. The response is plotted in Figure 5-6-(a) and Figure 5-6-(b). The predicted values from the network were plotted versus the values obtained from the parametric study. As shown in the figures, the network has successfully learned the relationships between the input and corresponding output values. The network performance was satisfactory and an AAE of 0.99% was observed for the training data, while an AEE of 2.90% was observed for the cross-validation data.

5.7.2 Performance of ANN using testing data

As explained earlier, the acceptance/rejection of a trained neural network is determined by its ability to generalize its predictions beyond the training data. The network model should be able to successfully predict the reduction factor β when presented with new data and unfamiliar to the network (not used in training). The model was presented with an input vector consisting of 150 input patterns that are new to the network and no knowledge of the exact values of β was provided. Figure 5-6-(c) shows that the model successfully predicted the testing data. An AAE of 4.20% was observed, indicating that the model predictions are appropriate.

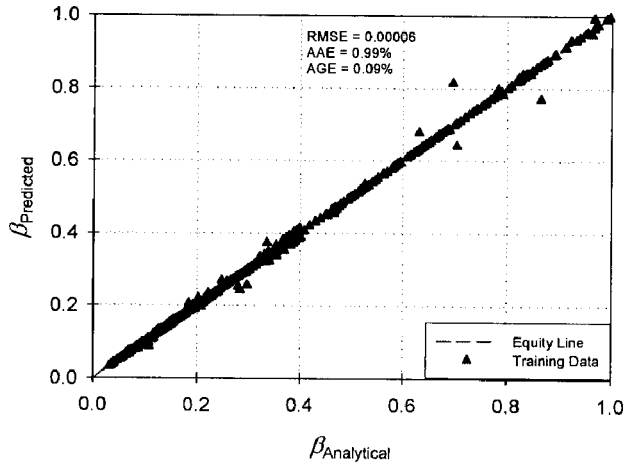

(a) Training data

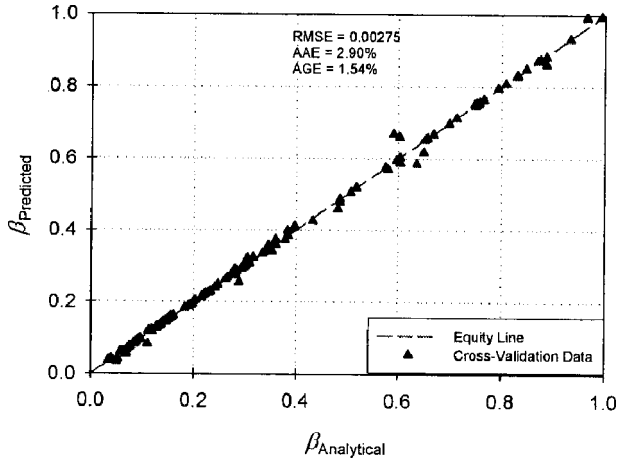

(b) Cross-validation data

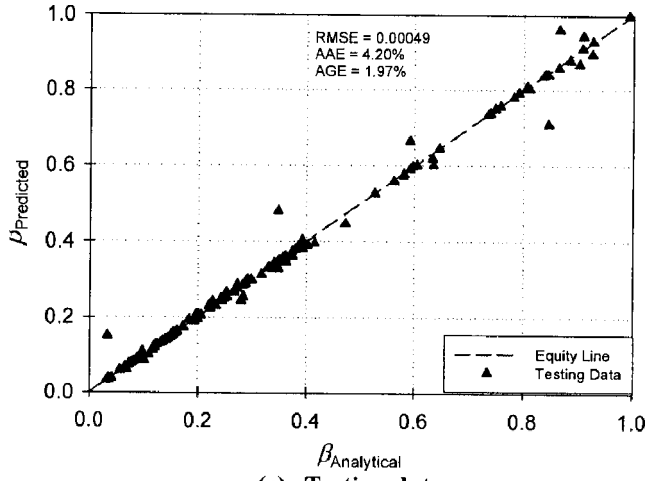

(c) Testing data

Figure 5-6: ANN model response in predicting the training, cross-validation, and testing data output.

5.8 Sensitivity analysis

The ANN model thus developed showed superior performance and demonstrated its ability to predict the reduction factor β. This section examines the ability of the developed model to capture the effects of the individual input parameters on the desired output value β. The strategy adopted to examine the sensitivity of the developed model to the input parameters consists of randomly selecting one database pattern from the training data, and subsequently create other database patterns by changing the parameter of interest, while keeping all other input parameters unchanged. The levels of the parameters of interest in the created database records are not similar to those of the training data to avoid the possibility that the ANN had memorized the output of such data.

The sensitivity of the proposed model to h/b, L/h, and f_c' values was evaluated. Two input records that have a reinforcement ratio of 0.40% and 0.62% were used in the analysis. Values of 0.25% and 0.35% were assigned to the ρ_s/ρ_b input parameter, while a value of 40,000 MPa was assigned to the E input parameter. The load level was kept constant with M_a/M_{cr} = 1.20. The h/b input parameter was varied from 0.85 to 2.60 with a step of 0.05. A step of 0.1 was used to increase the L/h input parameter from 8.00 to 15.00. The f_c' input parameter was varied within the normal strength concrete range, 20 MPa to 55 MPa. Figures 5-7-(a) to 5-7-(c) indicate a minor sensitivity of the proposed model to the h/b, L/h, and f_c' input parameters, respectively.

The effect of the ρ_s/ρ_b and E input parameters on the predicted value of β was studied by constructing two separate databases which have constant input parameters while varying

the ρ_s/ρ_b and E input parameters, respectively. The h/b, L/h, f_c', and M_a/M_{cr} input parameters were chosen as 2.00, 10.00, 40 MPa, and 1.20, respectively. The ρ_s/ρ_b input parameter was varied between 0.18% to 1.70%. A step of 0.05 was used. Values between 20,000 MPa and 65,000 MPa were assigned to the E input parameter. As shown in Figure 5-7-(d) and Figure 5-7-(e), a significant increase in the β value was observed with the increase in the ρ_s/ρ_b and E input parameters.

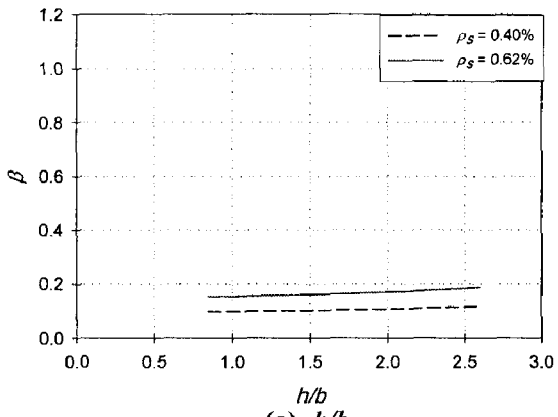

(a) *h/b*

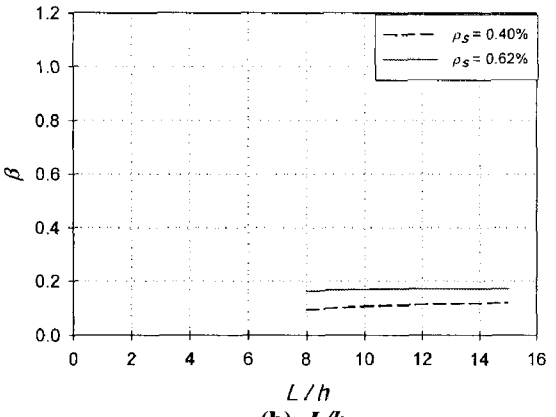

(b) *L/h*

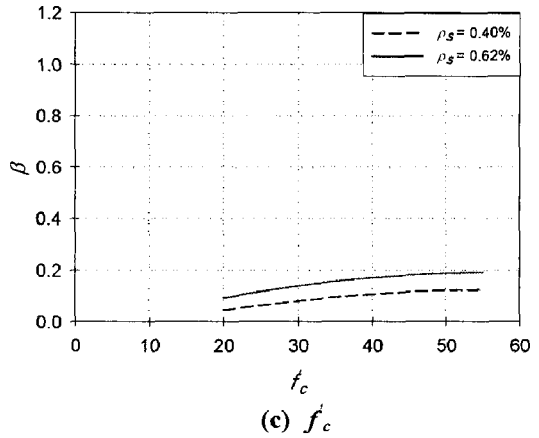

(c) f'_c

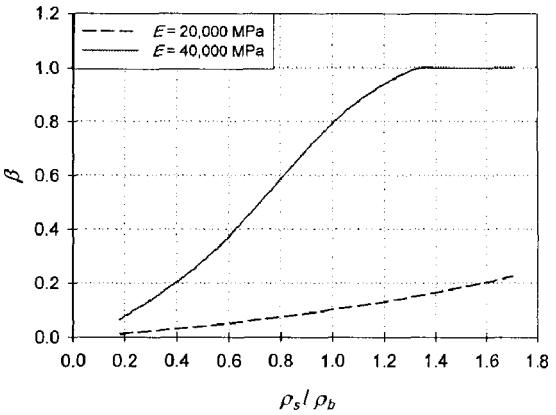

(d) ρ_s/ρ_b

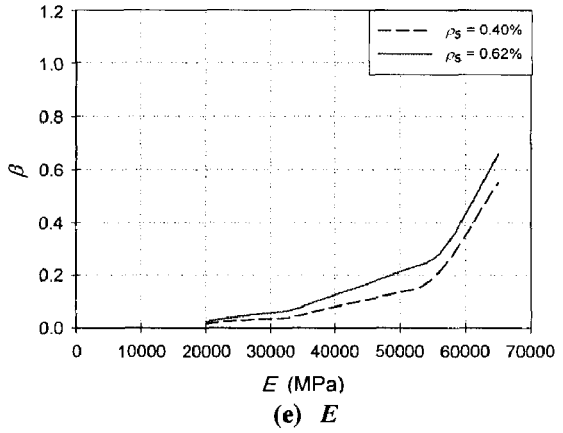

(e) *E*

Figure 5-7: Sensitivity of the ANN model.

5.9 Proposed model

From the sensitivity analysis carried out in the previous section, it is clear that the main factors affecting the reduction factor β are the section reinforcement ratio, and the reinforcement modulus of elasticity. Thus, a new database was developed with constant parameters b/h, L/h, f'_c, ρ_s/ρ_b varying between 0.17 to 1.0, and modulus of elasticity values of 20,000 MPa, 25,000 MPa, 30,000 MPa, 35,000 MPa, 40,000 MPa, and 50,000 MPa. The response of the model was summarized in Figure 5-8. Knowing the section reinforcement ratio, and the reinforcement modulus of elasticity value, the reduction factor β value can be obtained from this figure. This chart can offer a simplified design tool.

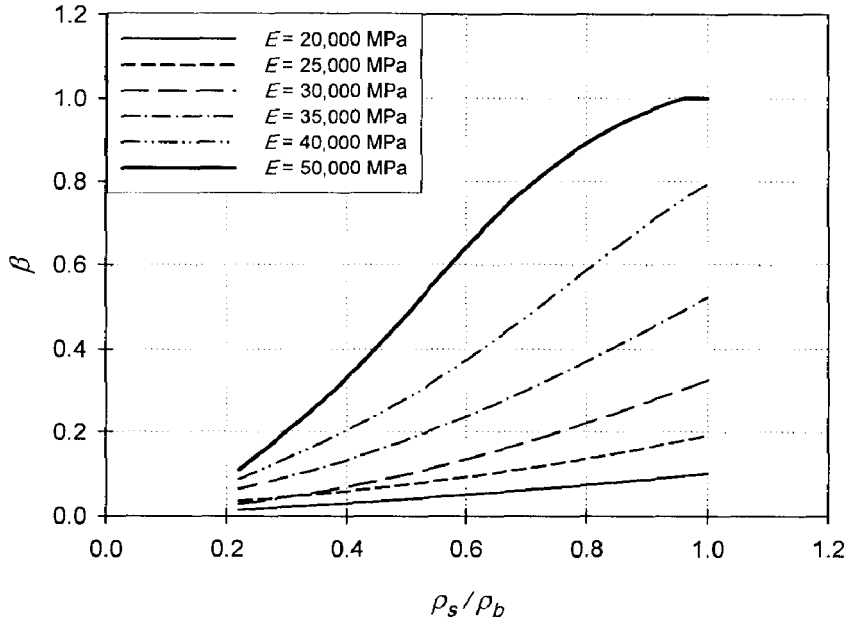

Figure 5-8: Developed chart for predicting the reduction factor β.

5.10 Design example

A design example is worked out for a 7.0 m span simply supported beam. The beam is reinforced with SMA that has a yield stress of 401 MPa. The concrete is assumed to be normal-strength concrete with a compressive strength of 35 MPa. As shown in Figure 5-9, the beam has a cross-section height and width of 700 mm, and 300 mm, respectively. In addition to its own weight, the beam supports two point loads at third span. As the service load can be represented by a range rather than a specific value, total service moment levels of 1.2 M_{cr}, 1.5 M_{cr}, 2.0 M_{cr}, and the moment causing a stress of 0.6 $f_{y\text{-}SMA}$ in the SMA were chosen to represent the range of service load conditions.

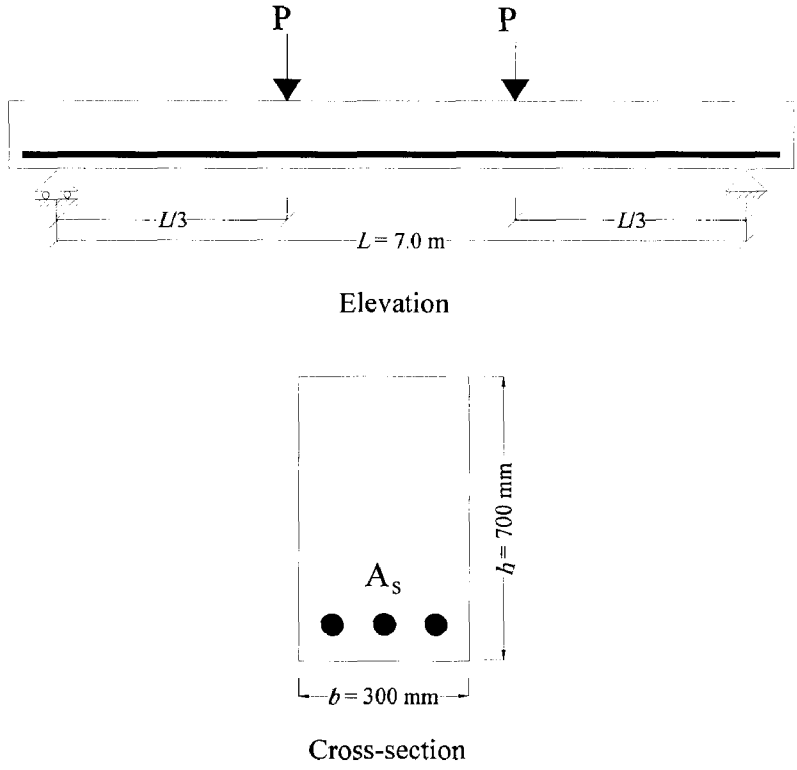

Figure 5-9: Elevation and cross-section details of the beams used in the design example.

As explained above, the cross-section reinforcement ratio and the reinforcement modulus of elasticity greatly affect the deflection of SMA RC members. Thus, in this example, three different reinforcement ratios were chosen as 0.35%, 0.70%, and 0.90%. For each reinforcement ratio, modulus of elasticity values of 20,000 MPa, 25,000 MPa, 30,000 MPa, 35,000 MPa, 40,000 MPa, and 50,000 MPa were assigned. The deflection analysis was performed first using the moment-area method. Then, the deflection analysis was performed using Branson (1963), ACI 440.1R-03 (2003), ACI 440.1R-04 (2004), and the proposed β values (Figure 5-10). The exact deflection values were plotted versus the different models predictions as shown in Figure 5-10. Superior performance for the ANN model can be observed.

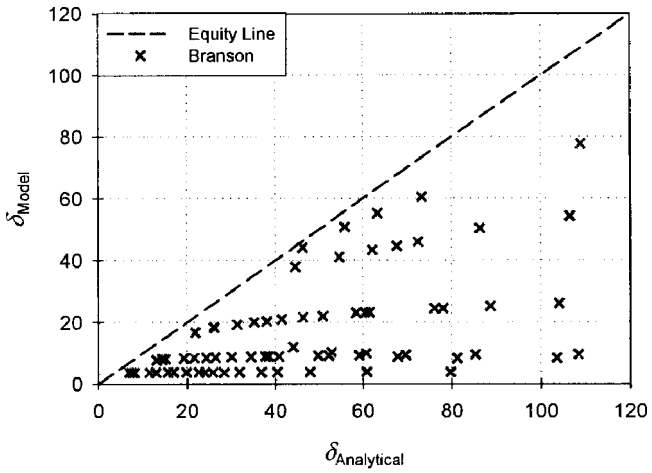

(a) Branson (1963)

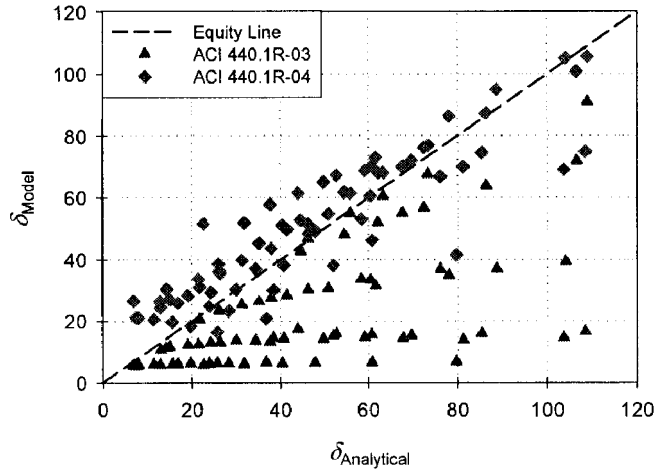

(b) ACI 440.1R-03 (2003) and ACI 440.1R-04 (2004)

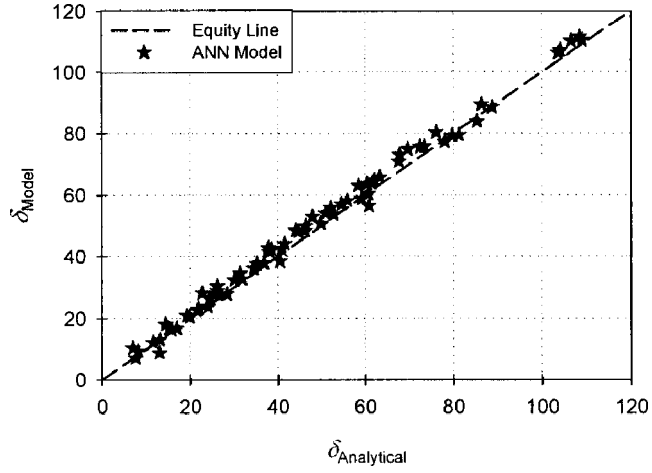

(c) ANN

Figure 5-10: Design example: moment-area method versus different models deflections.

5.11 Conclusions

This paper presents a non-traditional approach for predicting the deflection of SMA RC members. ANN model was developed to predict the reduction factor β to be used in the calculation of the effective moment of inertia I_e. First, a database was developed using the results obtained from the parametric study conducted in Chapter 4. The database includes the main factors affecting the effective moment of inertia I_e: cross-section height to width ratio h/b, beam slenderness ratio L/h, the ratio between the used reinforcement ratio to the balanced reinforcement ratio ρ_s/ρ_b, reinforcement modulus of elasticity E, concrete compressive strength f_c', and the applied load level as a ratio between the applied moment and cracking moment M_a/M_{cr}. The network architecture that results in the optimum performance was subsequently selected based on a trial and error approach.

After the ANN model was successfully trained, the ANN model showed superior performance not only in predicting the training data output, but also in predicting the output for testing data unfamiliar to the model. A sensitivity analysis was carried out to study the effects of the individual input parameters on the predicted values of β. While h/b, L/h, and f_c' did not have a significant effect on the predicted β values, ρ_s/ρ_b and E were found to greatly affect β.

A new database was developed using a range of ρ_s/ρ_b and different E values. The results for this database were presented in a chart format that can be easily used by designers to estimate the deflection of SMA RC members. Knowing the cross-section reinforcement ratio and the reinforcement modulus of elasticity, the reduction factor β can be obtained

from the chart. To illustrate the feasibility of using the developed chart to predict the deflection of the SMA RC members, a deign example was discussed. The developed chart showed superior performance to that of existing design tools.

5.12 References

ACI 318 (2005). Building Code Requirements for Structural Concrete and Commentary, American Concrete Institute, Farmington Hills, Michigan.

ACI 440 (2003). Guide for the Design and Construction of Concrete Reinforced with FRP Bars, American Concrete Institute, Farmington Hills, Michigan, 42 p.

ACI 440 (2004). Guide for the Design and Construction of Concrete Reinforced with FRP Bars, Proposed Revision, American Concrete Institute, Farmington Hills, Michigan, 35 p.

Ackley, D.H., Hinton, G.E., and Sejnowski, T.J. (1985). "A Learning Algorithm for Boltzmann Machines." Cognitive Science, 9(1), 147-169.

Alam, M.S., Youssef, M.A., and Nehdi, M. (2007). "Utilizing Shape Memory Alloys to Enhance the Performance and Safety of Civil Infrastructure: a Review." Canadian Journal of Civil Engineering, 34(9), 1075-1086.

Bischoff, P.H. (2005). "Reevaluation of Deflection Prediction for Concrete Beams Reinforced with Steel and Fiber Reinforced Polymer Bars." Journal of Structural Engineering, 131(5), 752-762.

Bischoff, P.H., and Scanlon, A. (2007). "Effective Moment of Inertia for Calculating Deflections of Concrete Members Containing Steel Reinforcement and Fiber-Reinforced Polymer Reinforcement." ACI Structural Journal, 104(1), 2007, 68-75.

Branson, D.E. (1963). "Instantaneous and Time-Dependent Deflections of Simple and Continuous Reinforced Beams." HPR Rep. No. 7, Part 1, Alabama Highway Department, Bureau of Public Roads, Montgomery, Ala, 78 p.

Charniak, E., and McDermott D. (1985). Introduction to Artificial Intelligence, Addisoon-Wesley Publishing Company, Reading Massachusetts, USA, 701 p.

CSA A23.3-04 (2004). Design of Concrete Structures, Canadian Standards Association, Rexdale, Ontario, Canada, 240 p.

Demuth, H., and Beal, M. (1998). "Neural Network Tool Box for Use with MATLAB Version 3." The Math Works Inc., 5.20-5.58.

Dolce, M., and Cardone, D. (2001). "Mechanical Behaviour of Shape Memory Alloys for Seismic Application 1: Martensite and Austenite NiTi bars subjected to torsion." International Journal of Mechanical Sciences, 43, 2631 56.

Eggeler, G., Hornbogen, E., Yawny, A., Heckmann, A. and Wagner, M. (2004). "Structural and Functional Fatigue of NiTi Shape Memory Alloys." Materials Science and Engineering, A 378 (1-2), 24-33.

Elbahy, Y.I., Youssef, M.A., and Nehdi, M. (2008). "Flexural Behaviour of Concrete Memebers Reinforced with Shape Memory Alloys." 2nd Canadian Conference on Effective Design of Structures, McMaster University, Hamilton, Ontario, Canada, 477-486.

El-Chabib, H., and Nehdi, M. (2006). "Effect of Mixture Design Parameters on Segregation of Self-Consolidating Concrete." ACI Materials Journal, 103(5), 374-383.

El-Chabib, H., Nehdi, M., and Sonebi, M. (2003). "Artificial Intelligence Model for Flowable Concrete Mixtures Used in Underwater Construction and Repair." ACI Materials Journal, 100(2), 165-173.

Grandhi, F., and Wolons, D. (1999). "Characterization of the Pseudoelastic Damping Behavior of Shape Memory Alloy Wires Using Complex Modulus." Smart Materials and Structures, 8, 49 56.

Haykin, S. (1994). Neural Networks: a Comprehensive Foundation, Macmillan, New York, 842 p.

Hopfield, J.J. (1982). "Neural Networks and Physical Systems with Emergent Collective Computational Abilities." Proceedings, National Academy of Science, USA, 79(8), 2554-2558.

Hornbogen, E. (2004). "Review: Thermo-Mechanical Fatigue of Shape Memory Alloys." Journal of Material Science, 39(2), 385-399.

Ip, K.H. (2000). "Energy Dissipation in Shape Memory Alloy Wire under Cyclic Bending." Materials and Structures, 9, 653 9.

Janke, L., Czaderski, C., Motavalli, M., and Ruth, J. (2005). "Applications of Shape Memory Alloys in Civil Engineering Structures - Overview, Limits and New Ideas." Materials and Structures, 338(279), 578-592.

Kohonen, T. (1982). "Self-Organized Formation of Topologically Correct Feature Maps." Biological Cybernetics, 43, 59-69.

Nehdi, M., Djebbar, Y., and Khan, A. (2001a). "Neural Network Model for Preformed-Foam Cellular Concrete." ACI Materials Journal, 98(5), 402-409.

Nehdi, M., El-Chabib, H., and El-Naggar, M. (2001b). "Predicting the Performance of Self-Compacting Concrete Mixtures Using Artificial Neural Networks." ACI Materials Journal, 98, 394-401.

Piedboeuf, M.C., and Gauvin, R. (1998). "Damping Behaviour of Shape Memory Alloys: Strain Amplitude, Frequency and Temperature Effects." Journal of Sound and Vibration, 214(5), 885 901.

Rosenblatt, F. (1958). "The Perceptron: A Probabilistic Model for Information Storage and Organization in the Brain." Psychological Review, 65(6), 386-408.

Rumelhart, D.E., Hinton, G.E., and William, R.J. (1986). "Learning Internal representation by error Propagation." Parallel Distributed Processing, Foundation, MIT Press, Cambridge, Mass, 1, 318-362.

Saiidi, M.S., Sadrossadat-Zadeh, M., Ayoub, C., and Itani, A. (2007). "Pilot Study of Behavior of Concrete Beams Reinforced with Shape Memory Alloys." ASCE, Journal of Materials in Civil Engineering, 19(6), 454-461.

Smithers, T., Conkie, A., Doheny, J., Logan, B., Millington, K., and Tang, M. X. (1990). "Design as Intelligent Behavior: an AI in Design Research." Journal of Artificial Intelligence in Engineering, 5(2), 78-109.

Chapter 6 Summary and Conclusions

6.1 Summary and conclusions

This thesis examines the behaviour of shape memory alloy (SMA) reinforced concrete (RC) members and addresses the advantages of using the SMAs as primary reinforcement for concrete structures. A literature review on the SMAs manufacturing process, material modelling, and unique properties from the civil engineering point of view was first carried out. Known applications of SMAs as primary reinforcement for reinforced and prestressed concrete structures were summarized. The reviewed studies showed the superior performance of SMA RC members in recovering deformations upon unloading. Because of the lack of design standards for SMA RC members, the author decided to study the flexural behaviour of SMA RC members for both strength and serviceability requirements.

6.1.1 Strength requirements

The flexural behaviour of SMA RC sections was investigated and compared to steel RC members. The validity of using sectional analysis for SMA RC members was confirmed through comparison with available experimental work. A parametric study was then conducted. Effect of cross-section height, cross-section width, tensile and compressive reinforcement ratios, concrete compressive strength, and axial load level on the flexural behaviour of SMA RC sections was discussed. For each of the studied sections, the

moment capacity M_u, the corresponding curvature Φ_{max}, and maximum top concrete strain $\varepsilon_{c\text{-}max}$ were recorded. Based on the obtained results, the following conclusions were drawn:

(1) SMA bars did not yield for axial loads with $ALI > 0.2$. This is attributed to their modulus of elasticity and high ultimate strain.

(2) Failure of steel RC sections varied between rupture of steel reinforcement and concrete crushing. However, the failure of SMA RC sections occurred only by crushing of concrete. This is attributed to the high ultimate strain of SMA bars.

(3) Results from the parametric study at different axial load levels were used to develop normal force-moment interaction diagrams for SMA RC sections. SMA RC sections did not exhibit the balanced condition (simultaneous concrete crushing and reinforcement yielding). However, a similar point was obtained that corresponds to ALI of about 0.4.

(4) The ultimate top concrete strain $\varepsilon_{c\text{-}max}$ was found to be dependent on the axial load level for SMA RC sections. A relationship between $\varepsilon_{c\text{-}max}$ and the axial load level was developed based on linear interpolation. Two equations were proposed to calculate α_1 and β_1 values for SMA RC sections. These equations were validated by comparing the moment capacity calculated based on these equations to that obtained from the moment-curvature relationship. The proposed equations showed superior performance compared to the equations proposed by the Canadian standards.

6.1.2 Serviceability requirements

The load deflection behaviour of SMA RC members was investigated through a parametric study. The studied parameters were cross-section height, cross-section width, reinforcement ratio, reinforcement modulus of elasticity, and concrete compressive strength. Moment-curvature analysis was utilized to calculate deflections through the moment-area method. Ability of the moment-area method to predict deformations of SMA RC members was confirmed by comparing its predictions to available experimental work. Results from the parametric study were used to assess the suitability of the available models for deflection analysis of SMA RC members. Based on the observed results, the following conclusions were drawn:

(1) The equation provided by the Canadian standards, A23.3-04 (2004), for deflection calculation was found to significantly overestimate the flexural stiffness of SMA RC members, and thus significantly underestimate the member deflection. This overestimation of the member flexural stiffness is attributed to the significant difference between the modulus of elasticity of steel and SMA.

(2) The model proposed by Bischoff (2007) was found to have the best performance in predicting the deflection of SMA members having reinforcement ratios greater than 0.6%. For lightly reinforced members (ρ < 0.6%), Bischoff's model was found to be un-conservative and ISIS design manual (2001) gave good estimates.

The need for a new model that is capable of accurately predicting the deflection of SMA RC members motivated the author to utilize artificial neural networks (ANNs) to develop such a model. The main idea is calculating a reduction factor β to be used in the calculation of the effective moment of inertia for SMA RC members. First, a database was developed using the results obtained from the previously explained parametric study. The main factors affecting the moment of inertia I_e such as cross-section height to width ratio h/b, beam slenderness ratio L/h, the ratio between the used to the balanced reinforcement ratio ρ_s/ρ_b, reinforcement modulus of elasticity E, and the ratio between the applied to the cracking moments M_a/M_{cr} were considered. Based on trial and error approach, the network architecture that results in the optimum performance was selected.

After the ANN model was successfully trained, it showed superior performance in predicting both the training and testing data. Sensitivity analysis was carried out to study the effect of individual input parameters on the predicted values of β. It was observed ρ_s/ρ_b and E input parameters have a significant effect on the predicted values of β. A new database was developed for ranges of ρ_s/ρ_b and E values. Results obtained using the ANN model were plotted in a figure to facilitate the design process. Based on the cross-section reinforcement ratio and reinforcement modulus of elasticity, the reduction factor β can be obtained. A design example was discussed where the developed model showed superior performance compared to the existing models.

6.2 Recommendation for future work

This study examines the flexural behaviour of SMA reinforced unconfined normal strength concrete members. More research is still needed to address the behaviour of SMA reinforced confined concrete members.

Utilizing SMAs as reinforcing bars for confined high strength concrete will result in taking full advantages of the high strain range of SMA bars. More research is needed to address its behaviour and develop design equations.

Experimental program is needed to investigate the cracking behaviour of SMA RC members. Analytical models needs to be developed to calculate the crack width of SMA RC members.

6.3 References

CSA A23.3-04 (2004). Design of Concrete Structures, Canadian Standards Association, Rexdale, Ontario, Canada, 240 pages.

Bischoff, P. H. (2007b). "Effective Moment of Inertia for Calculating Deflections of Concrete Members Containing Steel Reinforcement and Fiber-Reinforced Polymer Reinforcement." ACI Structural Journal, 104(1), 68-75.

ISIS Canada (2001). Reinforcing Concrete Structures with Fibre Reinforced Polymers, Design Manual 3, Winnipeg, Manitoba.

Appendix I: Finite Element Analysis of SMA RC Beam-Column Joints

To overcome the limitation of the moment-area method to account for the column rotation and joint deformations of the beam-column joint tested by Youssef et al. (2008), non-linear finite element (FE) analysis was carried out to predict the load-deflection behaviour and the beam tip load-beam rotation response using Seismo-Struct (Seismosoft 2008). A 3D inelastic beam-column element has been used in modelling the column and the beam elements of the samples. Static Pushover analysis was carried out to predict the beam tip load-displacement relationship and the beam tip load-rotation relationship. Displacement control loading approach was used in applying the load. As the FE analysis was able to account for the nonlinearity in both geometry and material behaviour, FE analysis was able to accurately predict the load-deformation behaviour of the tested joint and was superior to the moment-area method discussed in Chapter 4, Figure I-1and Figure I-2.

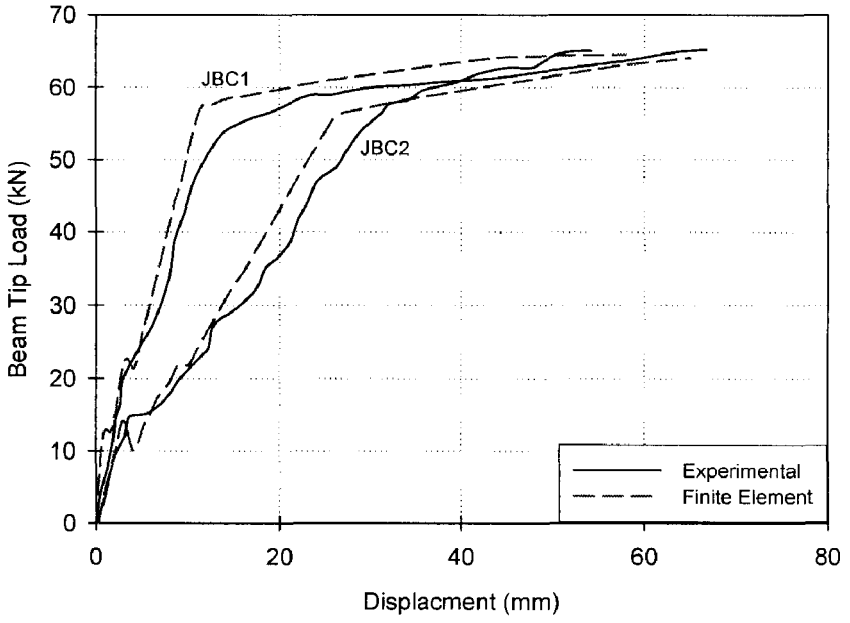

Figure I-1: Load-displacement (Finite Element vs. Experimental)

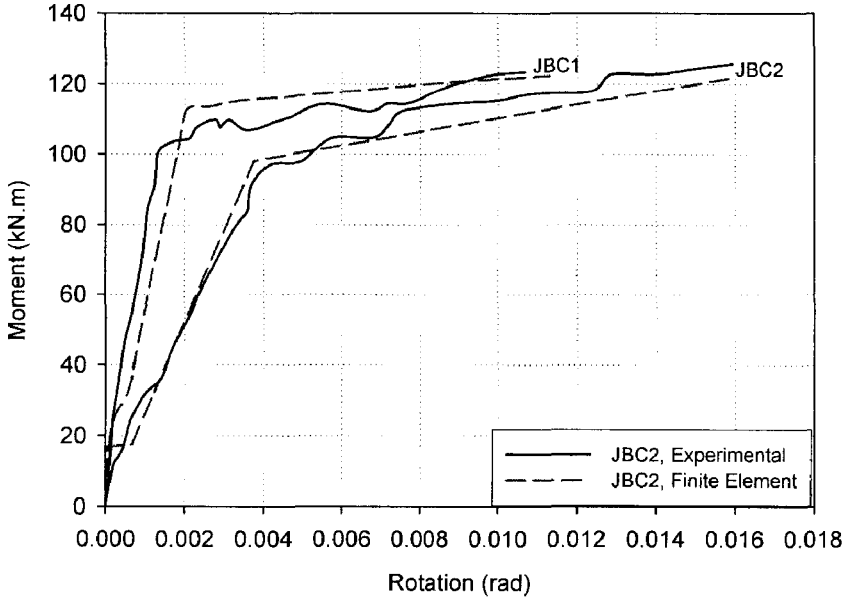

Figure I-2: Moment- beam rotation (Finite Element vs. Experimental)

Appendix II: Crack Width Calculations for SMA Reinforced Concrete Members

Cracking in concrete is unavoidable because of its low tensile strength. Reinforced concrete structures having low reinforcement stresses under service loads undergo very limited cracking, except for the cracks that occurs due to shrinkage of concrete and temperature changes. However, in cases where service loads cause high reinforcement stresses, some visible cracks may be expected under service loads. If these cracks are too wide, the aesthetic of the structure is affected which may provoke adverse criticism. In addition, they expose the reinforcement to the environment, and thus accelerate its corrosion. To minimize the adverse effects of cracking, the design of reinforced concrete structures must ensure that the widths of crack under normal service conditions are within acceptable limits.

Alam et al. (2008) utilized some of the available models in the literature to predict the crack width of the SMA reinforced beam-column joint tested by Youssef et al. (2008). These models were originally developed for steel RC members. The significant difference in the modulus of elasticity of steel and SMA resulted in poor predictions. In this section, the models developed for FRP RC members are examined. The used models are summarized in the following section.

II.1 Crack width models

The control of crack width is addressed in ACI 318-05 (2005) in clause 10.6 (distribution of flexural reinforcement in beams and one-way slabs). For reinforcement with nominal yield strength less than 40 ksi (300 MPa), no specific requirements are necessary. For reinforcement with yield strength greater than 40 ksi (300 MPa), an empirical expression based on the Gergely-Lutz (1968) equation is provided. The expression proposed by Gergely-Lutz is given by Equation [II-1].

$$W = 7.6 \times 10^{-5} \frac{h_2}{h_1} f_s \left(d_c \frac{A_e}{m} \right)^{1/3} \quad \text{[II-1]}$$

ENV 1992-1 (1992) recommends the calculations of the crack width based on the average crack spacing S_m for steel reinforced concrete members subjected to axial tension and/or bending. The expression is given by Equation [II-2].

$$S_m = 50 + 0.5 \, k_1 \, k_2 \frac{d_p}{\rho} \quad \text{[II-2a]}$$

$$w = S_m \cdot \varepsilon_s \cdot \zeta \quad \text{[II-2b]}$$

Nawy and Neuworth (1977) extended the work done by Nawy et al. (1971) and tested additional twelve FRP simply supported beams to failure. The beams were loaded at third-span points. The reinforcement ratio varied from 0.65% to 2.28%. Beams with lower percentage of FRP reinforcement developed very few cracks whereas specimens

with greater amount of reinforcement developed larger number of considerably narrower cracks. Equation [II-3] was proposed as a modified version of Equation [II-1].

$$W = 2.0 \times 10^{-3} \frac{h_2}{h_1} f_f \left(d_c \frac{A_e}{m} \right)^{1/3} \quad \text{[II-3]}$$

Faza and Gangarao (1992a, 1992b) observed that the existing ACI 318 equation is invalid because the modulus of elasticity of FRP is approximately four times smaller than that for steel. Based upon the assumption that the maximum crack width can be approximated by an average bar strain multiplied by the crack spacing, the following expression for the maximum crack width was obtained.

$$W_{max} = \left(\frac{f_f}{E_f} \right) \left(\frac{2 f_t' A}{\mu \pi D} \right) \quad \text{[II-4]}$$

Through theoretical correlation with experimental results, Masmoudi et al. (1998) introduced a coefficient, K_g, to Gergely-Lutz equation in the following form.

$$W = K_g \frac{h_2}{h_1} f_f \left(d_c \frac{A_e}{m} \right)^{1/3} \quad \text{[II-5]}$$

Six FRP RC beams with different amounts of reinforcement were tested by Tountanji and Saafi (1999). Tests were conducted in three series with the number of reinforcing bars being variable in each. It was found that the crack spacing decreased with the increase in

applied load and reinforcement ratio. The following equation was proposed to evaluate the crack width.

$$W = \frac{2 f_o}{E_f}[d + A \tanh\ (\cosh^{-1} \sqrt{\frac{fo}{f_o - \frac{f_t'}{\rho}}})] \qquad \text{[II-6a]}$$

$$A = 70 + f_o\ \ e^{[0.479 - 0.214\, f'^{2/3}_c]} \qquad \text{[II-6b]}$$

Gao et al. (1998) modified the expression proposed by Nawy and Neuworth (1977) to the following expression:

$$W_{max} = 11.2 \times 10^{-6}\ K_f\ \frac{h_2}{h_1}\ f_f\ (d_c\ A)^{1/3} \qquad \text{[II-7a]}$$

The modification coefficient, K_f takes into account the behaviour of FRP bars and is given by the following expression:

$$K_f = K_b \left(\frac{E_s}{E_f} \right) \qquad \text{[II-7b]}$$

ISIS Canada manual (2001) gave an equation similar to that proposed by ACI committee 440 (2000) for FRP RC sections, this equation is given by:

$$W_{max} = 11 \times 10^{-6} \frac{E_s}{E_f} K_b \frac{h_2}{h_1} f_f (d_c A)^{1/3} \quad \text{[II-8]}$$

II.2 Results and discussions

The introduced models were used in calculating the crack width at the maximum load level for the experimental program carried out by Youssef et al. (2008). The predictions are summarized in Table II-1. It is clear from the results that ACI (2005), Masmoudi et al. (1998), and Gao et al. (1998) models were found to significantly underestimate the crack width of the SMA RC at the maximum loading conditions. The model proposed by Nawy and Neuworth (1977) underestimated the crack width by 20%. Eurocode 2 (1992) and Faza and Ganagaro (1992a) models were found to have the best match with the experimental results (5.6%, and 7.5% error, respectively). Toutanji and Saafi (1999), and ISIS design manual (2001) models were much conservative in predicting the crack width. However, ISIS design manual (2001) was found to significantly overestimate the crack width of the SMA RC sections.

Table II-1: Crack width predictions

Used Model	Crack width (mm)
Experimental Results	10.70
ACI 318-95 (1995)	1.15
EuroCode-2 (1992)	10.1
Nawy and Neuworth (1977)	8.60
Faza and Gangarao (1992)	11.50
Masmoudi et al. (1998)	1.67
Toutanji and Saafi (1999)	13.4
Gao et al. (1998)	6.10
ISIS Canada (2001)	17.00

II.3 Conclusions

The available models in the literature for predicting the crack width of FRP RC members were used to predict the crack width of the SMA RC beam-column joint tested by Youssef et al. (2008). The models proposed by EuroCode (1992), and Faza and Ganagaro (1992a) were found to have the best matching with the experimental results. However, more experimental work is required to guarantee the applicability of using these models at different load levels, or to propose new models to calculate the crack width of SMA RC members.

II.4 References

ACI 318 (2005). Building Code Requirements for Structural Concrete and Commentary, American Concrete Institute, Farmington Hills, Michigan.

Alam, M.S., Youssef, M.A., Nehdi, M. (In-press). "Analytical Prediction of the Seismic Behaviour of Superelastic Shape Memory Alloys Reinforced Concrete Elements." Journal of Engineering Structures, Accepted May 2008.

ENV 1992-1 (1992). Eurocode 2: Design of concrete structures – Part 1: General rules and rules for buildings, European Committee for Standardization, rue de Stassart 36, B-1050, Brussels, Belgium.

Faza, S.S., Gangarao, H.V.S. (1992). "Bending and Bond Behaviour of Concrete Beams Reinforced with Fibre Reinforced Plastic Rebars." WVDOH-RP-83 Phase 1 Report, West Virginia University, USA, 128-173.

Faza, S.S., Gangarao, H.V.S. (1992). "Theoretical and Experimental Correlation of Behaviour of Concrete Beams Reinforced with Fiber Plastic Rebars. Fiber-Reinforced-Plastic Reinforcement for Concrete Structures." ACI International Symposium, SP-138, 559-614.

Gao, D., Benmokrane, B., Masmoudi, R. (1998). "A calculating Method of Flexural Properties of FRP-Reinforced Concrete Beams, Part 1: Crack Width and Deflections." Technical Report, Department of Civil Engineering, Université de Sherbrooke, Sherbrooke, Canada.

Gergely P, Lutz LA. (1968). "Maximum Crack Width in Reinforced Concrete Flexural Members. Causes, Mechanism and Control of Cracking in Concrete." American Concrete Institute, SP-20, 87-117.

ISIS Canada (2001). Reinforcing Concrete Structures with Fibre Reinforced Polymers, Design Manual 3, Winnipeg, Manitoba.

Masmoudi R, Thériault M, Benmokrane B. (1998). "Flexural Behavior of Concrete Beams Reinforced with Deformed Fiber Reinforced Plastic Reinforcing Rods." ACI Structural Journal, 95, 665-676.

Nawy, E.G., Neuwerth, G.E. (1977). "Fibreglass Reinforced Concrete Slabs and Beams." ASCE Structural Journal, 103(2), 421-440.

Nawy, E.G., Neuwerth, G.E., Phillips, C.J. (1971). "Behaviour of Fibrer Glass Reinforced Concrete Beams." ASCE Structural Journal, 97(ST9), 2203-2215.

Toutanji, H.A., Saafi, M. (1999). "Deflection and Crack Width Predictions of Concrete Beams Reinforced with Fiber Reinforced Polymer Bars." Proceedings of Fourth International Symposium on Non-Metallic (FRP) Reinforcement for Concrete Structures.

Youssef MA, Alam MS, Nehdi M. (In-press). "Experimental investigation on the seismic behaviour of beam-column joints reinforced with superelastic shape memory alloys." Journal of Earthquake Engineering, accepted January 2008.

Appendix III: Artificial Neural Network Model Performance versus Existing Models

To compare the performance of the developed artificial neural network (ANN) model with the existing models, the predictions of deflection models provided in the design example of Chapter 5 were compared with the deflection values obtained from the moment-area method. The evaluation of the results was done using basic statistical tools such as absolute average error *AEE* and the average algebraic error *AGE*. The *AAE* is given by Equation [III-1] while the *AGE* is given by Equation [III-2].

$$AAE = \frac{1}{n}\sum_{i=1}^{n}\frac{|\delta_{exact} - \delta_{predicted}|}{\delta_{predicted}} \qquad [III\text{-}1]$$

$$AGE = \frac{1}{n}\sum_{i=1}^{n}\frac{|\delta_{exact} - \delta_{predicted}|}{\delta_{predicted}} \qquad [III\text{-}2]$$

Figures (III-1) to (III-6) illustrates the AEEs and the AGE for different modulus of elasticity values of each reinforcement ratio. It is clear from the figures that Branson's equation significantly underestimates the deflection of the SMA RC members. The AAE and the AGE were approaching a value of 100% in some cases. The ACI 440.1R-03 (2003) showed poor predictions in case of low modulus of elasticity values (i.e. E = 20,000 MPa to E = 35,000 MPa). For higher modulus of elasticity values, better predictions were obtained using this model. The ACI 440.1R-04 (2004) showed

satisfactory performance with some cases. However, for low reinforcement ratio (ρ_s = 0.35%), the AEE and the AGE values were not small enough to be neglected. For the ANN model, superior performance was observed for all reinforcement ratios for different modulus of elasticity values.

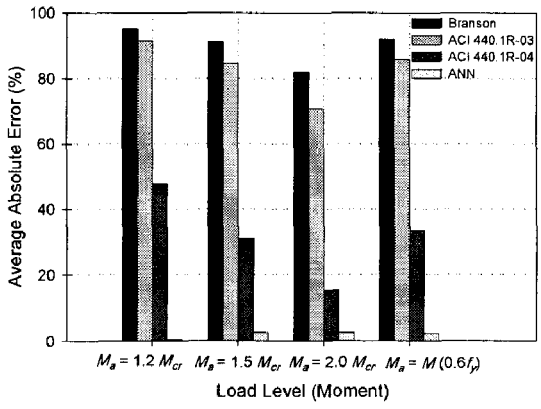

(a) $E = 20{,}000$ MPa

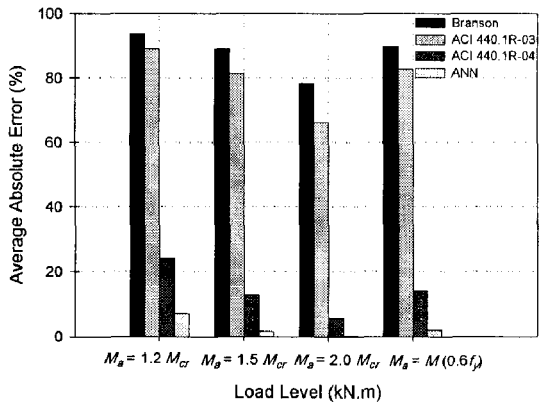

(b) $E = 25{,}000$ MPa

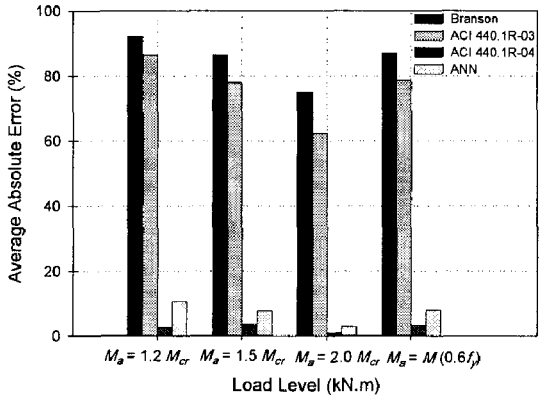

(c) $E = 30{,}000$ MPa

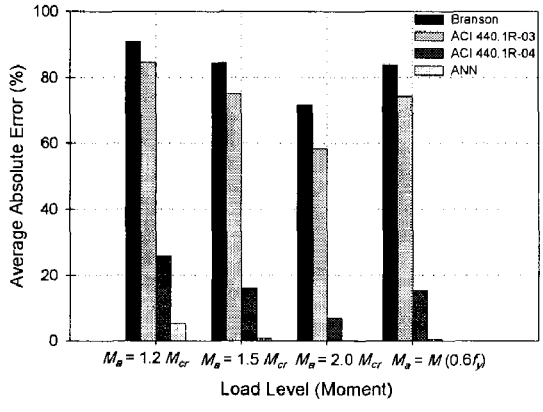

(d) $E = 35{,}000$ MPa

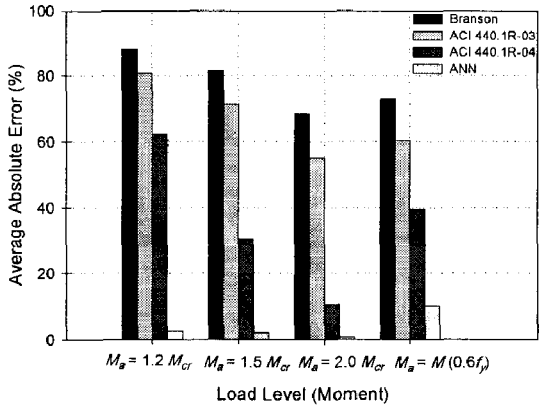

(f) $E = 40{,}000$ MPa

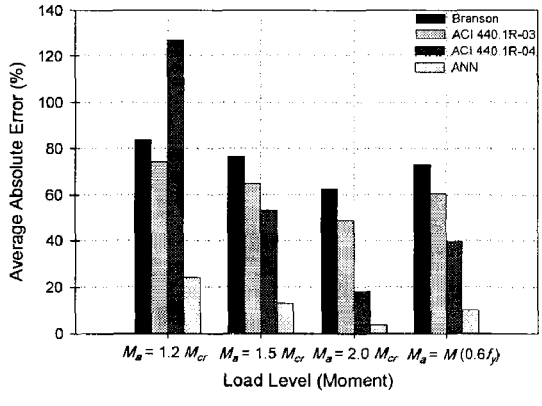

(g) $E = 50{,}000$ MPa

Figure III-1: Average absoluter error for $\rho_s = 0.35\%$ case

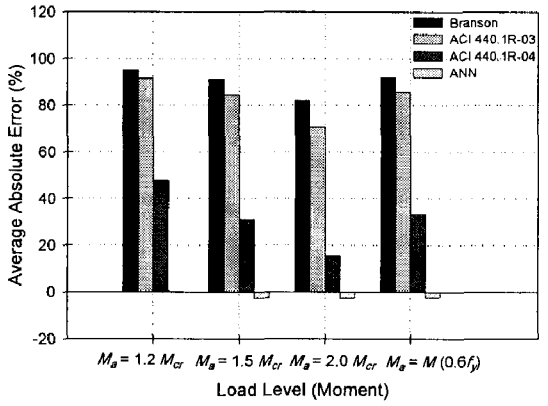

(a) E = 20,000 MPa

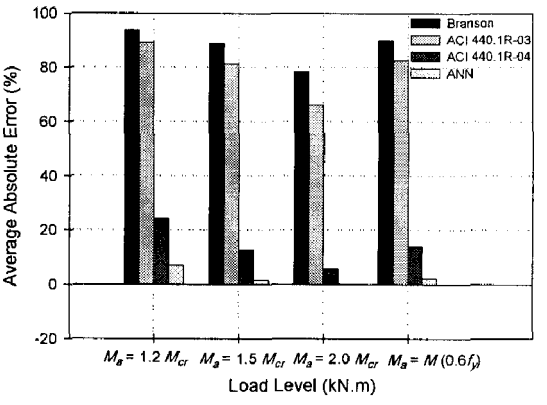

(b) E = 25,000 MPa

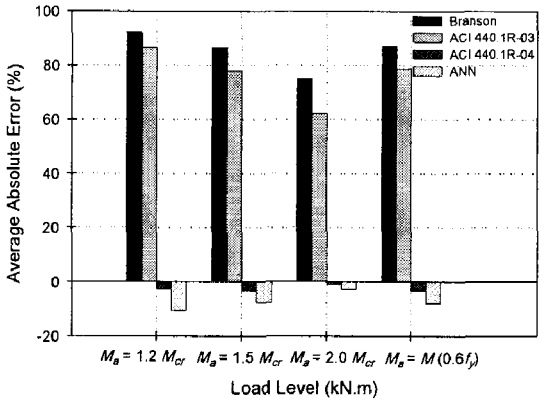

(c) E = 30,000 MPa

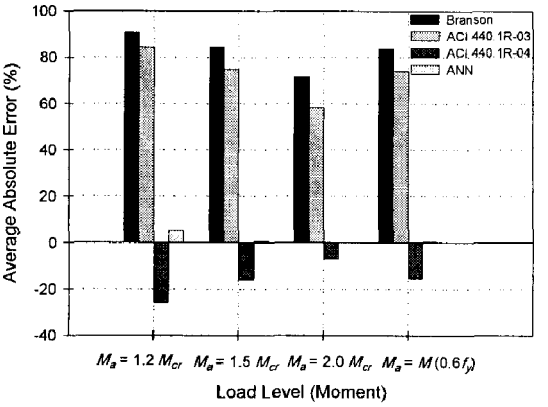

(d) E = 35,000 MPa

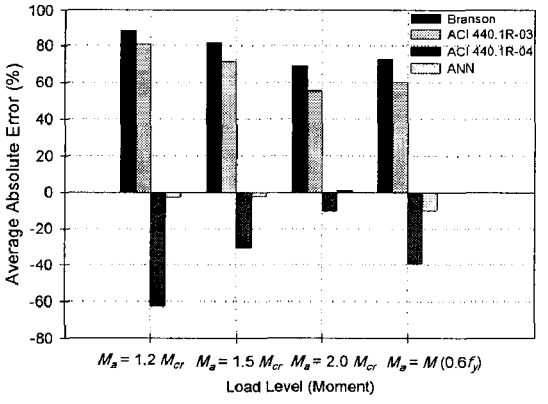

(e) E = 40,000 MPa

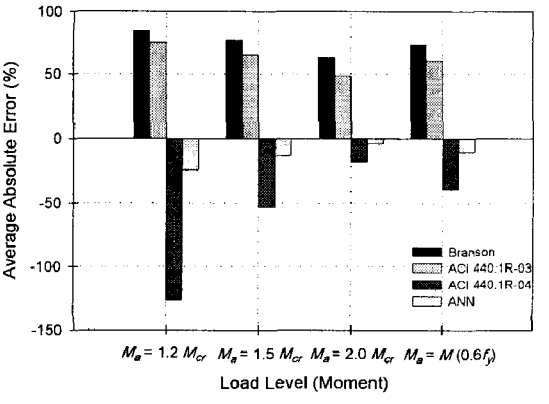

(f) E = 50,000 MPa

Figure III-2: Average algebraic error for ρ_s = 0.35% case

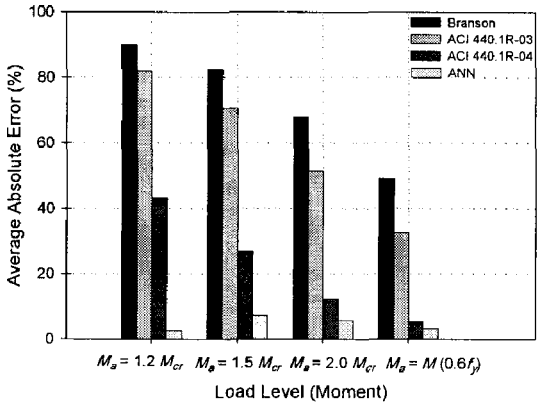

(a) $E = 20{,}000$ MPa

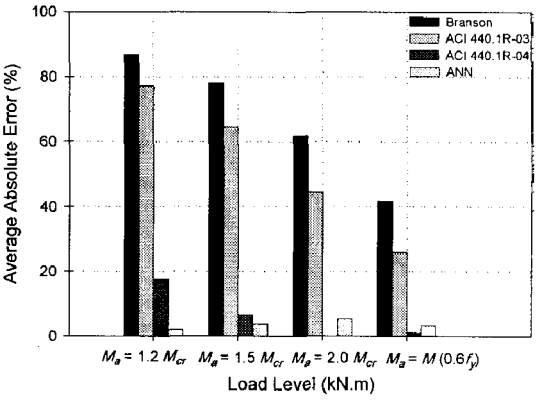

(b) $E = 25{,}000$ MPa

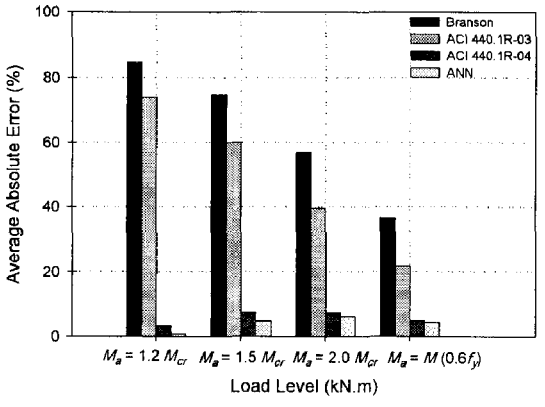

(c) $E = 30{,}000$ MPa

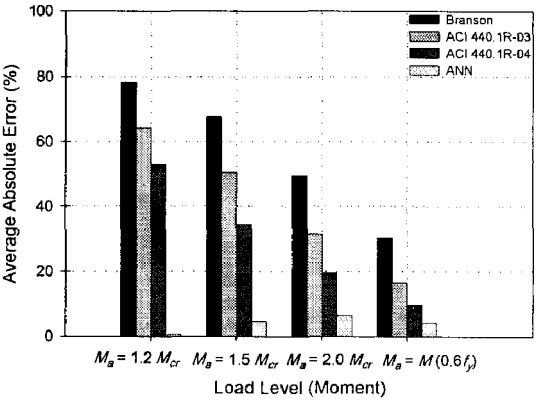

(d) $E = 35{,}000$ MPa

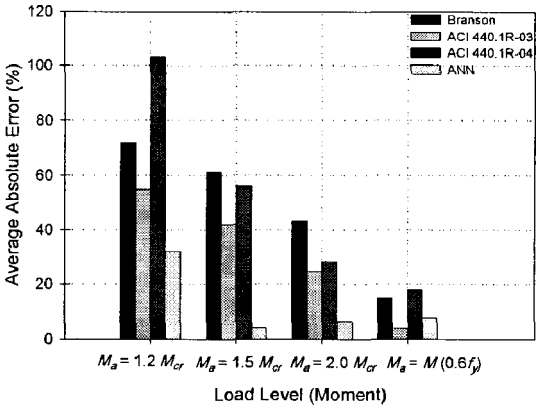

(e) $E = 40{,}000$ MPa

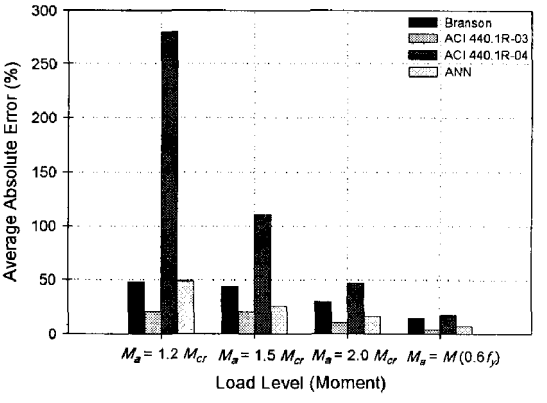

(f) $E = 50{,}000$ MPa

Figure III-3: Average absoluter error for $\rho_s = 0.70\%$ case

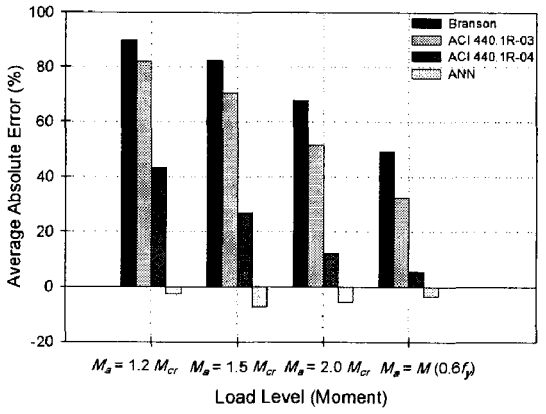

(a) E = 20,000 MPa

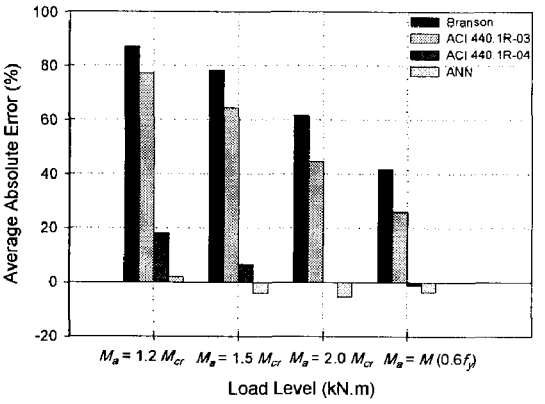

(b) E = 25,000 MPa

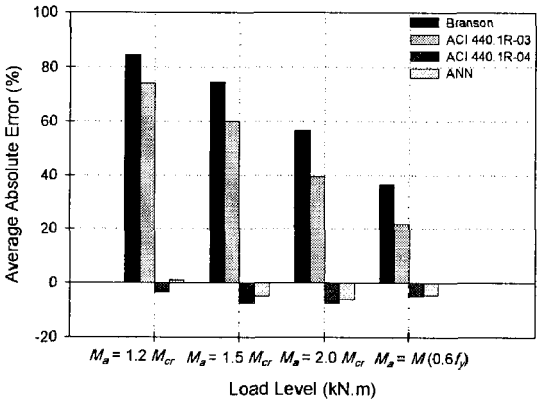

(c) E = 30,000 MPa

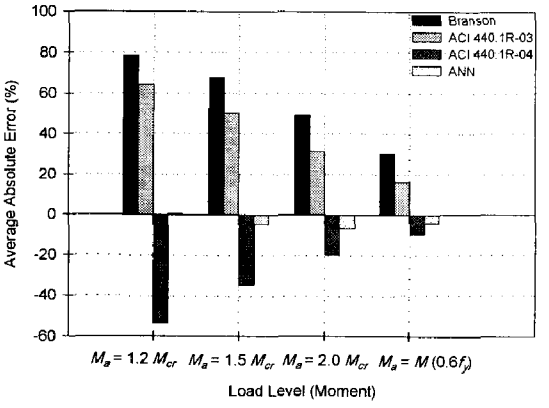

(d) E = 35,000 MPa

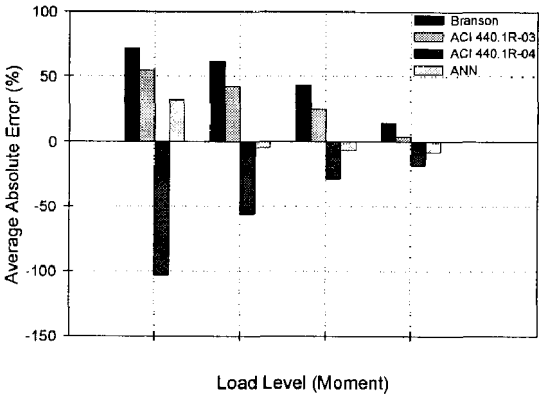

(e) E = 40,000 MPa

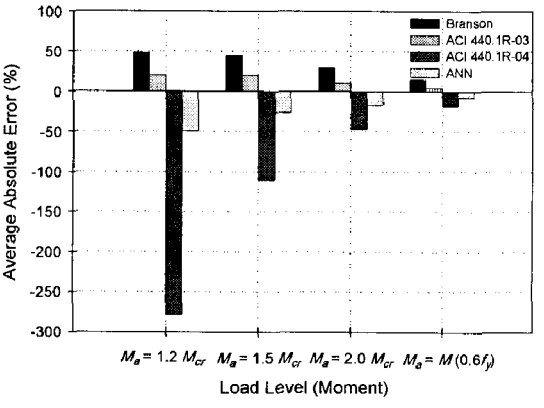

(f) E = 50,000 MPa

Figure III-4: Average algebraic error for ρ_s = 0.70% case

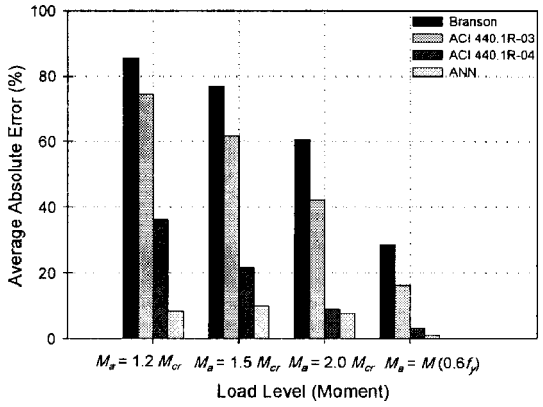

(a) E = 20,000 MPa

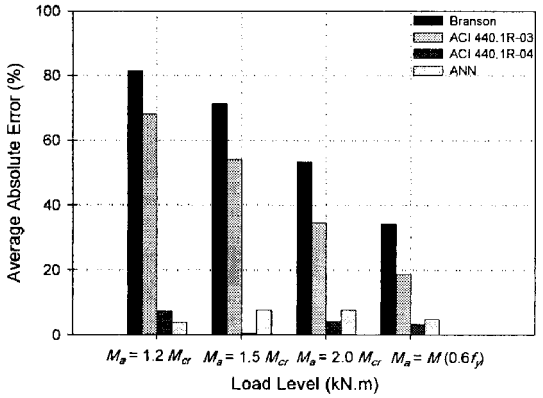

(b) E = 25,000 MPa

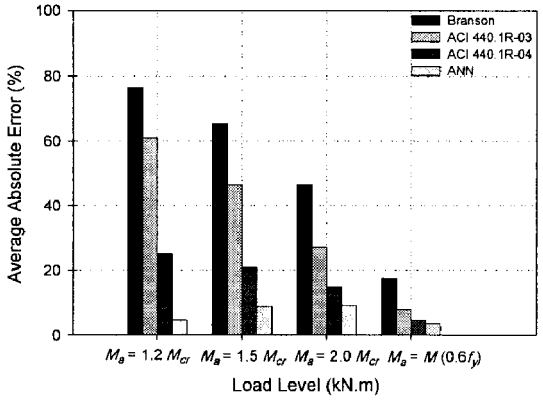

(c) E = 30,000 MPa

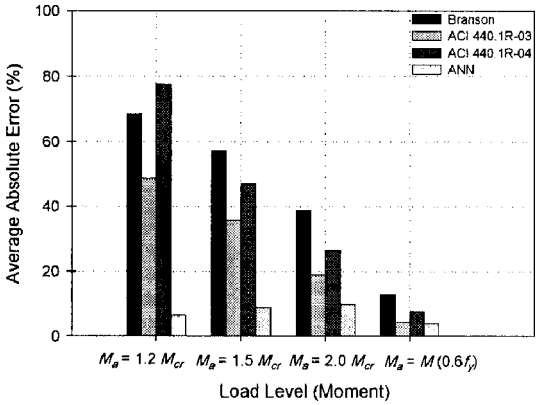

(d) E = 35,000 MPa

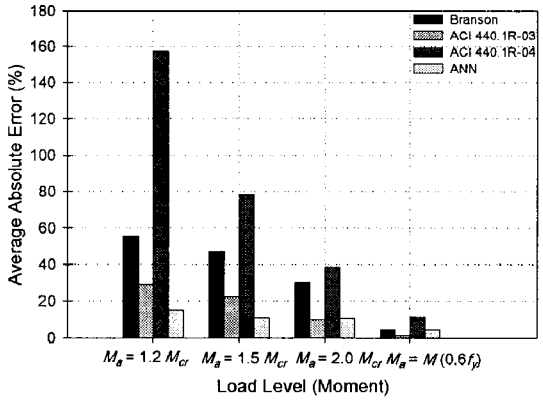

(e) E = 40,000 MPa

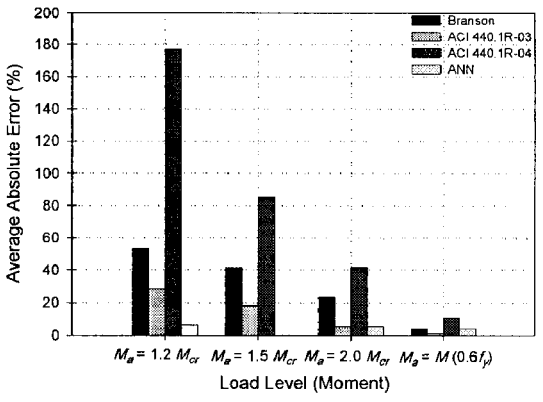

(f) E = 50,000 MPa

Figure III-5: Average absoluter error for ρ_s = 0.90% case

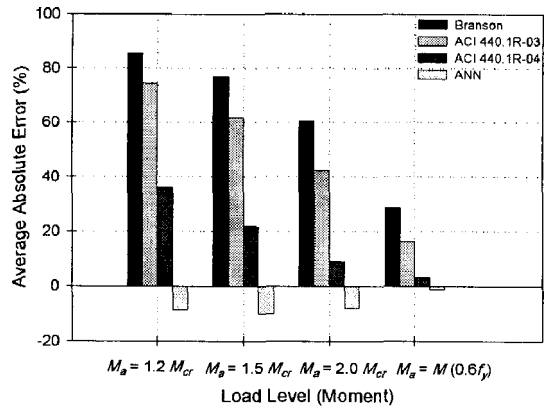

(a) E = 20,000 MPa

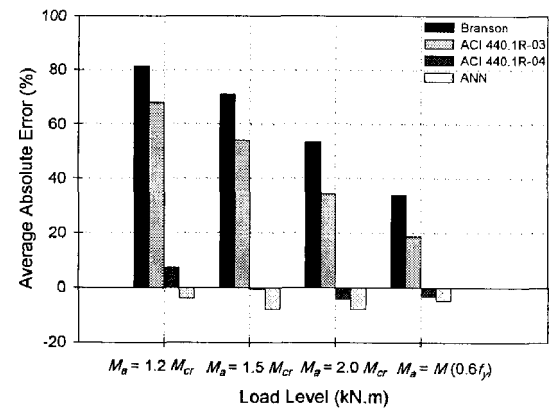

(b) E = 25,000 MPa

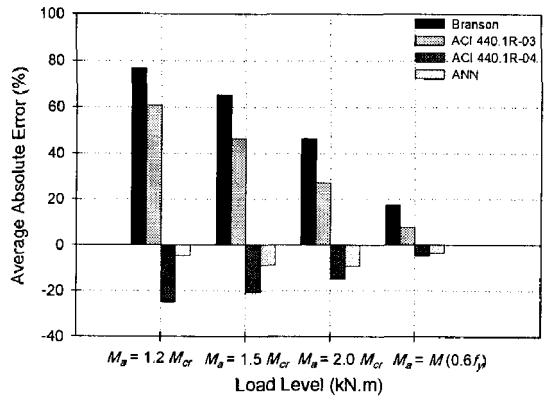

(c) E = 30,000 MPa

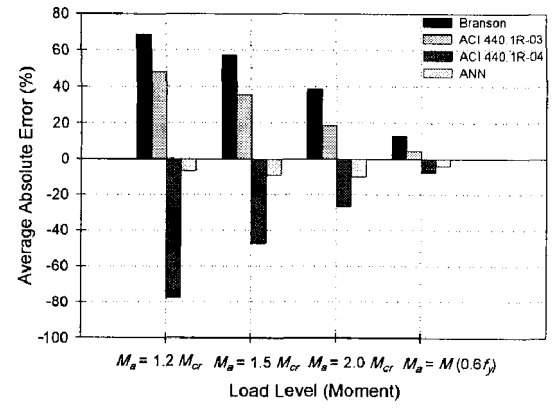

(d) E = 35,000 MPa

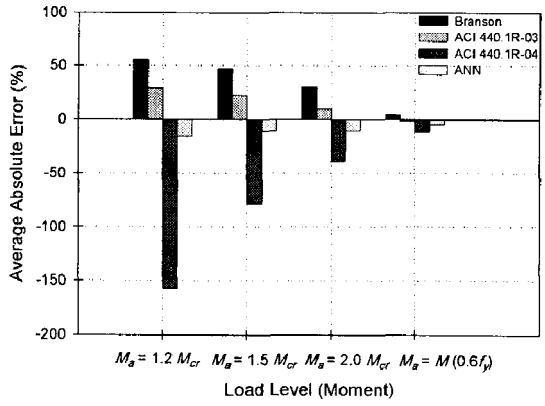

(e) E = 40,000 MPa

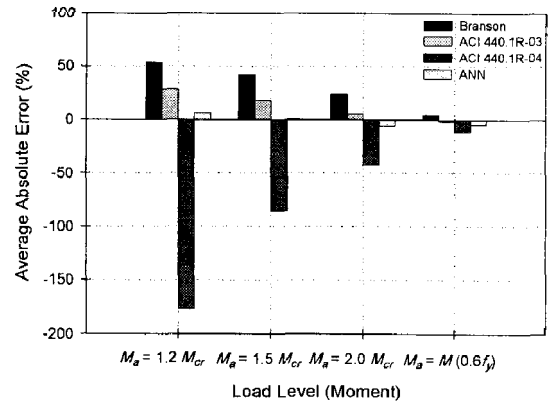

(f) E = 50,000 MPa

Figure III-6: Average algebraic error for ρ_s = 0.90% case

III.1 References

ACI 440 (2003). Guide for the Design and Construction of Concrete Reinforced with FRP Bars, American Concrete Institute, Farmington Hills, Michigan, 42.

ACI 440 (2004). Guide for the Design and Construction of Concrete Reinforced with FRP Bars, Proposed Revision, American Concrete Institute, Farmington Hills, Michigan, 35.

Branson, D. E. (1963). "Instantaneous and time-dependent deflections of simple and continuous reinforced beams." HPR Rep. No. 7, Part 1, Alabama Highway Department, Bureau of Public Roads, Montgomery, Ala.